Order Number 9224870

Diffusing wave spectroscopy

Zhu, Jixiang, Ph.D.

City University of New York, 1992

U·M·I
300 N. Zeeb Rd.
Ann Arbor, MI 48106

A

DIFFUSING WAVE SPECTROSCOPY

by

Jixiang Zhu

A dissertation submitted to the Graduate Faculty in Physics in partial fulfillment of the requirements for the degree of Doctor of Philosophy, The City University of New York.

1992

This manuscript has been read and accepted for the Graduate Faculty in Physics in satisfaction of the dissertation requirement for the degree of Doctor of Philosophy.

4/27/92
Date

L. G. Ferrari
Chair of Examining Committee

4/30/92
Date

Joseph B. Krieger
Executive Officer

Dr. D.A. Weitz

Dr. D.J. Pine

Prof. J. Gerstern

Prof. Fisher

Supervisory Committee

The City University of New York

Abstract

DIFFUSING-WAVE SPECTROSCOPY

By Jixiang Zhu

Adviser: Dr. David A. Weitz

We present the development of Diffusing-Wave Spectroscopy (DWS) and the applications of DWS to study concentrated colloidal suspensions. DWS is an extension of the traditional photon correlation spectroscopy to the multiple scattering limit. It is a unique tool for studying the dynamics and the structures of optically opaque materials and thus it opens up for study a new class of systems. An important feature is that DWS probes the motion of scatterers at very short length scale.

To utilize DWS, one must account for the effects of internal reflection which results from the index of refraction mismatch at the boundaries between the scattering medium and its surroundings. We develop a model which accounts for the internal reflection by amending the boundary conditions for the diffusion equation for the propagating light. We show that static angular correlation functions can be used to measure the effect of internal reflection. After doing a series of experiments, we find that the theory is in excellent agreement with the experiments.

As an important application of DWS we study the effect of hydrodynamic interactions on the short time non-diffusive motion of Brownian particles suspended in a fluid. We measure the mean square displacement, $\langle \Delta r^2(\tau) \rangle$, for concentrated suspensions at times short to observe the retarded nature of hydrodynamic interactions. A power-law decay of the velocity autocorrelation function, $R(\tau) \sim \tau^{-3/2}$, is observed for all concentrations. A remarkable scaling behavior of the time dependent diffusion

coefficient, $D_s(\tau)=\langle\Delta r^2(\tau)\rangle/6\tau$, with particle volume fraction is observed: if $D_s(\tau)$ is scaled by its asymptotic value and if time is scale by a viscous time constant inversely proportional to the shear viscosity of the suspension, all the data fall onto a single universal curve.

Using DWS in backscattering, we find that light backscattered from an optically dense random medium exhibits a pronounced polarization dependence. An unexpected memory of the incident circular polarization of multiply scattered light arises because the wave's helicity is randomized less rapidly than is its direction. We develop a simple model to account for the observed polarization dependence of the intensity and temporal correlation of the intensity fluctuations of backscattered light.

ACKNOWLEDGMENTS

I wish to acknowledge many people who have helped me and encouraged me during the preparation of this thesis, as well as during the thesis research at Exxon Corporate Research labs and my graduate course works at the Hunter College and the Queens College of the City University of New York.

I owe a great deal of my successful completion of this thesis to my thesis adviser Dr. David A. Weitz. Four years ago I was very fortunate to have the opportunity to come to the Exxon Corporate Research labs to work on my thesis research with Dr. Weitz. He worked very hard to help me in every aspects of my research work. Not only did He teach me how to do physics experiments, but also the fundamental ways of doing research. He insisted that I must understand the physics of my research projects and he went a great length to teach me how to present our research work in very simple terms. He is a bright, tough, very responsible adviser. I deeply appreciate his great efforts in helping me gaining my knowledge and ability. He is the best and I can not thank him enough for his work in training me to be a physicist.

Special thanks go to Dr. David J. Pine who helped me in many ways during the thesis research. He is a great thinker and the best writer. He helped me to understand the physics, as well as writing papers. I enjoyed working with Mr. J. Müller who built the ultra fast correlator which made my last project possible, Drs. J.Z. Xue, D.J. Durian and A.J. Liu with whom I had many helpful discussions. Thanks also go to Prof. Mark Hillery who taught me many courses, L.A. Ferarri, N.G. Garcia, and A.Z. Genack for their help while I was in the Queens College.

I like to thank the members of my dissertation committee, among them are Prof. Ferrari, Prof. H.Z. Cummin, Prof. Fisher and Prof. J. Gerstern who gave me many good instructions. I wish to acknowledge the financial support from the Hunter College, the Queens College, and Exxon Research & Engineering Company.

I wish to thank my parents, my brothers, and my sister who assisted me to come to the United States for my Ph.D. study. The cost of the airfare was astronomical to them. Without their selfless financial support, I would not even be able to come here to study.

Finally, I should acknowledge my indebtedness to my wife, Linda M. Lam, for her patience, great care, and encouragement.

Annandale, NJ.

May 1992.

CONTENTS

Lists of Figures

Chapter I. INTRODUCTION

In this thesis, we present recent developments and applications in diffusing-wave spectroscopy (DWS), which have a significant impact on the range of problems that can be addressed and on the type of systems that can be studied. DWS is an extension of dynamic light scattering (DLS) to very highly multiple scattering media. This technique extends the technique of DLS to opaque samples such as concentrated suspensions without diluting or index matching. In addition, DWS can be used to study particle dynamics on length scales that are so short that the conventional DLS is not suitable. In this chapter, we present a summary of the theoretical principles underlying DWS, and the characteristics of DWS, both in extending traditional DLS techniques, and in studying new physical phenomena.

There are many similarities between diffusing-wave spectroscopy and conventional dynamic light scattering. Both involve the detection of the intensity fluctuation of a single speckle spot of the scattered light. In both cases, these fluctuations are characterized by their temporal autocorrelation function. In both cases, these intensity fluctuations reflect the dynamics of the scattering medium. By contrast, there are also major differences in terms of the kind of samples the length scale they probe. DWS is used in studying strongly scattering opaque medium while DLS is used to study weakly scattering transparent medium. DWS typically probes motions at length scale much shorter than the wavelength of the light while DLS probes motions at length scale about the wavelength.

In traditional dynamic light scattering, motion of the scatterers on the length scale set by the inverse of the scattering wave vector, q^{-1}, leads to a change in the path length of the scattered light by a wavelength. This changes the phase of the detected light by 2π, and hence to a change in the intensity of the scattered light. The characteristic decay

time of the correlation function is related to the dynamics of the medium through this length scale. This characteristic time scale for the intensity fluctuations can be obtained by analyze the experimentally measured temporal autocorrelation function. Therefore, to obtain meaningful information about the dynamics of the medium from this characteristic time scale requires knowledge of the length scale set by the scattering wave vector. This requirement limits the application of traditional DLS to the strictly single scattering limit. If light has been multiply scattered, the intermediate scattering wave vector is unknown, precluding simple, meaningful interpretation of the measured decay time of the autocorrelation function of the scattered light. Diffusing-wave spectroscopy approaches the problem of multiple scattering from an entirely different limit, that of very high multiple scattering. In this limit, the light does not undergo only one, or even a small number of scattering events, but instead is scattered a *very* large number of times. In this limit, the direction of the light is totally randomized. Then, the propagation of the light, and the effect of the dynamics of the scattering medium, can both be treated with *statistical* approximations. This approach allows useful information to be obtained from the temporal autocorrelation function of the scattered light in the high multiple scattering limit.

The length scale of the motion of particles that causes the decay of the temporal autocorrelation function of the multiply scattered light measured with DWS is very short. The decay results from a change in phase of the scattered light by 2π, just as for conventional DLS. In DWS the total path length of the light through the sample change by a wavelength and thus the fluctuation in the intensity. Since light has been multiply scattered, each scatterer needs to move a very short length scale to cause the total path length to change a wavelength. The calculation of this phase change, and hence the temporal autocorrelation function in DWS, has two fundamental approximations. The first approximation is in the description of the light propagation through the scattering medium. In the limit of very high multiple scattering, each photon is scattered a very

large number of times, and its path can be described as a random walk. The simplest description of the light propagation is with the diffusion approximation[1]. This approximation neglects any interference effects of the light as it propagates through the scattering medium, and assumes that photon flux are conserved. The neglect of interference effects within the medium is predicated on the assumption that the light scattering is not so strong as to approach the localization of light due to random scattering. It is an excellent approximation in virtually every instance of practical importance. The use of the diffusion approximation makes it possible to calculate the distribution of paths taken by the photons propagating through the medium.

The second fundamental approximation inherent in DWS is in the treatment of the effect of the dynamics of the scatterers on the phase of the light. Since each photon is scattered a large number of times as it is transported through the medium, the details of individual scattering events play a less critical role. In particular, the conservation of scattering momentum at every point along the full path can be neglected. Instead, the individual scattering events are approximated by the contribution of an average scattering event. Then, the knowledge of the path length, obtained through the use of the diffusion approximation, determines the number of these average scattering events that contribute to each path. It is these two approximations that make the DWS approach tractable, and allows the calculation of the autocorrelation function. Diffusing-wave spectroscopy is an extension of the diffusion approximation to dynamic light scattering.

Within the diffusion approximation, light propagation is parameterized by the diffusion coefficient for light, $D_\ell = v\ell^*/3$, where v is the speed of light in the medium and ℓ^* is the transport mean free path in the medium. The effective speed of light in the medium can be substantially smaller than that in a homogeneous medium[2]. The average distance a photon travels between scattering events is called scattering mean free path, ℓ.

For scatterer sizes small comparing with the wavelength, one scattering event will randomize the direction of the scattered photon. The random walk step size is the scattering mean free path. By contrast, for large sized scatterers, the photons tend to be scattered in forward direction, and whence taking many scattering events to randomize the direction of the incident photon. The random walk step size is typically substantially larger than the scattering mean free path, ℓ. This length scale is called the transport mean free path, ℓ^*, which characterizes the scattering medium itself. By definition, it is apparent that $\ell^* > \ell$.

To use of the diffusion approximation to describe the propagation of the light places limitations on which media can and cannot be studied using DWS. Samples that scatter light very strongly, and have a opaque or milk-like appearance, are suitable. For example, concentrated samples of latex spheres in water can be studied. However, the requirement that light diffuse through the sample also leads to some restrictions in the choice of samples. Absorption becomes much more important in highly scattering samples since the path length followed by the light is greatly increased. While the effects of absorption can easily be included in the theoretical treatment of DWS, even a relatively small amount of absorption can preclude the use of DWS. Thus, the applicability of DWS to samples that are colored is much more limited than to samples that are white. Furthermore, the requirement that the light diffuse through the sample also restricts the application of DWS to those samples that scatter highly enough. The sample must be sufficiently opaque that all light transmitted through the sample is scattered many times. Even with these limitations, DWS greatly broadens the range of samples that can be studied using dynamic light scattering techniques. In particular, DWS can be used to study samples at length scales that had not been possible to study with DLS, including a wide range of concentrated suspensions.

The use of the diffusion approximation to describe the propagation of light ensures that the scattering wave vector, which relates the incident and detected light, has little relevance to the resultant correlation function, because the light has undergone such a large number of intermediate scattering events. Thus, unlike DLS, the angle between the incident and detected light is not important in DWS. As a consequence, there are two basic experimental geometries that have proven useful. The first is backscattering, where the light is incident of one side of the sample and the scattered light is detected from the same side. The other geometry is transmission, where the light is incident on one side of the sample and the scattered light transmitted through the sample is detected. In either case, the exact angle of the detected light is not critical. However, the exact experimental geometry is critical, as it determines the length of the paths that the scattered photons follow. Thus, for example, the thickness of the sample or the diameter of the incident beam strongly affect the decay time of the autocorrelation functions.

In DWS the internal reflection resulting from the index mismatch between the medium and its surroundings can play a important role in correctly interpreting the results of DWS. We measure the effect of internal reflection. We show that effect of internal reflection can be quantitatively account for by incorporating a reflection coefficient into the boundary condition for the diffusive light. Physically, the consequences of internal reflections can be understood by considering their effect on the distribution of photon path lengths through the sample. The internal reflection due to the mismatch of the index of refraction at the boundary of the random media causes photons to remain inside the medium for a longer time, and thus, increases the photon path lengths by an amount determined by the index mismatch. In all backscattering experiments, and in transmission experiments through *thin* samples where path lengths are comparable to ℓ^*, the increase in path length due to internal reflection is generally a significant fraction of the total path length. By contrast, in transmission experiments

through *thick* samples, where all paths are long, the increase in path length due to internal reflections is only a small fraction of total path length. Thus, the effect of internal reflection is significant for backscattering experiments and transmission experiments through thin samples, and relatively less significant for transmission experiments through very thick samples.

One of the most important applications of traditional DLS has been used in particle sizing measurements. Although traditional DLS is a well developed method for particle sizing, it is only good for sufficiently dilute suspension so that the light is scattered only once. DWS can be used in particle sizing for *concentrated* suspensions. Since most suspensions during the manufacturing processes are sufficiently concentrated that they scatter very highly, DWS may provide a means of using light scattering for monitoring particle size in these materials without requiring dilution. We show that the backscattering geometry is the most convenient one for particle sizing, and it is certainly possible to obtain a measure of the average particle size that is accurate to within about 10 to 20%.

In studying DWS in the backscattering geometry, we discover a unexpected polarization memory effect of circularly polarized light. For long time, single Rayleigh scattering is known to result in the polarization of scattered light in a cloudless blue sky. Multiple scattering is expected to randomize the phase, direction, and polarization of photons. What is surprising is that for *circularly* polarized light, randomization of the polarization requires many more scattering events than are required for the complete randomization of the wave's direction. This polarization memory has important consequences both for the average scattered intensity and for the temporal correlation of the intensity fluctuations of light backscattered from a time varying medium. For circularly polarized light backscattered from anisotropic scatterers, the scattered intensity of the same helicity is higher than that of the opposite helicity. The temporal

autocorrelation function decays slower for the same helicity channel than that of the opposite helicity.

In transmission, the length scale DWS probes can, theoretically, be arbitrarily small so long as we choose the sample sufficiently thick. We use this feature of DWS to study the short time Brownian motion of particle suspension at both high and low volume fractions. To probe the short time scale corresponding to the short length scale, we use a ultra fast correlator of which the sample time is as short as 12.5ns. At this short length scale the Brownian motion of the particles is no longer diffusive, in the sense that the mean square displacement, $\langle \Delta r^2(\tau) \rangle$, of a particle does not increase linearly as a function of time. For the first time, we find that for all volume fractions the velocity correlation function decays as a power law, $R(\tau) \sim \tau^{-3/2}$. This slow decay of the velocity correlation function reflects the fact that the flow pattern develops slowly around the particle in question. A remarkable scaling behavior with the volume fraction is observed for the time dependent diffusion coefficient, $D_S(\tau) = \langle \Delta r^2(\tau) \rangle / 6\tau$: if $D_S(\tau)$ is scaled by its asymptotic value and if time is scaled by a viscous time inversely proportional to the shear viscosity of the suspension, all the data fall onto to single master curve. This finding gives great inside of the time evolution of the hydrodynamic interaction between suspended particles.

This thesis is organized as follows: In Chapter II. we present the theoretical background and experimental details of DWS, in Chapter III. we discuss the effect of internal reflection, and the memory effect of multiply scattered light will be discussed in Chapter IV. and finally, we present the study of the short time motion of Brownian particles at various concentration.

CHAPTER II.

THEORETICAL AND EXPERIMENTAL BACKGROUNDS

In this chapter, we present the theoretical principles underlying DWS and a derivations of its analytical expressions. We begin by considering the case where the concentration of particles is large enough to produce high multiple scattering, but small enough that both potential and hydrodynamic interactions need not be considered. This simplifies the discussion of the effects of the particle dynamics and allows us to consider the consequences of the diffusive propagation of the light. This is followed by a more detailed discussion of the consequences of particle interactions, both potential and hydrodynamic, on the theoretical treatment. We then discuss the details of the experimental setup.

The key to the theory of DWS is the description of the propagation of light in a multiply-scattering medium in terms of the diffusion approximation. Within this approach, the phase correlations of the scattered waves within the medium are ignored, and only the scattered intensities are considered[3]. Thus, the path followed by an individual photon can be described as a random walk. Whether the diffusion approximation is valid in a given system depends on the length scales over which the transport of light is described. For length scales less than the mean free path (or extinction length), ℓ, of the coherent field, the wave equation for the electric field must be used. For length scales longer than ℓ, the phase correlation of the waves must be considered only for limited, specialized cases. The most commonly studied example is that of enhanced backscattering where the phase coherence of the scattered fields plays an essential role[4,5]. More generally, it is only in the case of extremely strong scattering, where the Ioffe-Regel limit is approached, and light localization is predicted to occur, that the use of the full wave equation is essential[6]. However, achieving this criterion has

proven elusive and, for nearly all cases of practical interest, the transport of light can be described in terms of the intensity or energy density.

For scatterers much smaller than λ, the scattering is isotropic and the direction of the light propagation is randomized by a single scattering event or, equivalently, over a distance ℓ. In this case the transport of the light energy density, $U(\mathbf{r},t)$, can be described over length scales longer than ℓ by the diffusion equation

$$\frac{\partial}{\partial t}U(\mathbf{r},t)=D_\ell\nabla^2U(\mathbf{r},t) \qquad (2.1)$$

where D is the diffusion coefficient of the light. Then, $D_\ell=c\ell/3$ where c is the speed that the light travels through the effective background medium. For particles which are not small compared to λ, the scattering is anisotropic, and the mean number of scattering events, n_0, required to randomize the direction of light propagation is greater than one. The length scale over which this randomization occurs is the transport mean free path, ℓ^*, defined by $\ell^*=n_0\ell$. Thus, for $n_0>1$, the diffusion equation is valid only over length scales longer than ℓ^* and $D=c\ell^*/3$. In practice, this means that the theory for DWS based solely on the diffusion approximation will provide an accurate description of the temporal fluctuations of the scattered light when the sample dimensions are greater than ℓ^* and the distance that photons travel through the sample is much greater than ℓ^*.

Two theoretical approaches have been used to describe the fluctuations in the scattered electric field. The first approach starts from the wave equation for the propagation of light and uses a diagrammatic expansion to describe of the scattering from random fluctuations in the dielectric constant. The lowest order term in this expansion corresponds to the diffusion approximation. The consequences of motion of the scatterers were first considered by Golubentsev[7] and temporal autocorrelation functions for different scattering geometries were calculated by Stephen. Subsequently,

MacKintosh and John[8] refined this approach by considering the effects of anisotropic scatterers and non-diffusive modes of propagation.

The second theoretical approach differs from the first by considering the diffusive transport of individual photons directly, rather than starting from the wave equation[9,10]. The path of each photon is determined by random, multiple scattering from a sequence of particles. The fluctuations in the phase of the electric field due to the motion of the scatterers is calculated for each light path. The contributions of all paths, appropriately weighted within the photon diffusion approximation, are then summed to obtain the temporal autocorrelation function. In this paper, we adopt the second approach. It is mathematically simpler and physically more transparent than diagrammatic methods. It can also be more easily generalized to larger particles which scatter light anisotropically.

For simplicity, we consider a suspension of identical spherical particles randomly dispersed in a fluid and illuminated with laser light of wavelength. For specificity, we assume a slab geometry, as shown in Fig. 2.1; other geometries will be discussed later. The suspension must be optically thick so that all the light entering the sample is scattered many times before exiting. Scattered light exiting the sample is collected from a small area near the sample surface (within approximately one mean free path, ℓ^*) and partially collimated so that roughly one coherence area is detected. The motion of the particles is probed by monitoring the time dependence of the fluctuations of the scattered light. In DLS experiments, these fluctuations are usually characterized by the normalized temporal autocorrelation function,

$$g_1(\tau)=\frac{\langle E(0)E^*(\tau)\rangle}{\langle |E(0)|^2\rangle} \qquad (2.2)$$

where $E(\tau)$ is the electric field of the scattered light collected by the detector and τ is the delay time. To calculate $g_1(\tau)$, we first consider a single light path through the sample.

For a given sequence of scattering events at positions $\mathbf{r}_1$, ..., $\mathbf{r}_n$ and with corresponding successive wavevector transfers $\mathbf{q}_i = \mathbf{k}_i - \mathbf{k}_{i-1}$, the product of the scattered electric field at time τ with that at time 0 will be

$$E^{(n)}(\tau)E^{(n)*}(0) = |E^{(n)}(0)|^2 \exp\left[i\sum_{i=1}^{n}\mathbf{q}_i \cdot \Delta\mathbf{r}_i(\tau)\right] \qquad (2.3)$$

where $\Delta\mathbf{r}_i(\tau) = \mathbf{r}_i(\tau) - \mathbf{r}_i(0)$ is the distance the i^{th} particle moves in a time τ. The argument of the exponential,

$$\Delta\Phi^{(n)}(\tau) = \sum_{i=1}^{n}\mathbf{q}_i \cdot \Delta\mathbf{r}_i(\tau) \qquad (2.4)$$

represents the aggregate phase shift of the scattered light due to the motion of all n scatterers in the time interval τ. Assuming that the fields belonging to different paths add incoherently, the average contribution to the normalized autocorrelation function of all paths of order n is

$$\langle E^{(n)}(\tau)E^{(n)*}(0)\rangle = I(0)P(n)\left\langle \prod_{i=1}^{n} e^{-i\mathbf{q}_i \cdot \Delta\mathbf{r}_i(\tau)} \right\rangle \qquad (2.5)$$

Here $P(n)$ is the fraction of the total scattered intensity, I_0, in the n^{th} order paths and $\langle\ \rangle$ denotes averages over both the particle displacement, $\Delta\mathbf{r}(\tau)$, and the distribution of wavevectors $\mathbf{q}$. For large n, that is $n>>n_0$, the transport of light through a sample is accurately described within the diffusion approximation. This allows $P(n)$ to be easily evaluated. Furthermore, the large number of scattering events in each path greatly simplifies the evaluation of the averages in Eq. (2.5).

For large n, we can relax the condition that the sum of the intermediate scattering vectors must equal the difference between the incident and exiting wavevectors,

$\sum_{i=1}^{n} \mathbf{q}_i \Delta\mathbf{r}_i(\tau)=\mathbf{k}_n-\mathbf{k}_0$. In addition, we also assume that successive scattering events are uncorrelated. Thus, the distribution of the $\mathbf{q}_i$ is determined solely by the scattering form factor of a single sphere. Then, for independent particles, the right hand side of Eq. (2.5) becomes $P(n)\langle\exp[-i\mathbf{q}\,\Delta\mathbf{r}(\tau)]^n\rangle$. For Brownian motion, the distribution of $\Delta\mathbf{r}(\tau)$ is Gaussian and the average over particle motion is readily performed yielding

$$\langle E^{(n)}(\tau)E^{(n)*}(0)\rangle = I_0\, P(n) \left\langle e^{-q^2\langle\Delta r^2(\tau)\rangle/6}\right\rangle_q^n \qquad (2.6)$$

where $\langle\ \rangle_q$ denotes the average over q. For simple diffusion, $\langle\Delta r^2(\tau)\rangle = 6D\tau$ where D is the diffusion coefficient of the particles.

The average over q can be performed explicitly for point-like scatterers which scatter light isotropically; this gives

$$\langle E^{(n)}(\tau)E^{(n)*}(0)\rangle = I_0\, P(n) \left[\frac{\tau_0}{4\tau}\left[\,1-e^{-\tau_0/4\tau}\,\right]\right]^n \qquad (2.7)$$

where $\tau_0 \equiv (Dk_0^2)^{-1}$ and $k_0=2\pi/\lambda$. However, for larger particles which scatter light anisotropically, the average over q is more difficult to perform. Thus, we restrict ourselves to small delay times, $\tau<<\tau_0$, and retain only the first term in a cumulant expansion,

$$\langle e^{-Dq^2\tau}\rangle_q^n = \langle 1-Dq^2\tau\rangle_q^n = (1-D\langle q^2\rangle\tau)^n = e^{-Dn\langle q^2\rangle\tau} \qquad (2.8)$$

We can compare this more general approximation with the exact expression, Eq. (2.7), for point-like scatterers by evaluating $\langle q^2\rangle$ for a flat distribution,

$$\langle q^2\rangle = \frac{\int q^2 d\Omega}{\int d\Omega} = \frac{\int q^2 q\,dq}{\int q\,dq} = 2k_0^2 \qquad (2.9)$$

which gives,

$$\langle E^{(n)}(\tau)E^{(n)*}(0)\rangle = I_0\, P(n)\, e^{(-2\tau/\tau_0)n} \qquad (2.10)$$

Expanding the exact expression in Eq. (2.7) gives

$$\langle E^{(n)}(\tau)E^{(n)*}(0)\rangle = I_0\, P(n)\, e^{-2n\tau/\tau_0}[1-1/3(\tau/\tau_0)+O(\tau/\tau_0)^3] \qquad (2.11)$$

so that the cumulant expansion gives the correct results to leading order in τ/τ_0. Furthermore, the effective decay time is $\tau_0/2n$, so that for large n, $\langle E^{(n)}(\tau)E^{(n)*}(0)\rangle$ decays essentially to zero before the higher order terms make a significant contribution. Nevertheless, for large τ/τ_0 the cumulant expansion must fail since the exact expression in Eq. (2.7) decays as a power law, $(\tau/\tau_0)^{-n}$, due to the contributions of scattering at small q. We note, however, that at these long times low order scattering events dominate. For small n, the distribution of $\mathbf{q}_i$ is not random but must satisfy the condition that $\sum_{i=1}^{n}\mathbf{q}_i\cdot\Delta\mathbf{r}_i(\tau)=\mathbf{k}_n-\mathbf{k}_0$. This will modify the average in Eq. (2.8) and could have the effect of at least partially offsetting the error introduced by the cumulant expansion.

Equation (2.8) can be readily generalized to treat the anisotropic scatterers typically used in experiments. Here, the single particle scattering intensity is peaked in the forward direction and $\langle q^2\rangle$ is less than $2k_0^2$. Using the relation $\ell/\ell^* = \langle\, 1 - \cos\theta \,\rangle$[3,11], we have

$$\langle q^2\rangle = \langle\, [2k_0\sin(\theta/2)]^2 \,\rangle = 2k_0^2\langle\, 1 - \cos\theta \,\rangle = 2k_0^2\ell/\ell^* \qquad (2.12)$$

Using this result and the cumulant expansion in Eq. (2.8), we can evaluate the average over q in Eq. (2.6) and obtain a simple expression for the contribution of the n^{th} order scattering paths to the autocorrelation function,

$$\langle E^{(n)}(\tau)E^{(n)*}(0)\rangle = I_0\, P(n)\, e^{(-2\tau/\tau_0)(\ell/\ell^*)n} \qquad (2.13)$$

For isotropic scatterers, $\ell = \ell^*$, and we recover Eq. (2.10), the approximate result for point-like scatterers. We note that the accuracy of Eq. (2.13) improves as the scattering becomes more anisotropic. The second cumulant of $\langle e^{-Dq^2\tau} \rangle$ is $e^{-\frac{1}{2}(D\tau)^2[\langle q^4 \rangle - \langle q^2 \rangle^2]}$. For typical single-particle form factors, $F(q)$, we expect $\langle q^4 \rangle \sim \langle q^2 \rangle^2 \sim (\ell/\ell^*)^2$, so that the leading order correction to the cumulant expansion in Eq. (2.8) is $O[(\tau/\tau_0)(\ell/\ell^*)^2]$. Thus, for large scatterers, where $\ell^* >> \ell$, the range of validity of Eq. (2.13) may extend up to τ/τ_0.

The total field autocorrelation function, $g_1(\tau)$, is obtained by summing over scattering paths of all orders

$$g_1(\tau) = \sum_{n=1}^{\infty} P(n)\, e^{-(2\tau/\tau_0)(\ell/\ell^*)n} \qquad (2.14)$$

If we rescale n by defining $n^* \equiv n/n_0 = (\ell/\ell^*)n$, the exponential term in this equation is identical to Eq. (2.10) for isotropic scatterers. Furthermore, for $n >> n_0$, $P(n)$ can be written as a function of n^* rather than n. Physically, this reflects the fact that over length scales longer than ℓ^*, the scattering appears to be isotropic ($n > n_0$), and the photon diffusion equation should be adequate to describe the transport of light. As a result, in this approximation,

$$g_1(\tau) = \sum_{n^*=1}^{\infty} P(n^*)\, e^{-(2\tau/\tau_0)n^*} \qquad (2.15)$$

This reflects a renormalization of the mean free path for anisotropic scatterers, so that the light may be viewed as undergoing an isotropic random walk with an average step length ℓ^*. We note that the decay rate of a given path depends critically on its length. Long paths reflect the aggregate contribution of many scattering events. Thus, each particle

need move only a small distance for the total path length to change by a wavelength. This occurs in a short time, leading to a rapid decay rate. By contrast, short paths reflect the contribution of a small number of scattering events. Thus, each particle must undergo substantial motion for the total path length to change by a wavelength. This takes a longer time, leading to a slower decay.

The key to the solution of Eq. (2.15) is the determination of $P(n^*)$. This task is greatly simplified if we pass to the continuum limit. Thus, we approximate the sum over n^* by an integral over the path lengths, $s=n^*\ell^*$ $(=n\ell)$, and obtain

$$g_1(\tau) = \int_0^\infty P(s)\, e^{-(2\tau/\tau_0)(s/\ell^*)} ds \qquad (2.16)$$

In this case, $P(s)$ is the fraction of photons which travel a path of length s through the scattering medium. Physically, Eq. (2.16) reflects the fact that a light path of length s corresponds to a random walk of s/ℓ^* steps and that $g_1(\tau)$ decays, on average, $\exp(-2\tau/\tau_0)$ per step. Now we can use the diffusion approximation to describe the random walk of the light, and $P(s)$ can be obtained from the solution of the diffusion equation for the appropriate experimental geometry. We emphasize, however, that the continuum approximation to the discrete scattering events will break down whenever there are significant contributions from short light paths.

Our method for determining $P(s)$ can be illustrated by considering a simple thought experiment. An instantaneous pulse of light is incident on the face of a sample which multiply scatters the light. The scattered photons will execute a random walk until they escape the sample. Here, we focus on those photons which exit the sample at some specified point, $\mathbf{r}_d$, on the boundary where they are detected. The flux of photons reaching $\mathbf{r}_d$ is zero at $t=0$, then increases to a maximum, and finally decreases back to zero at long times when all the photons have left the sample. At time t, the photons

arriving at point r_d are those that have traveled a path length $s=ct$ through the sample. Thus, the time dependence of the flux of photons arriving at point $\mathbf{r}_d$ is directly proportional to $P(s)$. The details of this time dependence, and hence the shape of $P(s)$, will depend on the experimental geometry.

To obtain $P(s)$ for a given experimental geometry we use Eq. (2.1), the diffusion equation for light, to determine the dispersion induced in a delta function pulse as it traverses the scattering medium. We denote the density of diffusing photons within the medium by $U(r)$. For initial conditions, we take the source of diffusing light intensity to be an instantaneous pulse at a distance $z=z_0$ inside the illuminated face, where we expect that $z_0 \sim \ell^*$, that is

$$U(z,t=0) = \delta(z-z_0,t) \tag{2.17}$$

We will discuss the consequence of the this approximation in Chapter IV.

In addition to the initial condition, we also need the boundary conditions. The detailed discussion of the boundary conditions and their relationship to internal reflection are presented in Chapter III. In the absence of internal reflection, the boundary must ensure that there is no flux of diffusing photons *entering* the sample from the boundaries. This is achieved to a good approximation with the boundary condition

$$U+\frac{2}{3}\ell^*\mathbf{n}\cdot\nabla U=0 \tag{2.18}$$

where $\mathbf{n}\cdot\nabla$ is the outward normal derivative[3]. Solving the diffusion equation for a given experimental geometry, the time-dependent flux of light emerging from the sample is obtained from the normal derivative of the solution evaluated at the exit point. Since all light emerging from the sample at time t has traveled a distance $s=ct$,

$$P(s) \propto U(\mathbf{r},t)\big|_{\mathbf{r}_d} \tag{2.19}$$

Having determined $P(s)$ for a given geometry, Eq. (2.15) can be used to calculate $g_1(\tau)$.

The calculation of $g_1(\tau)$ can be greatly simplified by noting that Eq. (2.15) is essentially the Laplace transform of $P(s)$. Thus, instead of solving the diffusion equation to obtain $P(s)$, we can solve the Laplace transform of the diffusion equation and obtain $g_1(\tau)$ directly. To this end, we introduce a simple change of variables in Eq. (2.1) and let $t=s/c$. Recalling that $D_{\ell}=c\ell^*/3$, Eq. (2.1) becomes,

$$\nabla^2 U - \frac{3}{\ell^*}\frac{\partial U}{\partial s} = 0 \qquad (2.20)$$

Multiplying both sides by $\exp(-ps)$ and integrating with resect to s from 0 to ∞, we obtain the Laplace transform of the diffusion equation,

$$\nabla^2 \overline{U} - \frac{3p}{\ell^*}\frac{\partial \overline{U}}{\partial s} = -\frac{3}{\ell^*} U_0(\mathbf{r}) \qquad (2.21)$$

where $\overline{U} = \overline{U}(\mathbf{r},p)$ is the Laplace transform of $U(\mathbf{r},s)$,

$$\overline{U}(\mathbf{r},p) = \int_0^{\infty} e^{-ps}\, U(\mathbf{r},s)\, ds \qquad (2.22)$$

and $U_0(\mathbf{r}) = \lim_{t \to 0} U_0(\mathbf{r},t) = \delta(z-z_0,t)$.[12] Then, from Eq. (2.18), the Laplace transform of $P(s)$ is given by

$$\overline{P}(p) = \int_0^{\infty} e^{-ps}\, P(s)\, ds \propto \frac{c}{2}\, \overline{U}(\mathbf{r},p)\,|_{\mathbf{r}_d} \qquad (2.23)$$

Comparing Eqs. (2.16) and (2.23), we see that

$$g_1(\tau) = \frac{\overline{U}(\mathbf{r},p)|_{\mathbf{r}_d}}{\overline{U}(\mathbf{r},0)|_{\mathbf{r}_d}} \qquad (2.24)$$

where we have made the identification, $p=(2\tau/\tau_0)/\ell^*$, and $\overline{U}(r,p)$ has been normalized so that $g_1(0)=0$. Thus, by solving the Laplace transform of the diffusion equation we can obtain the desired autocorrelation function directly.

For comparison to our experiments we note that we usually measure normalized intensity autocorrelation functions, $g_2(\tau)=\langle I(\tau)I(0)\rangle/\langle I\rangle^2$. For most systems of experimental interest, the scattered electric field is a complex Gaussian random variable and the intensity autocorrelation function is related to the field autocorrelation function calculated above by the Siegert relation,

$$g_2(\tau) = 1 + \beta|g_1(\tau)|^2 \qquad (2.25)$$

where β is a constant determined primarily by the collection optics. Wolf *et al.* have experimentally verified that there is no observable deviation from Gaussian statistics for strong multiple scattering in samples similar to ours[11]. In addition, by measuring $g_1(\tau)$ directly in heterodyne experiments, we have verified the validity of Eq. (2.25) for the correlation functions reported here.

The first experimental geometry we consider is transmission through a slab of thickness L and infinite extent[10,13].[St88, PWCH88] The light is incident on one side of the slab, and is detected after it has diffused a distance L across the sample. The incident light beam can either be focused to a point on the face, as illustrated in Fig. 2.1, or expanded to uniformly fill the face of the slab, as illustrated in Fig. 2.2. The autocorrelation functions for these two experimental geometries are different and can be calculated by solving the Laplace transform of the diffusion equation as previously discussed. In both cases, we take the source of diffusing intensity to be a distance $z=z_0$ inside the illuminated face where we expect that $z_0 \sim \ell^*$.

We first consider the case of uniform illumination of one side by an extended source so that $U(x,y,x,t) = \delta(z-z_0,t)$. The solution of the diffusion equation using the Laplace transform is given in Carslaw and Jaeger[12] (§ 14.3) for this geometry and for these boundary and initial conditions. They obtain

$$\overline{U} = \frac{1}{2D\ell\alpha} e^{-\alpha|z-z_0|} + A \sinh \alpha z + B \cosh \alpha z \qquad (2.26)$$

where $\alpha^2=6\tau/\tau_0\ell^{*2}$ and $D=c\ell^*/3$. The coefficients A and B are chosen so that the boundary condition, Eq. (2.18), is satisfied at $z=0$ and $z=L$. After tedious, but straightforward algebra, we obtain

$$g_1(\tau) = \frac{\dfrac{L+(4/3)\ell^*}{z_0+(2/3)\ell^*}\left\{\sinh\left[\dfrac{z_0}{\ell^*}\sqrt{\dfrac{6\tau}{\tau_0}}\right] + \dfrac{2}{3}\sqrt{\dfrac{6\tau}{\tau_0}}\cosh\left[\dfrac{z_0}{\ell^*}\sqrt{\dfrac{6\tau}{\tau_0}}\right]\right\}}{\left[1+\dfrac{8\tau}{3\tau_0}\right]\sinh\left[\dfrac{L}{\ell^*}\sqrt{\dfrac{6\tau}{\tau_0}}\right] + \dfrac{4}{3}\sqrt{\dfrac{6\tau}{\tau_0}} + \dfrac{4}{3}\sqrt{\dfrac{6\tau}{\tau_0}}\cosh\left[\dfrac{z_0}{\ell^*}\sqrt{\dfrac{6\tau}{\tau_0}}\right]} \qquad (2.27a)$$

$$\approx \frac{\left[\dfrac{L}{\ell^*}+\dfrac{4}{3}\right]\sqrt{\dfrac{6\tau}{\tau_0}}}{\left[1+\dfrac{8\tau}{3\tau_0}\right]\sinh\left[\dfrac{L}{\ell^*}\sqrt{\dfrac{6\tau}{\tau_0}}\right] + \dfrac{4}{3}\sqrt{\dfrac{6\tau}{\tau_0}} + \dfrac{4}{3}\sqrt{\dfrac{6\tau}{\tau_0}}\cosh\left[\dfrac{z_0}{\ell^*}\sqrt{\dfrac{6\tau}{\tau_0}}\right]} \qquad (2.27b)$$

where the second expression holds for $\tau<<\tau_0$. The characteristic time scale in these expressions is $\tau_0(\ell^*/L)^2$.

For the second geometry, we consider light incident from a point source on axis with the detector so that $U(x,y,x,t) = \delta(x,y,z-z_0,t)$. The solution for this geometry and these boundary and initial conditions can again be found in Carslaw and Jaeger[12] (§ 14.10):

$$\overline{U} = \frac{1}{4\pi D\ell}\int_0^\infty \frac{\xi J(\xi R)}{\eta}\left[e^{-\eta|z-z_0|} + A \sinh \eta z + B \cosh \eta z\right] d\xi \qquad (2.28)$$

where $\eta=\sqrt{\xi^2+\alpha^2}$ and $R=0$ when the source is on axis with the detector. The coefficients A and B are again found by applying the boundary conditions. We obtain,

$$g_1(\tau) \propto \int_{(L/\ell^*)\sqrt{\frac{6\tau}{\tau_0}}}^{\infty} [\, A(s) \sinh s + e^{-s(1-z_0/L)}]ds \qquad (2.29a)$$

where

$$A(s) = \frac{(\varepsilon s - 1)\,[\,\varepsilon s\, e^{-sz_0/L} + (\sinh s + \varepsilon s \cosh s)\, e^{-s(1-z_0/L)}\,]}{(\sinh s + \varepsilon s \cosh s)^2 - (\varepsilon s)^2} \qquad (2.29b)$$

and $\varepsilon=2\ell^*/3L$. The characteristic time scale for the decay of the autocorrelation function in Eq. (3.4) is $\tau_0(\ell^*/L)^2$. This reflects the diffusive nature of the transport of the light, which introduces a characteristic path length, $s_c=n_c\ell=n_c^*\ell^*$, where $n_c^*=(L/\ell^*)^2$ is the mean number of steps for a random walk of end-to-end distance L and average step length ℓ^*. Physically, this characteristic time scale corresponds to the time taken for the characteristic path length to change by λ, so that the total phase shift is roughly unity. Thus, we can estimate the typical distance an individual particle has moved from $n_c\langle q^2\rangle\langle\Delta r^2\rangle \approx 1$, which gives $\Delta r_{rms} \approx \lambda\ell^*/2\pi L$. *Since $\ell^*/L<<1$, the typical length scale over which particle motion is probed by DWS in transmission is much smaller than the wavelength.* This reflects the fact that the decay of the autocorrelation function is due to the cumulative effect of many scattering events, so that the contribution of individual particles to the total decay is small. *This is in striking contrast to ordinary dynamic light scattering where, by varying q, length scales greater than or roughly equal to the wavelength are probed.* Similarly, the time scale over which particle motion is probed with DWS is much shorter than with DLS. Thus, by adjusting the sample thickness L in transmission measurements, DWS provides a means for varying the range of length and

time scales over which particle motion can be measured using dynamic light scattering techniques.

Another significant difference between DLS and DWS is the dependence on scattering angle. In DLS, varying the angle changes the scattering vector, q, thus varying the length scale over which motion is probed. By contrast, in DWS, the diffusive nature of the transport ensures that the transmitted light has no appreciable dependence on angle and we find that the measured autocorrelation functions are independent of detection angle in transmission.

Autocorrelation functions measured in transmission are shown in Fig. 2.3. The sample consisted of an aqueous suspension of 0.605-μm-diam. polystyrene latex spheres at a volume fraction of ϕ=0.012 in a 1.0 mm thick cuvette. There is no unscattered light transmitted through the sample, insuring that the strong multiple scattering limit is achieved. The data in the lower curve were obtained when the sample was illuminated uniformly by a 1-cm diameter beam from an argon ion laser with λ=488 nm. Imaging optics collected the transmitted light from a 50 μm spot on the opposite side of the sample from a point near the center of the illuminated area. For comparison, the upper curve shows data obtained when the incident beam was focused to a point on one side of the sample and transmitted light was collected from a point on axis with the incident spot. These data clearly decay somewhat more slowly than the data obtained with an extended source illumination. Physically, this difference reflects the fact that for the extended source there is a larger contribution from long paths, resulting in a somewhat faster decay than for the point source.

To compare these data to the expression for the autocorrelation function derived above, we take $z_0=(4/3)\ell^*$, but note that the solutions are insensitive to the exact value used since, in general, $z_0 \sim \ell^*$ and $\ell^*/L >> 1$. The value chosen for z_0 affects only the first

few steps of a random walk which typically consists of a great number of steps. Thus, the relative contribution of the first few steps is small. In Fig. 2.3, the solid lines through the data are fits to the appropriate equations above. The time constant $\tau_0 \equiv (Dk_0^2)^{-1}$ is set equal to 4.52 msec where D was obtained from a DLS measurement in the single scattering limit using $\phi=10^{-5}$. The diffusion D coefficient remains independent of concentration for the particle concentrations used in these measurements. For both cases, excellent agreement is found between the data and the predicted forms of $g_2(\tau)$. The only fitting parameter is ℓ^* and values of $\ell^*=167$ æm for the extended source and $\ell^*=166$ æm for the point source are obtained. This excellent consistency for the fitted values of ℓ^* confirms that the somewhat different decay rates in Fig. 2.3 are due solely to geometric effects. The values obtained from the fit to the data are in reasonable agreement with Mie scattering theory, $\ell^*=180$ μm. Nevertheless, there is a discrepancy of about 7%, with the measured values lower than predicted. This in not experimental error, as a similar discrepancy is found for other polystyrene latex samples with different sizes and different volume fractions. The values obtained from DWS measurements in transmission are consistently lower than the predicted values, typically by about 10%. This discrepancy is probably not due to the consequences of particle correlation on the value of ℓ^*. The particle interactions in these polystyrene samples can be approximated as hard sphere repulsion, allowing the particle correlations to be determined. These are relatively weak for $\phi<0.1$, leading to negligible effect on ℓ^*. Instead, we believe that the discrepancy arises from the approximate nature of the boundary condition that we use, Eq. (2.18). In particular, we neglect the possibility of ay reflection of the light due to the discontinuity of the average index of refraction at the boundary. Including this effect will modify the boundary condition and will result in a renormalization of the value of ℓ^* obtained from DWS transmission measurements. If this effect is not included, the apparent ℓ^* measured will be less than the correct value.

Another interesting geometry we consider is that of backscattering[9,10,13,14]. Here, the light is incident uniformly on one face of a slab of thickness, L, and the scattered light is collected from the same face, as illustrated in Fig. 2.4. In deriving a functional form for the autocorrelation function, we would like to maintain the simplicity and elegance of the Laplace transform approach used in the case of transmission. However, we must be extremely cautious in using this approach for backscattering. In obtaining the Laplace transform in Eq. (2.16), we have used a continuum approximation to change the summation over paths in Eq. (2.15) to an integral. However, since $s=n$ and we must have at least one scattering event, we require $n \geq 1$; thus, the lower bound on s must be ℓ rather than 0. Equivalently, for isotropic scatterers, where $z_0=\ell^*$, the decay time for a path of length s is $\exp[-(2\tau/\tau_0)s/\ell]$. Allowing $s<\ell$ leads to unphysically long decay times, since $\tau_0/4$ represents the shortest decay time possible, corresponding to light singly scattered through 180°. Similarly, for anisotropic scatterers, where $\ell^*>\ell$, we require $s \geq \ell^*$ to obtain physically meaningful decay times. However, in order to maintain the simplicity of the Laplace transform, the lower bound on the integral must be zero. For transmission, this does not present a problem as the shortest possible paths are $s=L$, so that $n \geq 1$. By contrast, for backscattering, short paths do contribute and thus, in using the diffusion approximation, we must ensure that the contribution of the unphysically short paths is suppressed.

A simple way of achieving this is to solve the diffusion equation using an initial condition of a source a fixed distance, z_0, in from the illuminated face at $z=0$. This ensures that there are no contributions from paths shorter than z_0. Physically we can regard this as the source of the diffusing intensity, which we expect to be peaked at $z_0 \sim \ell^*$. Thus, for the initial condition we take $U(\mathbf{r},t=0)=\delta(x,y,z-z_0,t)$ and for the boundary conditions again we use Eq. (2.18). The solution for this geometry is the same as for the

case of transmission with an extended source, but here we evaluate it at the incident face and obtain,

$$G_1(\tau) = \frac{\sinh\left[\sqrt{\frac{6\tau}{\tau_0}}\left(\frac{L}{\ell^*}-\frac{z_0}{\ell^*}\right)\right] + \frac{2}{3}\sqrt{\frac{6\tau}{\tau_0}}\cosh\left[\sqrt{\frac{6\tau}{\tau_0}}\left(\frac{L}{\ell^*}-\frac{z_0}{\ell^*}\right)\right]}{\left[1+\frac{8\tau}{3\tau_0}\right]\sinh\left[\frac{L}{\ell^*}\sqrt{\frac{6\tau}{\tau_0}}\right] + \frac{4}{3}\sqrt{\frac{6\tau}{\tau_0}} + \frac{4}{3}\sqrt{\frac{6\tau}{\tau_0}}\cosh\left[\frac{z_0}{\ell^*}\sqrt{\frac{6\tau}{\tau_0}}\right]} \qquad (2.30)$$

For a sample of infinite thickness, Eq. (2.30) simplifies,

$$G_1(\tau) = \frac{e^{-(z_0/\ell^*)\sqrt{6\tau/\tau_0}}}{1+\frac{2}{3}\sqrt{\frac{6\tau}{\tau_0}}} \qquad (2.31)$$

We note that the initial condition of a source at z_0 appears explicitly in the solution, reflecting the importance of the contribution of the short paths. In fact, we expect there to be a distribution in the position of the apparent source, z_0. Thus we must integrate Eq. (2.31) over a distribution of sources, $f(z_0)$. While the exact form of $f(z_0)$ is unknown, we do know that $f(z_0)$ goes to zero as $z_0 << \ell^*$ and for $z_0 >> \ell^*$. Furthermore, we expect $f(z_0)$ to be peaked near $z_0 \sim \ell^*$. Thus, to leading order in $\sqrt{\tau/\tau_0}$, $g_1(\tau)$ is given by Eq. (2.31), with z_0/ℓ^* replaced by $\langle z_0\rangle/\ell^*$, the average over the source distribution $f(z_0)$. The first order correction is $[\langle z_0^2\rangle/\langle z_0\rangle^2 - 1]\tau/\tau_0$ which is small for a narrow distribution $f(z_0)$. Physically, we can think of $\langle z_0\rangle$ as the average position of the source of diffusing intensity, and we expect that the exact form of the distribution $f(z_0)$, and therefore $\langle z_0\rangle$, will depend on the anisotropy of the scattering as reflected by ℓ^*/ℓ.

In contrast to transmission, in backscattering there is no well-defined characteristic path length set by the sample thickness. In fact, since paths of all lengths contribute in

backscattering, the autocorrelation function consists of contributions from all orders of multiple scattering. As a consequence, there is a much broader distribution of time scales in the decay. The longer paths consist of a larger number of scattering events and thus decay more rapidly, probing the motion of individual particles over shorter length and time scales. By contrast, the shorter paths consist of a smaller number of scattering events thus decaying more slowly and probing the motion of individual particles over longer length and time scales. This feature is particularly advantageous for exploring the dynamics of interacting systems, which can have a broad distribution of relaxation rates associated with motion over different lengths scales.

An autocorrelation function measured in backscattering is shown in Fig. 2.5. The sample consisted of an aqueous suspension of 0.412-μm-diam. polystyrene latex spheres at a volume fraction of ϕ=0.05 in a 5 mm thick cuvette. It was illuminated by a uniform beam, 1 cm in diameter; light from a 50 μm diameter spot near the center of the illuminated area was imaged onto the detector. The scattering angle was ~175°, although we found virtually no dependence of the results on scattering angle when it was varied 20° from that used here, as expected for diffusing light. After subtracting the baseline, the logarithm of the autocorrelation function, normalized by the baseline is plotted as a function of time, in Fig. 5a. The large amount of curvature exhibited by the data reflects the contributions of paths with a wide range of length scales, leading to a wide range of decay times. As suggested by the expression for $G_1(\tau)$ for DWS in backscattering, we replot the data in Fig. 5b as a function of the square root of time, in units of τ_0. We use τ_0=3.01 msec, as measured experimentally in the single scattering limit, and consistent with the value calculated from the Stokes-Einstein relation. The solid line is a fit to the functional form given by Eq. (2.31), and is in reasonably good agreement with the data. However, to within the precision of experiment, the data shown in Fig. 5 is linear over

nearly three decades of decay when plotted logarithmically as a function of the square root of time. This suggests that the data can be more simply described using

$$G_1(\tau) = e^{-\gamma\sqrt{6\tau/\tau_0}} \qquad (2.32)$$

where $\gamma=\langle z_0\rangle/\ell^*+2/3$. This result was obtained previously using the simpler, but less rigorous, boundary condition, $U(z=0)=0$.[10]

The behavior of the autocorrelation function shown in Fig. 2.5 is in fact quite general. For particles with diameters comparable to or greater than λ where $\ell^*/\ell >> 1$, the simple exponential form given in Eq. (2.32) is always observed. For small particles where $\ell^*/\ell \sim 1$, there is some curvature for data plotted logarithmically *vs* square root of time. The data curves upward or downward, depending on whether polarized or depolarized light is detected. However, the theory we develop, expressed in Eq. (2.31), always exhibits a subtle upward curvature when plotted logarithmically *vs* square root of time. MacKintosh and John have obtained similar results using diagrammatic techniques. Therefore, since the curvature is generally small and may be either up or down, it is most convenient to use the very simple form in Eq. (2.32) to describe the shape of the autocorrelation function. The slope of the autocorrelation function, when plotted in this fashion, is determined solely by τ_0 and by γ. While we have derived this functional form using rather heuristic arguments, similar results are also obtained using more rigorous diagrammatic techniques[8]. However, it is again essential to properly account for the contributions of the short paths. This can be done by ensuring that the difference between initial and final wavevectors is strictly $2k_0$, as required for backscattering, and by limiting the momentum transfer in any single scattering event to properly reflect the form factor of the scatterers. By contrast, if this is not done, the contributions of the short paths are over estimated in the diagrammatic approach, leading to a prediction[13] for the autocorrelation function that describes the initial decay

reasonably well, but fails at longer times by predicting a power-law decay, in sharp disagreement with the data.

[1] A. Ishimaru, *Wave Propagation and Scattering in Random Media* (Academic, New York, 1978).

[2]M.P. van Albada, B.A. van Tiggelen, A. Lagendijk, and A. Tip,Phys. Rev. Lett. **66**, 3132 (1991).

[3] A. Ishimaru, *Wave Propagation and Scattering in Random Media, vol. I* (Academic, New York) 1978.

[4] M.P. van Albada and A. Legendijk, Phys. Rev. Lett. **55**, 2692, (1985).

[5] P.E. Wolf and G. Maret, Phys. Rev. Lett. **55**, 2696 (1985).

[6] A.F. Ioffe and A.R. Regel, *Prog. Semicond.* **4**, 237, (1960)

[7] A.A. Golubentsev, Zh. Eksp. Teor. Fiz. **86**, 47 (1984) [Sov. Phys. JETP **59**, 26 (1984)].

[8] F. MacKintosh and S. John, Phys. Rev. B **40**, 2383 (1989).

[9] G. Maret and P.E. Wolf, Z. Phys. B **65**, 409 (1987).

[10] D.J. Pine, D.A. Weitz, P.M. Chaikin, and E. Herbolzheimer, Phys. Rev. Lett. **60**, 1134 (1988).

[11] P.E. Wolf, G. Maret, E. Akkermans and R. Maynard, J. Phys. (France) **49**, 63 (1988).

[12] H.S. Carslaw and J.C. Jaeger, *Conduction of Heat in Solids* (Clarendon, Oxford) 1959.

[13] St88. M.J. Stephen, Phys. Rev. B **37**, 1 (1988).

[14] M. Rosenbluh, M. Hoshen, I. Freund, and M. Kaveh, Phys. Rev. Lett. **58**, 2754 (1987).

Chapter III

INTERNAL REFLECTION OF DIFFUSIVE LIGHT IN RANDOM MEDIA

Abstract

The consequences of internal reflection of multiply scattered light at the boundaries of disordered media are studied. We show that the effect of internal reflection due to index mismatch can be quantitatively accounted for with a single parameter by incorporating a reflection coefficient into the boundary condition for the diffusive light. We measure the angular correlation functions in transmission and reflection at different thicknesses for both high and low index mismatch. By including the effect of internal reflection, we are able to obtain consistent quantitative agreement between experiment and theory. Extensions to other experiments including diffusing-wave spectroscopy, coherent backscattering, frequency correlations, and pulse propagation are discussed.

3.1. INTRODUCTION

The problem of the propagation of light in optically dense random media represents a significant challenge that has attracted considerable attention in recent years[1,2]. One approach that has met with considerable success is the photon diffusion approximation. This approximation is valid provided the scattering is not too strong, so that $k\ell >> 1$, where ℓ is the scattering mean free path and $k=2\pi n/\lambda$, with λ the wavelength of the light and n the average index of refraction of the medium. In addition, the diffusion approximation applies only for distances greater than the transport mean free path, ℓ^*, the length scale over which the direction of light is randomized by scattering. When these conditions are satisfied, diverse phenomena, such as the spatial and temporal fluctuations of multiply scattered light, pulse propagation, and coherent backscattering, can be understood within this simple, yet powerful framework. While good agreement between experiment and theory is generally achieved, many measurements exhibit systematic deviations from the quantitative predictions of the theory. Recently Lagendijk *et al.*[3] suggested that the source of these discrepancies may be a failure to properly account for the reflection of light at the boundaries of the random medium. Indeed, by incorporating the effects of internal reflection into the diffusion propagator, they found that internal reflection can lead to significant corrections in the apparent photon diffusion coefficient for pulse propagation through a slab of an optically dense medium. Subsequently, Freund *et al.*[4] demonstrated that reducing reflections at the sample interface leads to a substantial improvement between experiment and theory for measurements of angular intensity autocorrelation functions. More recently, they used Green's function methods\cite[5] to show that internal reflection could account for the discrepancies between their earlier reported data and theoretical predictions. Pine *et al.* have also noted that measurements of the temporal correlations of multiple scattered light leads to

systematically low estimates of the transport mean free path and have suggested that this may be due to not properly accounting for reflection of light at the sample interface.[6,7]

In this chapter, we show that the effects of internal reflection at the boundaries due to index mismatch can be accounted for quantitatively with a single parameter by incorporating a reflection coefficient into the boundary conditions for the diffusion equation for light. We discuss measurements of the decay of the angular correlations in the intensity of multiply scattered light when an optically dense sample is rotated with respect to the incident laser beam. These correlations were first considered by Feng *et al.*[8] using diagrammatic techniques. Here, we present an alternate theoretical derivation of the correlations using the diffusion equation for light. In addition to being more physically transparent, this approach allows us to incorporate a more realistic treatment of the boundary conditions. By properly accounting for the internal reflection of light in the boundary conditions, we are able to obtain consistent quantitative agreement between experiment and theory for different sample thicknesses and for different index mismatch. An important additional feature of the theory we develop is that it enables us to quantitatively predict value of the reflection coefficient. Exploiting transmission measurements for samples of different thickness, we are able to accurately determine both the internal reflection parameter and the absorption length in the sample. These same parameters can then be used to interpret the angular correlations of backscattered light. In contrast to the transmission measurements, the correlations of the backscattered light are also very sensitive to the nature of the initial conditions which describe the conversion of the incoming plane wave to diffusing light. Here, we obtain good agreement with data by using the rather crude approximation that this conversion occurs at a fixed distance into the sample. An estimate of this distance is obtained from the backscattering results.

The angular correlation of the scattered light upon sample rotation is the simplest of the correlations between incoming and outgoing light described by Feng *et al.*[8] These correlations do not depend on any phase interference within the sample, but merely reflect the fact that the light propagation is diffusive. As we will show, it is the very simple dependence of the angular correlations on the diffusive propagation that enables us to quantitatively determine the consequences of internal reflection on the boundary conditions. Once these consequences are determined, the new boundary conditions can be used to properly interpret other experiments.

Physically, the consequences of internal reflections can be understood by considering their effect on the distribution of photon path lengths through the sample. The internal reflection due to the mismatch of the index of refraction at the boundary of the random media causes photons to remain inside the medium for a longer time, and thus, increases the photon path lengths by an amount determined by the index mismatch. In all backscattering experiments, and in transmission experiments through *thin* samples where path lengths are comparable to ℓ^*, the increase in path length due to internal reflection is generally a significant fraction of the total path length. By contrast, in transmission experiments through *thick* samples, where all paths are long, the increase in path length due to internal reflections is only a small fraction of total path length. Thus, the effect of internal reflection is significant for backscattering experiments and transmission experiments through thin samples, and relatively less significant for transmission experiments through very thick samples.

3.2.THEORY

3.2.A. Angular autocorrelation functions

We consider a plane wave which is incident on one side of a slab of random static scatterers. Transmitted or backscattered photons emerge from the sample at a point on the boundary and are detected. The light transport within the sample is assumed to be diffusive and is described by the diffusion equation

$$\frac{\partial}{\partial t}U(\mathbf{r},t)=D\nabla^2U(\mathbf{r},t) \tag{3.1}$$

where U is the density of photons, $D=v\ell^*/3$ is the diffusion coefficient of light, v the speed of the light inside the sample, and $f(t,x,y,z)$ the source of diffusing light. The path of each diffusing photon is determined by random multiple scattering from a sequence of scatterers. The multiply scattered electrical field, E, emerging from the sample is made up of the contributions of fields following many different scattering paths

$$E=\sum_{p}E_p \tag{3.2}$$

where p denotes a scattering path. The scattering intensity is given by

$$I=\sum_{pp'}E_pE_{p'}^* \tag{3.3}$$

Rotating the sample changes the relative phase of the field between paths and, as a result, the scattered intensity fluctuates. The ensemble-averaged intensity is given by

$$\langle I\rangle=\sum_{p,p'}\langle E_pE_{p'}^*\rangle=\sum_{p}\langle E_pE_p^*\rangle \tag{3.4}$$

The second equality follows from our assumption that the positions of scatterers are randomly distributed and that the relative phases of fields from different paths are uncorrelated and therefore average to zero; the only non-vanishing terms in $\langle E_p E_{p'}^* \rangle$ are those with $p=p'$, where the random phases of fields are canceled by their conjugates. We measure the intensity correlation of backscattered or transmitted light as the sample is rotated along an axis normal to the direction of the incident light. The autocorrelation function is defined as

$$G_2(\theta) \equiv \langle I(0)I(\theta)\rangle = \sum_{p,p',p'',p'''} \langle E_p(0)E_{p'}^*(0)E_{p''}(\theta)E_{p'''}^*(\theta)\rangle \qquad (3.5)$$

where θ is the angle rotated and $I(\theta)$ the intensity of the light. Once again, because the relative phases of fields are random, the leading non-zero terms are those with $p=p'$ and $p''=p'''$ or $p=p'''$ and $p'=p''$. Then Eq. (3.5) factorizes:

$$\begin{aligned} G_2(\theta) \equiv \langle I(0)I(\theta)\rangle = & \sum_{p,p',p'',p'''} \langle E_p(0)E_{p'}^*(0)\rangle \delta_{p,p'} \langle E_{p''}(\theta)E_{p'''}^*(\theta)\rangle \delta_{p'',p'''} \\ & + \sum_{p,p',p'',p'''} \langle E_p(0)E_{p'''}^*(\theta)\rangle \delta_{p,p'} \langle E_{p''}(\theta)E_{p'}^*(0)\rangle \delta_{p',p''} \\ & = \langle I\rangle^2 + \left| \sum_p \langle E_p(0)E_p^*(\theta)\rangle \right|^2 \end{aligned} \qquad (3.6)$$

For later use, we define

$$g_2(\theta) \equiv \frac{G_2(\theta)}{\langle I\rangle^2} - 1 \qquad (3.7)$$

and

$$g_1(\theta) \equiv \frac{\sum_p \langle E_p(0) E_p^*(\theta) \rangle}{\langle I \rangle} \qquad (3.8)$$

From Eq. (3.6), we see that $g_2(\theta)$ and $g_1(\theta)$ are related:

$$g_2(\theta) = |g_1(\theta)|^2 \qquad (3.9)$$

This equation, known as the Siegert relation, allows us to obtain intensity correlation functions from calculations of the field correlation functions. Thus, in subsequent sections we always calculate the field correlation functions and use Eq. (3.9) to obtain intensity correlation functions for comparison with our experiments.

To calculate these autocorrelation functions we first determine the contribution of a single diffusive light path due to the rotation of the sample. This corresponds to calculating the argument of the summation in Eq. (3.8). Then the contributions of all paths, weighted by the distribution of the paths, are summed to obtain the desired correlation function. The photon path distributions for transmission and backscattering geometries can be determined by solving the diffusion equation *provided one uses boundary conditions which properly account for the behavior of the light at the sample interfaces*. In the following section, we discuss the behavior of light near interfaces and develop boundary conditions which account for the effect of internal reflection at the sample interfaces. We then use these results to obtain explicit expressions for the angular correlation functions of multiply scattered light. These results are compared with experiments and then generalized to several other types of measurements involving strong multiple scattering. We show that the simple angular correlation measurements allow the determination of the parameters that characterize the effects of internal reflection. These parameters can then be used directly to account for the effects of internal reflection in other measurements.

3.2.B. Internal reflections and boundary conditions

A variety of boundary conditions have been used to describe the behavior of diffusing light at a sample interface. The simplest approach is to use perfectly absorbing boundary conditions, U=0. Feng *et al.*[8] have used these boundary conditions within a diagrammatic expansion to obtain an expression for the angular correlation function for transmission through a slab of thickness L. They obtain

$$g_1(\theta) = \frac{k_0 \theta L}{\sinh(k_0 \theta L)} \tag{3.10}$$

where $k=2\pi/\lambda$. However, perfectly absorbing boundary conditions are known to be inconsistent with the exact Milne solution for scattering from uncorrelated point particles[1]. Furthermore, because perfectly absorbing boundary conditions cannot internal reflection of light at the interfaces, Eq. (3.10) fails to quantitatively describe the experimental results.[4] Thus, more accurate boundary conditions are required.

To obtain more realistic boundary conditions, we consider the flux of diffusing photons scattered through an arbitrary small area, dS, *inside the sample.* For simplicity, we will assume that the sample is made up of isotropic scatterers and that absorption can be neglected (these assumptions will be relaxed later). Without loss of generality, we let dS be at the origin and perpendicular to z axis, as shown in Fig. 3.1. The flux of photons scattered directly from the volume element dV through dS is given by the product of the number of photons in dV, $U(r,\theta,\varphi)dV$, the fractional solid angle, $\cos\theta\ dS/r^2$, the speed of light, v, and the loss due to the scattering between dV and dS, $\exp(-r/\ell)$.

$$U(r,\theta,\varphi)dV v \frac{\cos\theta\ dS}{r^2} e^{-r/\ell} \tag{3.11}$$

Replacing dV by $r^2\sin\theta\ dr d\theta d\varphi$, this can be rewritten as

$$\frac{dS}{4\pi}U(r,\theta,\varphi)v\cos\theta\,\sin\theta e^{-r/\ell}\,dr d\theta d\varphi; \qquad (3.12)$$

The total flux of photons scattered into the area dS per unit time in the negative z direction is obtained by integrating over the number coming from the entire half-space $z>0$. Denoting the photon flux in the $-z$ direction as J_-, we have

$$J_- dS=\frac{dS}{4\pi}v\int_0^{\pi/2}d\theta\int_0^{2\pi}d\varphi\int_0^{\infty}dr U(r,\theta,\varphi)\cos\theta\,\sin\theta\,e^{-r/\ell} \qquad (3.13)$$

To evaluate this integral, we expand $U(r,\theta,\varphi)$ about the origin. Since the primary contribution to the photon flux through dS is from the neighborhood of a few mean free paths away, we can restrict the expansion to first order terms in a Taylor expansion,

$$U(r,\theta,\varphi)=U_0+x\left[\frac{\partial U}{\partial x}\right]_0+y\left[\frac{\partial U}{\partial y}\right]_0+z\left[\frac{\partial U}{\partial z}\right]_0; \qquad (3.14)$$

where the derivatives are to be evaluated at the origin. The independent variables x, y, and z may be expressed in terms of spherical coordinates by

$$\begin{aligned} x&=r\sin\theta\cos\varphi\,,\\ y&=r\sin\theta\sin\varphi\,, \qquad (3.15)\\ z&=r\cos\theta\,; \end{aligned}$$

Since the integration over φ in Eq. (3.13) is between the limits of zero and 2π, the terms containing x and y will make no net contribution. Thus, replacing z by $r\cos\theta$ and integrating over r and φ, we obtain

$$\begin{aligned} J_- &= \frac{v}{4\pi}\int_0^{\pi/2}d\theta\int_0^{2\pi}d\varphi\int_0^{\infty}dr\left[U+\frac{\partial U}{\partial z}\cos\theta\right]\cos\theta\,\sin\theta\,e^{-r/\ell}\\ &= \frac{Uv}{4}+\frac{D}{2}\left[\frac{\partial U}{\partial z}\right] \qquad (3.16) \end{aligned}$$

where $D=v\ell/3$ is the diffusion coefficient of light and, for convenience, we neglect the subscript zero. Similarly the photon flux through dS in z direction, J_+, may be obtained by integrating the contributions from $z<0$:

$$J_+ = \frac{v}{4\pi}\int_{-\pi/2}^{0} d\theta \int_0^{2\pi} d\varphi \int_0^{\infty} dr \left[U - \frac{\partial U}{\partial z}\cos\theta\right] \cos\theta \sin\theta\, e^{-r/\ell}$$

$$= \frac{Uv}{4} - \frac{D}{2}\left[\frac{\partial U}{\partial z}\right] \qquad (3.17)$$

Equations (3.16) and (3.17) can be generalized to treat the anisotropic scatterers typically used in experiments. Here the single particle scattering is peaked in the forward direction so that the effective random walk step size is the transport mean free path ℓ^*, where ℓ^* is defined by the relation, $\ell/\ell^* = \langle 1 - \cos\theta \rangle$. It can be shown[9] that Eqs. (3.16) and (3.17) are satisfactory for anisotropic systems, provided that ℓ^* replaces ℓ in the definition of the diffusion coefficient, *i.e.*, $D=v\ell^*/3$.

Now we consider the photon flux at the boundaries at $z=0$ and L. If there is no internal reflection, there will be no photon flux from outside the sample, that is, $J_+ =0$ at $z=0$ and $J_-=0$ at $z=L$. This gives the mixed boundary conditions,

$$U - \frac{2\ell^*}{3}\frac{\partial U}{\partial z} = 0 \qquad \text{at } z=0 \qquad (3.18)$$

$$U + \frac{2\ell^*}{3}\frac{\partial U}{\partial z} = 0 \qquad \text{at } z=L; \qquad (3.19)$$

By contrast, if there is internal reflection, there will be some incoming flux due to the reflection at the boundaries. The simplest treatment is to define a reflection coefficient R which is the ratio of the incoming flux to the outgoing flux at the boundaries. Thus, the boundary conditions are $J_+ = RJ_-$ for $z=0$, and $J_- = RJ_+$ for $z=L$. This gives

$$U - \frac{2C}{3}\frac{\partial U}{\partial z} = 0 \qquad \text{at } z=0 \qquad (3.20)$$

$$U + \frac{2C}{3}\frac{\partial U}{\partial z} = 0 \qquad \text{at } z=L; \qquad (3.21)$$

where

$$C \equiv \frac{2\ell^*}{3}\frac{1+R}{1-R} \qquad (3.22)$$

When R=0, we recover the mixed boundary conditions for no reflections. If we assume $\partial U/\partial z$ is constant inside the sample near the boundaries, Eqs. (3.20) and (3.21) are essentially equivalent to extrapolating U to 0 at a distance C outside of the boundaries. In the limit that R=0, C=2ℓ^*/3 which is very near the frequently used extrapolation length of 0.7104 ℓ^* given by the Milne solution.[1] However, in the presence of reflections, this extrapolation length can be significantly larger.

3.2.C. Calculation of angular correlation functions

For convenience, we assume that the incident light is at near normal incidence on a slab of thickness, L, and that the wavevector of the detected light is approximately parallel to the incident light. As shown in Fig. 3.2, we define a coordinate system with an origin on one side of the sample where the light is incident at z=0 from the -z direction. The sample is rotated about the x axis. A typical diffusing light path through the sample is also shown in Fig. 3.2. A photon incident on the slab at a position $\mathbf{r}_i = (x_i, y_i, 0)$ follows a path of total length s through the sample and emerges at a position $\mathbf{r}_t = (x_t, y_t, L)$. We calculate the phase shift of photons traversing this same path after the sample rotates through a small angle θ. The phase shift arises from the change in the *total* length of this path. However, since the scatterers are stationary, the path length *within* the sample is unchanged upon rotation, and all the phase shift arises from the

change in path length *outside* the sample. As shown in Fig. 3.2, there are two contributions to the change in path length, one from each side of the sample. The path length of the incident light is decreased by $y_i\theta$ while that of the emerging light is decreased by $y_t\theta$. Defining a scattering wavevector $q=k_0\theta$, the total phase difference of the path on rotation is $\Delta\phi_T = \Delta\phi_i + \Delta\phi_t = q\,(y_t - y_i) + O(\theta^2)$. Thus, if the electric field at $\mathbf{r}_t$ is initially $E(0)$, then after the sample is rotated through an angle θ, the electric field will be

$$E(\theta)=E(0)e^{iq(y_t-y_i)}; \tag{3.23}$$

Photons incident at $\mathbf{r}_i$ can travel many different paths within the sample before emerging at $\mathbf{r}_t$. We denote by $p(s,\mathbf{r}_i,\mathbf{r}_t)$ the probability that, in the absence of absorption, a photon follows a path of length s whose end points are at $\mathbf{r}_i$ and $\mathbf{r}_t$. Since the light emerging at any single point from the sample is made up of contributions of different paths beginning anywhere on the incident face of the slab, we can calculate the angular correlation function of the electric field by summing over all paths and all incident points:

$$g_1(q) \equiv \frac{\langle E(0)E^*(\theta)\rangle}{\langle E(0)E^*(0)\rangle} \tag{3.24}$$

$$\cong \int ds\, dx_i\, dy_i\, p(s, \mathbf{r}_i, \mathbf{r}_t)\, e^{iq(y_t - y_i)}\, e^{-s/\ell_a}, \tag{3.25}$$

where we have also accounted for the possibility of absorption by including an exponential cutoff with an absorption length ℓ_a. Similarly, we can calculate the phase shift for a backscattered photon following the path shown in Fig. 3.2 and emerging at a positition on the incident face, $\mathbf{r}_t = (x_t, y_t, L)$. For this case, we obtain $\Delta\phi_B = \Delta\phi_b + \Delta\phi_i$ $= q\,(y_b + y_i) + O(\theta^3)$. The angular autocorrelation function of backscattered fields is then given by:

$$g_1(q) \cong \int ds\, dx_i\, dy_i\, p(s, \mathbf{r}_i, \mathbf{r}_b)\, e^{iq(y_b + y_i)}\, e^{-s/\ell a} \tag{3.26}$$

In addition to collecting light from a single point on the outgoing surface as discussed above, it is also instructive to consider collecting the light from the whole outgoing plane. This entails an additional integration over the outgoing surface to calculate the correlation function. However, the results can be seen immediately from symmetry arguments. For transmission, the phase shift depends only on the difference, y_t-y_i, and thus $g_1(q)$ is translationally invariant on the outgoing plane. Thus, summing over the whole plane yields the same result as for a point. By contrast, for backscattering the phase shift depends on the sum y_b+y_i. Thus, $g_1(q)$ is not translationally invariant on the outgoing plane. In this case summing over the plane results in no correlations at all.

To obtain explicit expressions for $g_1(q)$ from Eqs. (3.25) and (3.26), we must determine $p(s, \mathbf{r}_i, \mathbf{r}_b)$ for each scattering geometry. To this end, we consider an instantaneous pulse of light which begins to diffuse a distance z_0 inside the slab at t=0, so that the initial conditions for the diffusion equation are

$$f(t,x,y,z)=\Delta(t)\Delta(x-x_i)\Delta(y-y_i)\Delta(z-z_0), \qquad (3.27)$$

where we expect $z_0 \cong \ell^*$. Photons emerging at $\mathbf{r}_t$ at time t have all traveled a distance $s=vt$. The average number (or flux) of photons emerging from the sample at r_t at time t will be proportional to the probability that a photon travels a distance s from $\mathbf{r}_i$ to $\mathbf{r}_t$, that is, $p(s, \mathbf{r}_i, \mathbf{r}_t)$. The photon flux can be determined within the diffusion approximation by solving the diffusion equation, Eq. (3.1), for U, subject to the appropriate boundary conditions for U at z=0 and L, and then calculating the outward flux at the boundaries using Eqs. (3.16) or (3.17). The solution of Eq. (1) can be simplified by separating U into three parts,

$$U(x,y,z,t)=X(x,t)Y(y,t)Z(z,t) \qquad (3.28)$$

where

$$X(x,t) = \frac{1}{\sqrt{4\pi Dt}} \exp\left[-\frac{(x-x_i)^2}{4Dt}\right]$$

and

$$Y(y,t) = \frac{1}{\sqrt{4\pi Dt}} \exp\left[-\frac{(y-y_i)^2}{4Dt}\right]$$

are the solutions to the one dimensional diffusion equations $\partial X/\partial t - D\nabla^2 X = \delta(x-x_i)\delta(t)$ and $\partial Y/\partial t - D\nabla^2 Y = \delta(y-y_i)\delta(t)$ in an infinite medium, and $Z(z,t)$ is the solution to the equation

$$\partial Z/\partial t - D\nabla^2 Z = \delta(z-z_0)\delta(t) \qquad (3.29)$$

subject to the boundary conditions,

$$Z - \frac{2C}{3}\frac{\partial U}{\partial z} = 0 \qquad \text{at } z=0 \qquad (3.30)$$

$$Z + \frac{2C}{3}\frac{\partial U}{\partial z} = 0 \qquad \text{at } z=L; \qquad (3.31)$$

The transmitted flux from the sample at $\mathbf{r}_t$ is

$$J_+ = \frac{Uv}{4} - \frac{D}{2}\frac{\partial U}{\partial z}$$

$$= \frac{Uv}{2(1+R)} = \frac{v\,XYZ}{2(1+R)} \qquad \text{at } z=L, \qquad (3.32)$$

where the second equality follows from the boundary condition at $z=L$, Eq. (3.21). Similarly, the backscattered flux from the sample at $\mathbf{r}_b$ is

$$J_- = \frac{Uv}{4} + \frac{D}{2}\frac{\partial U}{\partial z}$$

$$= \frac{Uv}{2(1+R)} = \frac{v\,XYZ}{2(1+R)} \qquad \text{at } z=0, \qquad (3.33)$$

Equations (3.32) and (3.33) are directly proportional to $p(s, \mathbf{r}_i, \mathbf{r}_t)$ and $p(s, \mathbf{r}_i, \mathbf{r}_b)$, respectively, when the time dependence, t, in XYZ is replaced by s/v. Substituting these expressions for $p(s, \mathbf{r}_i, \mathbf{r}_t)$ and $p(s, \mathbf{r}_i, \mathbf{r}_b)$ into Eqs. (3.25) and (3.26), and then integrating over x_i and y_i, we obtain

$$g_1(q) \propto \int_0^\infty P(s) e^{-(q^2 + \alpha^2)\ell^* s/3} ds$$

where $\alpha^2 \equiv 3/\ell\hat{}^*\ell_a$ and $P(s) \propto Z(z,t)|_{z=L}$ for transmission and $P(s) \propto Z(z,t)|_{z=0}$ for backscattering where, once again, we use the transformation $t=s/v$. That is, $P(s)$ is proportional to the solution of the one-dimensional diffusion equation, Eq. (3.29), and thus, is the probability of a photon having a path length, s, regardless of its end points. From Eq. (3.34), we see that paths with large s decay more rapidly than paths with small s. Physically, this is because paths with large s have, on average, a larger transverse separation, y_t-y_i or y_b-y_i, of their end points. This larger separation results in a larger change in phase when the sample is rotated, as can be seen from the expression for θ-dependence for the electric field, Eq. (3.23). We note here, and we will discuss in more detail later that Eq. (3.34) has, apart from a simple transformation of variables, the same form as the expressions for the coherent backscattering cone and the temporal autocorrelation function. This is due to the fact that all these effects depend on changes in the phase of the multiply scattered light which scale linearly with the path length, s.

The calculation of $g_1(q)$ can be further simplified by noting that Eq. (3.34) is the Laplace transform of $P(s)$. Thus, instead of solving the diffusion equation to obtain $P(s)$, we can solve the Laplace transform of the one-dimensional diffusion equation, Eq. (1), and obtain $g_1(q)$ directly. The solution of the diffusion equation using the Laplace transform is given in Carslaw and Jaeger for this slab geometry.[10] They obtain

$$\bar{Z} = \int_0^\infty Z(z,t)e^{-pt}\,dt$$

$$= \frac{1}{2D\eta^2}e^{-\eta|z-z_0|} + A\sinh(\eta z) + B\cosh(\eta z) \qquad (3.35)$$

where $\eta = \sqrt{p/D}$ and the coefficients A and B are chosen so that the boundary conditions, the Laplace tranformations of Eqs. (3.30) and (3.31), are satisfied at z=0 and L, respectively. After and tedious, but straightforward algebra, we obtain,

$$\bar{Z} = \frac{\sinh[(L-z+z_0)\eta] + Cp\cosh[(L-z+z_0)\eta]}{(1+C^2\eta^2)\sinh(L\eta) + 2C\eta\cosh(L\eta)} \qquad (3.36)$$

Comparing Eqs. (3.34) and (3.35), we see that $\bar{Z}$ is equivalent to $g_1(q)$ if one makes the transformation of variables, $s \rightarrow t/c$ and $p=D\eta^2 \rightarrow (q^2+\alpha^2)v\ell^*/3$. The second transformation is equivalent to $\eta \rightarrow \sqrt{q^2+\alpha^2}$. Thus, in transmission, where $z=L$, we obtain

$$g_1(q) = \frac{(L+2C)/(z_0+C)[\sinh(z_0\sqrt{q^2+\alpha^2}) + C\sqrt{q^2+\alpha^2}\cosh(z_0\sqrt{q^2+\alpha^2})]}{[1+C^2(q^2+\alpha^2)]\sinh(L\sqrt{q^2+\alpha^2}) + 2C\sqrt{q^2+\alpha^2}\cosh(L\sqrt{q^2+\alpha^2})} \qquad (3.37)$$

For $z_0/L \ll 1$, $g_1(q)$ is insensitive to the exact value of z_0. Physically, this means that for light transmission through thick samples, the exact depth into the sample at which the light begins to diffuse is unimportant. For perfectly absorbing boundary conditions (C=0), Eq. (3.37) reduces to Eq. (3.10), $g_1(q)$=qL/\sinh(qL), derived by Feng *et al.*, provided there is no absorption (α =0) and the sample is very thick ($z_0/L \ll 1$).

For $C/L \ll 1$, Eq. (3.37) is equivalent to the results of Feng *et al.*, but for a sample with an effective thickness of L+2 C rather than L. Thus, the effect of reflections is to increase the apparent thickness of the sample. To see this, we consider a sample with an effective thickness of L+2 C. We use the simple boundary conditions, U=0 at z=- C and z=L+ C, and evaluate $g_1(q)$ at z=L. We obtain

$$g_1(q) \propto \frac{\sinh[(z+2\,C)\sqrt{q^2+\alpha^2}]+\sinh(z_0\sqrt{q^2+\alpha^2})}{\sinh[(L+2\,C)\sqrt{q^2+\alpha^2}]} \qquad (3.38)$$

In the case of $C/L \ll 1$, we can make the approximations $\sinh(2\,Cq) \cong 2\,Cq$ and $\cosh(2Cq) \cong 1+2\,C^2q^2$, to obtain

$$g_1(q) \propto \frac{[1+C^2(q^2+\alpha^2)]\sinh(z_0\sqrt{q^2+\alpha^2}) + C\sqrt{q^2+\alpha^2}\cosh(z_0\sqrt{q^2+\alpha^2})}{[1+2\,C^2(q^2+\alpha^2)]\sinh(L\sqrt{q^2+\alpha^2})+2\,C\sqrt{q^2+\alpha^2}\cosh(L\sqrt{q^2+\alpha^2})} \qquad (3.39)$$

Equations (3.37) and (3.39) are identical if we neglect terms with C^2. This calculation also suggests that the effects of internal reflection become less important for thick samples.

In contrast to transmission, the diffusion equation does not fully describe backscattered light because it consists of a significant contribution of paths of length comparable to the transport mean free path. However, Pine *et al.*[11] have shown that the diffusion equation can provide a surprisingly accurate description of temporal correlation functions of backscattered light with the boundary condition $U=0$ provided that the incident light is artificially assumed to start diffusing at a fixed distance $\gamma\,\ell^*$ inside the sample. The parameter γ then appears in their expression for the correlation function as the initial slope of the decay. Caution must be exercised in assigning a physical meaning to γ since it is observed to depend on the polarization of the incident and detected light and on the ratio of the transport and scattering mean free paths.[12] Here we show that the initial slope is also a function of the internal reflection.

To obtain an expression for the angular correlation in backscattering we let $z=0$ in Eq. (3.36) and obtain

$$g_1(q) \propto \frac{\sinh[(L-z_0)\sqrt{q^2+\alpha^2}] + C\sqrt{q^2+\alpha^2}\cosh[(L-z_0)\sqrt{q^2+\alpha^2}]}{[1+C^2(q^2+\alpha^2)]\sinh(L\sqrt{q^2+\alpha^2})+2\,C\sqrt{q^2+\alpha^2}\cosh(L\sqrt{q^2+\alpha^2})} \qquad (3.40)$$

For thick samples, where $L/z_0 >> 1$ and $L/C >> 1$, Eq. (3.40) becomes

$$g_1(q) \propto \frac{\exp(-z_0\sqrt{q^2+\alpha^2})}{1+C\sqrt{q^2+\alpha^2}} \qquad (3.41)$$

In the case of weak absorption, $\alpha << q$, the initial decay of Eq. (3.41) can be approximated by

$$g_1(q) = 1 - (z_0 + C)\, q = 1 - (z_0 + C)\, k_0 \theta ,$$

Here, the initial slope, $dg_1/d\theta = [z_0/\ell^* + \frac{2(1+R)}{3(1-R)}]k_0\ell^*$ depends critically on the internal reflection.

Internal reflection increases the photon path lengths and causes $g_1(q)$ to decay more rapidly. By contrast, absorption cuts off long paths and causes $g_1(q)$ to decay more slowly. We can exploit this fact to experimentally determine both α and C by making measurements in transmission as a function of sample thickness. For a thin sample, where $\alpha L << 1$, $g_1(q)$ depends only on the sample thickness and the internal reflection, that is, on L and C. By contrast, for a thick sample, where $C/L << 1$, the effect of internal reflection becomes small and $g_1(q)$ only depends on the sample thickness and the absorption, that is, on L and α. Thus, by measuring $g_1(q)$ in transmission and backscattering for different thicknesses, we can determine C and α. These quantities can then be used to interpret other phenomena involving multiple light scattering, such as frequency correlation and pulse propagation. We will show that the theory is in good agreement with our experiments for samples with both large and small index mismatch, in both transmission and backscattering geometries, and for several different sample thicknesses.

3.3. EXPERIMENT

3.3.A. Samples and procedure

In our experiment we use two sets of samples, one of which has a higher average index of refraction than the other. The first set is made of sintered polydisperse alumina particles with a mean diameter of about 2.5 μm, and a volume fraction of 0.96. Three samples with thicknesses of 0.615 mm, 0.385 mm, and 0.256 mm were used. The second set is from commercial glass frits with pore sizes between 10 and 20 μm and with a volume fraction of glass of approximately 0.96. The index of refraction of solid alumina is 1.7 while that of glass is 1.5. Thus, we expect that the effect of internal reflection should be stronger for the higher index alumina samples than for the lower index glass frit sample.

The samples were mounted on a vertical translation stage and placed at the center of a rotation stage. We used the 488 nm line of an Ar^+ laser; the beam was expanded to a diameter of 1 cm, collimated and then directed towards the sample at near normal incidence. Two methods were used to collect the scattered light in transmission or backscattering. In the first method, we measured the scattered intensity at a single point near the center of the sample, which was aligned to be on the axis of rotation. This central spot was imaged one to one onto a 25-μm pin-hole with a 50 cm focal length lens. A 4.3-mm aperture was placed in front of the lens to determine the angular width of the detected light and to ensure that only a single speckle spot, and thus a single wavevector was detected. In the second method, we measured all the transmitted or backscattered light with the wavevector the same or opposite to that of the incident wavevector. This was accomplished by placing the detector pin-hole at the focal plane of the collection lens. To accumulate the autocorrelation function, the sample was rotated about the center of the incident beam. It was turned from 85° to 95° relative to the incident beam

at a constant angular speed of $\omega = 5 \times 10^{-2}$ degrees per second. The scattered intensity was detected with a photomultiplier tube using photon counting electronics. A digital correlator was used to measure the temporal intensity correlation function. The temporal intensity correlation function was converted to $g_2(q)$ using the relation $\theta = \omega t$. To ensure good ensemble averaging, we averaged several runs illuminating different areas of the samples.

From the correlator, we obtain normalized intensity correlation functions, $\langle I(0)I(q)\rangle / \langle I\rangle^2 = 1 + \beta\, g_2(\theta)$, where β is a constant of order unity which is determined by the number of speckle spots detected. Our detection area was about half a speckle spot, corresponding to $\beta \cong 0.8$.

3.3.B. Results

In Fig. 3.3, we plot the normalized angular intensity autocorrelation functions obtained from a 0.385-mm-thick alumina sample. Angular correlation functions obtained in the transmission geometry are shown in Fig. 3.3(a) for the two cases of planar and point collection optics. They are identical to within experimental uncertainty. This reflects the vertical (y-direction) translational invariance of the expression for the change in phase, Eq. (3.25), for each light path upon sample rotation. By contrast, angular correlation functions obtained in the backscattering geometry decay very differently for planar and point collection optics, as shown in Fig. 3.3. The dashed curve in Fig. 3.3(b), was obtained by collecting light over the entire outgoing plane, an area approximately 1 cm in diameter. The dashed curve decays much more rapidly than the solid curve, which was obtained by collecting light from a single point. In fact, the residual correlation in the dashed curve reflects only the finite size of the collection optics and the resultant finite speckle size. Thus, the absence of translational invariance over the collection plane in the backscattering geometry results in drastically different correlation functions, depending on whether planar or point collection optics are used while in transmission, the translational invariance ensures that the two collection schemes yield identical results. In the remainder of this paper we report only measurements obtained using point collection optics.

In Fig. 3.4, we show autocorrelation functions obtained in the transmission geometry for alumina samples of three different thicknesses. As expected, the autocorrelation functions decay more rapidly with increasing sample thickness. This reflects the fact that longer paths dephase the light more rapidly than do shorter paths. The solid lines are fits to the data using Eq. (3.37) with a single set of fitting parameters: C=0.212 mm and α=0.8 mm^{-1} for all three samples. The fact that a single set of parameters describe the

data for all three samples strongly supports the theory developed in section II. For comparison we also show, by the dashed line, the result of the theory for the thickest (L=0.615 mm) sample with C=0 and α =0, *i.e.*, without any internal reflection or absorption. The disagreement between these calculations and the measurements is apparent. It is important to note that increasing internal reflection tends to move the dashed curve towards the data and improve the agreement between theory and experiment while increasing absorption tends to move the dashed curve away from the data. Physically, this follows from the fact that internal reflection increases the effective length of the light paths through the sample while absorption tends to attenuate the contribution of the longer paths. Thus, it is the inclusion of reflection in the theory which provides the improved agreement with the data.

To better appreciate the relationship between $g_2(q)$ and L we plot the halfwidth, θ_h, of the measured autocorrelation functions as L is varied. The values for the alumina samples are shown Fig. 3.5(a). The lower solid line through the data is a fit to Eq. (3.37) and is in excellent agreement with experimental data. From the fit we obtain C=0.212± 0.001 mm and α =0.8± 0.1 mm^{-1}, in excellent agreement with the values obtained from the fit to the individual autocorrelation functions. The dashed line is calculated from Eq. (3.10), without the effect of internal reflection and absorption, and cannot account for the observed behavior. The internal reflection has the strongest effect for those samples with the highest index mismatch, particularly the thinnest samples. Since the thinnest samples have the shortest characteristic photon path lengths without internal reflection, the fractional increase in path length due to internal reflection is greatest in these samples. In Fig. 3.5(b), we plot θ_h for the glass frit samples and fit the data with Eq. (3.37) to obtain C=0.143± 0.001 mm and α =0.5± 0.1 mm^{-1}. Again, the agreement between theory and experiment is excellent. Furthermore, the effect of the internal reflection is considerably less for these samples since their index mismatch is less. In fact, for the thickest sample,

L=2.92 mm, the effect of the internal reflection is negligible. Nevertheless, over the full range of sample thicknesses used, inclusion of internal reflection in the theory provides substantially better agreement with the data than the theory with C=0, which is shown by the dashed curve in Fig. 3.5(b).

In order to determine the reflection coefficient, R, from our measurements of C, we must know ℓ^* for our samples. We can obtain a good estimate of ℓ^* by combining our measurements of $g_2(\theta)$ in transmission with measurements of $g_2(\theta)$ in backscattering. In backscattering, the angular correlation function depends not only on C and α, as in transmission, but on z_0 as well. Since α and C are determined from transmission experiments, the measurements of $g_2(\theta)$ in backscattering can be used to determine the remaining unknown parameter, z_0. In previous measurements of the temporal autocorrelation functions in multiply-scattering colloidal suspensions, and in measurements of the coherent backscattering cone, z_0 was found to be approximately equal to ℓ^* to within ± 30\%. Thus, once z_0 is known, we can exploit this empirical relationship to determine ℓ^*. In Fig. 3.6 we plot the measured angular autocorrelation functions of the polarized intensity in the backscattering geometry for (a) the alumina sample with L=0.615 mm and (b) the glass frit sample with L=2.92 mm. The solid lines are fits to Eq. (3.40) which give z_0=50~μm for both samples. By contrast, we show, by the dashed lines the calculation using Eq. (3.40) with C=0, α =0 and z_0=50~μm. These results decay much more slowly than the data. By using ℓ^* =50~μm for both samples, we obtain R=0.73 for the alumina sample and R=0.63 for the glass frit. These values are substantially higher than the reflection coefficient for normal incidence from air to glass which is 0.04. However, much of the multiply-scattered light inside the sample is incident on the boundary at very large angles resulting in total or near total internal reflection. Thus, the internal reflection coefficient multiply can be quite high even for moderate index mismatch.

3.3.C. Estimation of R from Fresnel's law

We can obtain an estimate of the reflection coefficient, R, using Fresnel's law. We assume that the direction and polarization of diffusing light incident on the boundary from inside the sample is completely random and that the sample surface is flat. For an angle of incidence, θ, the reflection coefficient, $R(\theta)$, averaged over polarization is

$$R(\theta) \equiv \frac{R_{\perp}(\theta)+R_{\parallel}(\theta)}{2}, \qquad (3.43)$$

where $R_{\perp}(\theta)$ and $R_{\parallel}(\theta)$ are the Fresnel reflection coefficients for incident light polarized perpendicular and parallel to the plane of incidence, respectively.[13] The reflected flux for a given angle of incidence at z=0 is $R(\theta)J(\theta)$, where $J(\theta)$ is the angle-dependent flux incident on the interface from *inside* the sample. To obtain $J(\theta)$, we consider once again the flux, given by Eq. (3.12), from a volume element, dV, through an arbitrary small area, dS, inside the sample. Integrating over r and φ we obtain an expression for $J(\theta)$:

$$J(\theta)=\frac{Uv}{2}\cos\theta+\frac{v\ell^*}{2}\frac{\partial U}{\partial z}\cos\theta\sin\theta\,; \qquad (3.44)$$

At z=0 the only diffusive flux in the $+z$ direction is from *reflected* light. Thus, the total flux in the $+z$ direction at z=0 is obtained by integrating over light reflected through all θ

$$J_{+}=\int_{0}^{\pi/2} d\theta\, J(\theta)\, R(\theta); \qquad (3.45)$$

Away from the boundary inside the sample, J_+ is given by Eq. (3.17). Within the diffusion approximation, these two expressions for J_+, Eqs. (3.17) and (3.45), must be equal near the sample boundary at z=0. Thus, setting Eqs. (3.17) and Eq. (3.45) equal and using the expression for $J(\theta)$ in Eq. (3.44), we obtain the boundary condition at z=0,

$$U - \ell^* \frac{\frac{1}{3} + C_2}{\frac{1}{2} - C_1} \frac{\partial U}{\partial z} = 0 \qquad (3.46)$$

where

$$C_1 \equiv \int_0^{\pi/2} d\theta \, R(\theta) \sin\theta\cos\theta \qquad (3.47)$$

and

$$C_2 \equiv \int_{-\pi/2}^{0} d\theta \, R(\theta) \sin\theta\cos^2\theta \qquad (3.48)$$

At $z=L$, we obtain a similar boundary condition,

$$U + \ell^* \frac{\frac{1}{3} + C_2}{\frac{1}{2} - C_1} \frac{\partial U}{\partial z} = 0 \qquad (3.49)$$

Equations (3.46) and (3.49) have the same form as the boundary conditions we previously derived, Eqs. (3.30) and (3.31), provided we make the identification,

$$C = \ell^* \frac{\frac{1}{3} + C_2}{\frac{1}{2} - C_1}; \qquad (3.50)$$

We can obtain an expression for the parameter R, which depends only on the indices of refraction of the sample and the surrounding medium (*e.g.*, air or glass), by comparing Eq. (3.50) with Eq. (3.22). This gives,

$$R = \frac{3\,C_2 + 2\,C_1}{3\,C_2 - 2\,C_1 + 2}; \qquad (3.50)$$

Taking n=1.7 for the alumina and n=1.5 for the glass frit we obtain R=0.68 for the alumina sample and R=0.57 for the glass frit. These values are in reasonable agreement with the experimental estimates of 0.73 and 0.63, respectively.

We note that the treatment of reflections given above differs from the earlier treatment of Lagendijk *et al.*[3] in that it allows for angle- and polarization-dependent internal reflection of light. Thus, we are able to predict the value of the reflection coefficient incorporated into the boundary conditions in terms of known material parameters, namely the indices of refraction of the scattering medium and the sample container. Furthermore, in the absence of internal reflection, we recover boundary conditions which are more consistent with the Milne solution than the perfectly absorbing boundary conditions sometimes used.[3,8]

3.4. APPLICATIONS

Since internal reflection of light changes the path length distribution, $P(s)$, its effects must be taken into account in measurements of other quantities which involve multiply scattered light. Below, we discuss the effects of internal reflection on dynamic light scattering in the multiple-scattering limit, coherent backscattering, and frequency correlations. Because all of these measurements depend on $P(s)$ in essentially the same way, we can generalize our results for angular correlations to each of these measurements. In fact, in each of these cases we show how the expressions obtained in the absence of internal reflection can be modified to obtain more general expressions which apply when internal refections are not negligible. Furthermore, in all cases, the effects of internal reflection enter the expressions by means of the same parameter, C. Thus, at least in principle, it is possible to determine C, and the effects of internal reflection, from the angular correlation function in transmission, and use this value for other measurements. The angular correlation function in transmission has the unique advantage that, in the absence of absorption, the only other parameter it is dependent on is the sample thickness, which can easily be determined independently. It is this fact which makes the angular correlation function so useful.

A. Diffusing-Wave Spectroscopy

Diffusing Wave Spectroscopy (DWS) is the extension of dynamic light scattering to the multiple scattering regime and involves the analysis of the temporal fluctuations in the intensity of the light multiply scattered from mobile particles. The normalized intensity correlation function measured experimentally is $\langle I(0)I(\tau)\rangle/\langle I\rangle^2=1+\beta\ |g_1(\tau)|^2$ where β is again a constance which depends on the collection optics. For a suspension of colloidal particles undergoing Brownian motion, the normalized field autocorrelation function, $g_1(\tau)$, is given by

$$g_1(\tau) \propto \int_0^{\infty} P(s)\mathrm{e}\text{-}2(\tau/\tau_0)s/\ell^*; \qquad (3.51)$$

where τ_0 is the characteristic time for particle motion. For diffusing Brownian particles, $\tau_0=1/D_p k^2$ where D_p is the diffusion coefficient of the particles and $k=2\pi\ n/\lambda$ is the wavevector of the light in the sample. Equation (3.51) has exactly the same form as the general expression for the angular correlation function with no absorption, except that q is replaced by $\frac{1}{\ell^*}\sqrt{\frac{6\tau}{\tau_0}}$. Thus, for plane wave incidence, the form of $g_1(\tau)$ may be obtained from Eq. (3.37) by making the transformation, $q \rightarrow \frac{1}{\ell^*}\sqrt{\frac{6\tau}{\tau_0}}$. For example, in transmission we obtain

$$g_1(\tau) = \frac{(L+2C)/(z_0+C)\left[\sinh\left[\frac{z_0}{\ell^*}\sqrt{\frac{6\tau}{\tau_0}}\right] + \frac{C}{\ell^*}\sqrt{\frac{6\tau}{\tau_0}}\cosh\left[\frac{z_0}{\ell^*}\sqrt{\frac{6\tau}{\tau_0}}\right]\right]}{\left[1+\left[\frac{C}{\ell^*}\right]^2\frac{6\tau}{\tau_0}\right]\sinh\left[\frac{L}{\ell^*}\sqrt{\frac{6\tau}{\tau_0}}\right] + 2\frac{C}{\ell^*}\sqrt{\frac{6\tau}{\tau_0}}\cosh\left[\frac{L}{\ell^*}\sqrt{\frac{6\tau}{\tau_0}}\right]} \qquad (3.52)$$

For R=0, the above equation reduces to the same functional form obtained previously.[6]

If experimental data from a DWS measurement are interpreted without including the effects of internal reflection, the value of L/ℓ^* obtained by fitting the data to Eq. (3.52) with R=0 will be somewhat larger than its actual value. Physically, this reflects the increase in the effective path length due to the internal reflection. Thus, the value of ℓ^* will be underestimated. For example, with R=0.2 and L/ℓ^*=10, ℓ^* will be underestimated by 10% if internal reflection at the boundaries is not included. Previous reports of DWS measurements in transmission are consistent with these considerions.[6]

In the backscattering geometry, the effects of internal reflection on a DWS measurement can be even more pronounced. In previous reports, the autocorrelation

function in backscattering for a thick sample ($L>>\ell^*$) were found to be well approximated by[11]

$$g_1(\tau) = \exp(-\gamma\sqrt{6\tau/\tau_0}); \qquad (3.53)$$

where γ was observed to be a function of polarization and the ratio, ℓ^*/ℓ. Here we emphasize that γ is also a function of the reflection coefficient R. Making the substitution of $q \rightarrow \frac{1}{\ell^*}\sqrt{\frac{6\tau}{\tau_0}}$ in Eq. (3.41), we obtain an expression for the temporal autocorrelation function with internal reflection,

$$g_1(\tau) = \frac{e^{-z_0\sqrt{6\tau/\tau_0}/\ell^*}}{1 + C\sqrt{6\tau/\tau_0}/\ell^*}; \qquad (3.54)$$

Performing a small time expansion of Eqs. (3.53) and (3.54), we obtain the relationship

$$\gamma = \frac{z_0+C}{\ell^*} = \frac{z_0+\frac{2(1+R)}{3(1-R)}}{\ell^*}. \qquad (3.55)$$

Thus, the value of γ can depend on the optical properties of the sample container and its surroundings. For example, for $z_0=\ell^*$ and R=0, γ=1.67. By contrast, for R=0.2, γ=2. Note that finite values of R lead to larger values of γ. In Fig. 3.7 we show the reflection coefficient as a function of index mismatch.

3.4.B. Coherent backscattering

Another commonly performed experiment, which is also strongly affected by internal reflection, is the coherent enhancement of backscattered light.[2,14] The angular width of the coherent backscattered cone has been used as a direct measure of ℓ^*. The equation for the angular correlation function, Eq. (3.34), has exactly the same form as the expression for the coherent backscattering cone.[14] Thus, for very thick samples, the angular dependence of the coherent backscattering cone is given by Eq. (3.41) and the

inverse angular width is given by $[z_0/\ell^*+2(1+R)/3(1-R)]k_0\ell^*$. Even a modest index mismatch at the sample boundaries can lead to significant corrections to the apparent value of ℓ^* measured using coherent backscattering. For example, a reflection coefficient of R=0.2 increases the value of γ from 1.67 to 2. Thus, caution must be exercised in interpreting the width of the coherent backscattering cone, and the effects of internal reflection must be considered.

3.4.C. Frequency correlation

Another measurement which can also be strongly affected by internal reflection is the frequency correlation of transmitted light as the incident frequency is changed. Such measurements have been used, for example, to determine the diffusion coefficient, D, of light.[15] The phase shift of a path of length s due to a frequency shift, $\Delta\nu$, is $2\pi s\Delta\nu/v=2\pi\Delta\nu s\ell^*/3D$. An expression for the frequency autocorrelation function can be obtained within the diffusion approximation in a fashion analogous to that used to obtain other correlation functions by summing the contribution from all paths. The result is:

$$g_1(\Delta\nu) \propto \int_0^\infty P(s)e^{i2\pi\Delta\nu s\ell^*/3D-s/\ell_a}ds; \qquad (3.56)$$

Equation (3.56) has the same form as the general expression for the angular autocorrelation function, Eq. (3.37). Thus, explicit expressions for the frequency autocorrelation function for different geometries can be obtained from our formulas for the angular autocorrelaton function by making the substitution, $q\rightarrow\sqrt{i2\pi\,\Delta\,\nu\,/D}$ into Eqs. (3.37) and (3.40). Once again, the effect of reflections is to increase the effective length of light paths through a sample. Thus, if internal reflection is not taken into account, the apparent diffusion coefficient extracted from a fit to the data will be smaller than its actual value. However, because the effects of internal reflection decrease with increasing sample thickness, the fitted value of D should increase and saturate at the true value

when $L>> C$. These results are consistent with the recent report using microwave measurements.[16]

3.4.D. Pulse Propagation

Internal reflection can also strongly affect pulse propagation and the transmission coefficient of light through random media. For an instantaneous pulse of light incident on a random medium, the transmitted pulse is broadened in time. Physically, this reflects the fact that photons traverse a distribution of path lengths. Those with shortest paths escape from the sample first and those with longer paths escape later. The functional form of the transmitted pulse is simply $P(s)$ with the transformation of variables, $s=vt$. For plane wave incidence, the solution of the diffusion equation is given by Carslaw and Jaeger for the slab geometry.[10]

$$P(t) \propto \sum_{m=1}^{\infty} \frac{k_m[\sin(k_m z_0)+Ck_m\cos(k_m z_0)][\cos(k_m L) - Ck_m\sin(k_m L)]}{(C^2k_m^2+1)L+2C} e^{-D(k_m^2+\alpha^2)t} \quad (3.57)$$

where k_m is m^{th} positive root of the hyperbolic equation,

$$\tan(kL)=\frac{2kC}{C^2k^2-1} \quad (3.58)$$

$D=v\ell^*/3$ is the diffusion coefficient of light, and $\alpha^2=3/\ell_a\ell^*$. The internal reflection increases the path length which delays the peak of transmitted pulse and broadens its width. At long times, where $P(t)$ decays exponentially, the decay is slower when reflection is included. Thus, if internal reflection is not taken into account, the apparent diffusion coefficient extracted from a fit to the data will be smaller than its actual value. For example, fitting the exponentail tail of $P(t)$ by assuming $R=0$ and renormalizing D gives the apparent diffusion coefficient

$$D^* \approx D\left[1 - \frac{8R\ell^*}{3(1-R)L}\right]. \qquad (3.59)$$

A similar result was obtained by Lagendijk *et al.*[3] but with a slightly different numerical coefficient resulting from their assuming perfectly absorbing walls in the absence of reflection (see section 2 B).

3.5. CONCLUSIONS

We have developed a simple theory to describe the internal reflection of light at the sample boundaries in systems which multiply scatter light. We find that the effects of internal reflection can be accounted for by incorporating a single parameter, C, into the boundary conditions of the diffusion equation for light. Using these boundary conditions in the solution of the diffusion equation, we obtain explicit expressions for various experimentally measurable quantities, including the angular, temporal, and frequency autocorrelation functions, as well as the coherent backscattering cone and the shape of the transmitted pulse in a pulse propagation experiment.

We find that the measurements of the angular correlationfunctions are in excellent agreement with the theory only when the effect of internal reflection at the sample interface is properly taken into account. The angular autocorrelation functions depend on sample thickness, absorption, and internal reflection. The effects of reflection and absorption can be independently determined through their different dependences on sample thickness. Internal reflection increases the light path by a fixed amount which depends on the reflection coefficient. Therefore, in transmission experiments, internal reflection is most significant for thin samples. By contrast, absorption cuts off long paths and, therefore, is significant only for transmission through thick samples. Thus, measurements of $g_1(q)$ as a function of thickness can be used to determine the abosrption and reflection parameters, α and C, respectively. To obtain a value for the reflection coefficient, R, which appears in C, the transport mean free path, ℓ^*, must be known. An estimate of ℓ^* can be obtained from backscattering measurements of the angular correlation function. Thus, by measuring autocorrelation functions for different thicknesses in both transmission and backscattering, we can determine the absorption

parameter and obtain an estimate of the reflection coefficient and the transport mean free path.

Finally, using a simple model based on Fresnel theory, we calculated the dependence of the reflection coefficient on the index mismatch at the sample boundaries. As expected, larger index mismatch leads to larger reflection coefficients. The reflection coefficients we calculate are in good agreement with the measured values of R for samples with different index mismatch. Thus, reasonable *a priori* estimates of the effects of reflection are possible for a given experiment using multiple light scattering.

References

[1]A. Ishimaru, *Wave Propagation and Scattering in Random Media* (Academic, New York, 1978).

[2]*Scattering and Localization of Classical Waves in Random Media*, edited by P. Sheng (World Scientific, Singapore, 1990).

[3]A. Lagendijk, R. Vreeker, and P. DeVries, Phys. Lett. A **136**, 81 (1989).

[4]I. Freund, M. Rosenbluh, and R. Berkovits, Phys. Rev. B **39**, 12403 (1989).

[5]I. Freund, M. Rosenbluh, and R. Berkovits, Phys. Rev. B **41**, 496 (1990).

[6]D.J. Pine, D.A. Weitz, G. Maret, P.E. Wolf, E. Herbolzheimer, and P.M. Chaikin, *Scattering and Localization of Classical Waves in Random Media*, edited by P. Sheng (World Scientific, Singapore, 1990).

[7]D.J. Pine, D.A. Weitz, J. X. Zhu, and E. Herbolzheimer, J. Phys. (France) **51**, (1990) 2101-2127.

[8]S. Feng, C. Kane, and A. D. Stone, Phys. Rev. Lett. **61**, 834 (1988).

[9]S. Glasstone and M. C. Edlund *The Elements of Nuclear Reactor Theory* (D. Van Nostrand Company, Princeton, New Jersey, 1955).

[10]H. S. Carslaw and J. C. Jaeger, *Conduction of Heat in Solids*, 2nd edition (Clarendon, Oxford, 1990).

[11]D.J. Pine, D.A. Weitz, P.M. Chaikin, and E. Herbolzheimer, Phys. Rev. Lett. **60**, 1134 (1988).

[12]F.C. Mackintosh, J.X. Zhu, D.J. Pine, and D.A. Weitz, Phys. Rev. B. **40**, 9342 (1989).

[13]M. Born and E. Wolf, *Principles of Optics*, 4th edition (Pergamon, New York, 1990).

[14]P.E. Wolf, G. Maret, E. Akkermans, and R. Maynard, J. Phys. France **49**, 63 (1988).

[15]J.M. Drake and A.Z. Genack, Phys. Rev. Lett. **63**,259(1989).

[16]L. A. Ferarri, J. Appl. Phys. **68**, 4399 (1990).

Chapter IV

POLARIZATION MEMORY OF MULTIPLY SCATTERED LIGHT

ABSTRACT

Light backscattered from an optically dense random medium is shown to exhibit a pronounced polarization dependence. An unexpected memory of the incident circular polarization of multiply scattered light arises because the wave's helicity is randomized less rapidly than is its direction. A simple model is developed to account for the observed polarization dependence of the intensity and temporal correlations of the intensity fluctuations of backscattered light.

The propagation of light in optically dense random media is characterized by multiple scattering which randomizes the direction, phase, and polarization of the incident wave. This randomization accounts for the remarkable success of scalar diffusion theory in describing the transport properties of multiply scattered light[1-5]. Recent experiments[6,7] have demonstrated the power of this approach by extending traditional quasi-elastic light scattering to the multiple scattering regime, thereby allowing one to probe the structure and dynamics of optically dense media. The diffusion approximation, however, fails to fully describe *backscattered* light, because such light is comprised of a significant contribution of *multiply scattered modes* whose path lengths are comparable to the transport mean free path[8]. In this chapter, we demonstrate that these modes lead to a remarkable and unexpected persistence of polarization of multiply scattered light. Single Rayleigh scattering is known to result in the polarization of scattered light in a cloudless blue sky. What is surprising is that for *circularly* polarized light, randomization of the polarization requires many more scattering events than are required for the complete randomization of the wave's direction. This polarization memory has important consequences both for the average scattered intensity and for the temporal correlation of the intensity fluctuations of light backscattered from a time varying medium. In particular, we show that contrary to previous reports[9] the form of the autocorrelation functions is not universal, but instead depends on both particle size and polarization.

To demonstrate the polarization memory in a multiply scattering medium, we consider a system composed of uncorrelated and noninteracting spherical particles of radius a, suspended in a liquid. The multiply scattered light results in a random speckle pattern, which fluctuates as the particles undergo Brownian motion. The backscattered intensity is comprised of the contributions of light following many different scattering paths. Each path leads to a decay of the temporal correlations of the scattered field,

which depends on the number of scattering events, and consequently the path length. The field autocorrelation function is[6,7] $G_1(\tau) \equiv \langle E(\tau)E^{\wedge *}(0)\rangle \propto \int_0^\infty P(s)e^{-2(\tau/\tau_0)/\ell^*}ds$

Here, $P(s)$ is the number of scattering paths of length s and $\tau_0=(\lambda/2\pi)^2/D_S$, where λ is the optical wavelength in the liquid and D_S is the self-diffusion coefficient of the suspended particles. The time averaged intensity is given by $G_1(\tau)$. The transport mean free path, ℓ^*, signifies the distance the light must travel before its direction becomes completely randomized. For $s>\ell^*$, $P(s)$ can be calculated within the diffusion approximation. For shorter paths, however, the diffusion approximation fails to characterize $P(s)$. Backscattered light involves many photon paths which penetrate only ℓ^* into the medium. We focus on two limits, where a simple physical picture of the polarization dependence can be obtained. In the first case, $a<<\lambda$, so that $\ell=\ell^*$, where ℓ is the scattering length. Here, the non-diffusive paths involve a very small number of scattering events, and the polarization dependence reflects the behavior of single scattering at large angles. In the second case, $a\gtrsim\lambda$, and the scattering is highly anisotropic, so that $\ell^*>>\ell$. Here, the non-diffusive paths involve many scattering events, and the polarization memory results from a slower randomization of circular polarization than of direction of propagation. For our measurements with isotropic scatterers, with $\ell^*=\ell$, we use a 1-cm thick sample of 0.091-μm-diam polystyrene latex spheres in water with volume concentration ϕ=0.05. A linearly or circularly polarized beam from a 488-nm Ar^+ laser is expanded to 1-cm diameter and is incident on one side of the sample. Scattered light of the desired polarization is collected from the same side of the sample. We measure the time averaged intensity, $\langle I\rangle$, and the normalized intensity autocorrelation function $G_2(\tau) \equiv \langle I(\tau)I(0)\rangle/\equiv \langle I\rangle^2-1 \propto |G_1(\tau)|^2$, up to a constant determined by the optics. The autocorrelation functions can be approximated by[7]

$$G_2(\tau) \propto e^{-2\gamma\sqrt{\tau/\tau_0}}, \qquad (4.1)$$

where τ_0 is determined from the Stokes-Einstein relation for the self-diffusion coefficient: $D_S=k_BT(1-1.8\phi)/(6\pi\eta a)$. Here, η is the fluid viscosity, and we have corrected for the effects of hydrodynamic interactions[10]. The *slope* of the decay is characterized by the parameter γ, which directly reflects the fraction of non-diffusive paths contributing to $P(s)$, since short paths yield a slower decay of the correlations. The autocorrelation functions for the four polarization channels are plotted logarithmically as a function of $\sqrt{\tau/\tau_0}$ in Fig. 4.1. All four channels exhibit nearly linear behavior in this plot, consistent with Eq. (1). However, the slopes, γ, depend strongly on polarization. The two linear polarization channels exhibit the largest difference in slopes, with $\gamma_{||}=1.45$ for incident and scattered light of the same polarization, while $\gamma_{\perp}=3.06$ for light backscattered with perpendicular polarization. This difference is due to the fact that low-order backscattering sequences favor the parallel polarization channel, resulting in a smaller decay rate in this channel. The difference between the circular channels is also pronounced, with $\gamma_{+}=2.68$ for incident and scattered light of the same helicity, and $\gamma_{-}=1.59$ for the opposite helicity. For circularly polarized light, low-order sequences yield backscattered light primarily of the opposite *helicity*, for which incident and reflected photons are related by mirror symmetry. The greater contribution of short paths in the parallel and opposite-helicity channels is also directly reflected in the measured *intensity* of scattered light in these channels, with $\langle I_{||}\rangle/\langle I_{\perp}\rangle=1.78$ and $\langle I_{-}\rangle/\langle I_{+}\rangle=1.45$. In all cases the overall experimental error is about ±5%.

The values of γ in the four polarization channels can be calculated theoretically within the *white-noise* model[11], assuming uncorrelated particles, and $\ell^*=\ell$. The autocorrelation functions for the multiply scattered scalar[11] or vector[8] waves may be obtained from the sum of ladder diagrams, comprising the leading perturbative contribution for $\ell>>\lambda$. The inclusion of the non-diffusive modes[4,8] associated with the vector model leads to the same trends in the calculated as in the measured *initial* decay of correlations: we obtain $\gamma_{\perp}=2.7$, $\gamma_{||}=1.6$ for the linear polarization channels, and $\gamma_{+}=2.4$,

γ_-=1.7 for the circular polarization channels. The effects of polarization on backscattering are markedly different when $a \gtrsim \lambda$. This is illustrated in Fig. 4.2, which shows the measured autocorrelation functions for light backscattered from 0.605-μm-diam spheres, with ϕ=0.02. Here, $\ell^* \approx 10\ell$, and the two linear polarization channels have almost identical slopes: $\gamma_\perp$=2.18 and $\gamma_{||}$=1.96. In addition, the average intensities in the two linear channels are almost identical, with $\langle I_{||} \rangle / \langle I_\perp \rangle$=1.05. *By contrast, the circular polarization channels exhibit a high degree of polarization memory.* Their relative behavior, however, has reversed: the helicity-preserving channel decays more slowly than the opposite-helicity channel. Furthermore, the helicity-preserving channel exhibits more noticeable curvature. Thus we use the initial slope to obtain γ_+=1.72 and γ_-=2.62. This change is also reflected in the intensity, with $\langle I_+ \rangle / \langle I_- \rangle$=1.40. The key to understanding these polarization effects is the behavior of paths with $s \sim \ell^*$. For $a \gtrsim \lambda$, the scattering from individual particles is confined to a narrow cone of angular width λ/a about the incident direction. For multiple scattering, we may regard the intermediate unit wave vectors, $\hat{\mathbf{k}}_j$, as executing a random walk on the unit sphere between incident and final directions, with small step size λ/a. The number of scattering events required to completely randomize the wave direction, $n_0 \sim (a/\lambda)^2$, provides the definition of the transport mean free path: $\ell^* = n_0 \ell$. Backscattered light is comprised of a large contribution from paths of length $s \sim \ell^*$, which characteristically involve n_0 scattering events. For a sufficiently large n_0, the polarization vector for incident linearly polarized light is completely randomized. A simple geometric argument demonstrates this. For each scattering event, the polarization vector $\hat{\boldsymbol{\varepsilon}}_j$ is related to the previous vector $\hat{\boldsymbol{\varepsilon}}_{j-1}$ by $\hat{\boldsymbol{\varepsilon}}_j \propto \hat{\boldsymbol{\varepsilon}}_{j-1} - (\hat{\mathbf{k}}_j \cdot \hat{\boldsymbol{\varepsilon}}_{j-1}) \hat{\mathbf{k}}_j$. In the limit of small scattering angles θ_j, this is equivalent to parallel transport of the polarization vector on the surface of the unit sphere from $\hat{\mathbf{k}}_{j-1}$ to $\hat{\mathbf{k}}_j$, along a great circle. Backscattering corresponds to a random walk from one pole of the unit sphere to the other. If such a path results in a backscattered wave of parallel polarization, then an equally probable path, determined by the azimuthal rotation of the sphere

through an angle φ=45° about the incident direction, results in a backscattered wave of perpendicular polarization[8]. This reflects the azimuthal dependence of the linear polarized scattering amplitudes. Thus, paths of length $s \gtrsim \ell^*$ contribute equally to each linear polarization channel for large particles. This is not the case for the circular polarization channels. For scattering through a small angle the amplitude for helicity flip is small, *independent azimuthal rotations.* Physically, we can understand this by considering small particles. The Born approximation yields scattering amplitudes proportional to the overlap of the outgoing circular states $|R'\rangle$, $|L'\rangle$ with the incident states $|R\rangle$, $|L\rangle$:

$$\langle R'|R\rangle \propto \frac{1+\cos\theta}{2} \approx 1$$

and

$$\langle L'|R\rangle \propto \frac{1-\cos\theta}{2} \approx 0$$

For large particles, the probabilities for scattering with and without a helicity flip, $I^-(\theta)$ and $I^+(\theta)$ respectively, may be calculated within Mie theory[12]. The results are qualitatively the same as for small scatterers; for small θ, the probability of helicity flip is quite small. We may represent the *angular* average of the probabilities for scattering without (+) and with (-) helicity flip by

$$p_\pm = \langle I\pm\rangle / \langle I^+ + I^-\rangle \equiv \frac{1}{2}(1 \pm e^{-1/n'}).$$

Physically, $n'\ell$ represents the path length over which the helicity is randomized. The small amplitude for helicity flip makes this length greater than ℓ^*. This is the origin of the polarization memory. Paths of length $s=n\ell$ contributing to the two helicity channels are characterized by an even or odd number of helicity flips, respectively, each with probability p_-. The number of these paths is then given by

$$P_\pm(s) \approx \frac{1}{2}P(s)[(p_+ + p_-)^n \pm (p_+ - p_-)^n]$$
$$= \frac{1}{2}P(s)(1 \pm e^{-n/n'})$$

where $P(s)$ is the number of scattering paths for scalar waves. This leads to a simple expression for the autocorrelation functions in the two helicity channels in terms of the autocorrelation function for scalar waves:

$$G_1^{\pm}(\tau) \propto G_1(\tau) \pm G_1(\tau + \tau_0 n_0/(2n')). \qquad (4.2)$$

The second term represents a shift in the time variable, and is equivalent to the correlation function in an absorbing medium, with absorption length $n'\ell$. We can use Eq.(4.2) to compare with experiment by taking the scalar value of γ=2.05, obtained from the unpolarized autocorrelation function, and adjusting n' to simultaneously fit both circular polarization channels. The results for 0.605μm spheres, with n'=32, are shown by the dashed lines in Fig. 4.2. The shapes of the autocorrelation functions are reproduced quite well, including the curvature in the helicity-preserving channel. Physically, the polarization memory arises because n' increases with particle size more rapidly than n_0, so that more scattering events are required to randomize the helicity than to randomize the direction. The dependence on the scattering particle size is illustrated in Fig. 4.3, which shows the measured γ for the circular polarization channels. A striking polarization dependence is apparent for circularly polarized light in both limits of small and large scattering particles. For small scattering particles, the helicity is flipped by the non-diffusive paths and $\gamma_- < \gamma_+$. For large particles, where forward scattering dominates, the helicity is preserved over a longer length scale than ℓ^*, and this polarization memory results in $\gamma_- > \gamma_+$. This trend is correctly predicted by the values of γ calculated from Eq. (4.2) using Mie theory, as shown by the solid lines in Fig. 4.3. The oscillations reflect the resonances characteristic of Mie theory, and would be smeared out by any polydispersity in the scattering particles. The fitted values of n', however, are substantially less than calculated from Mie theory, as shown in the inset to Fig. 4.2. Nevertheless, they are still larger than n_0, reflecting the large degree of polarization memory. The discrepancy between the data and the Mie theory predictions may be due in part to the effects of particle concentration, and the resulting structure

factor, which tends to reduce the forward scattering. This will in turn increase the average angle of scattering from the individual particles, leading to a less pronounced polarization memory. Consistent with this, increasing ϕ to 0.05 further reduces the observed polarization memory. A full description of the multiple scattering of light in random media requires a detailed knowledge of the nature of short scattering paths, particularly for backscattering, where the characteristic path length is of order ℓ^*. These non-diffusive paths are responsible for the striking memory of the incident circular polarization. By contrast, linearly polarized light loses its polarization memory as the particle radius increases, independent of particle concentration, with $\gamma_{\parallel}$ and $\gamma_{\perp}$ monotonically approaching the asymptotic value of 2.05 as shown in the inset of Fig. 4.1. This behavior can be exploited to independently determine τ_0, by measuring the autocorrelation function for both linear polarization channels. This makes particle sizing possible using diffusing-wave spectroscopy[7], and demonstrates yet another way in which multiple dynamic light scattering can provide useful information about dense media.

References

[1]M. P. van Albada and A. Lagendijk, Phys. Rev. Lett. 55, 2692 (1985).

[2]P. E. Wolf and G. Maret, Phys. Rev. Lett. 55, 2696 (1985); E. Akkermans, P. E. Wolf and R. Maynard, Phys. Rev. Lett. 56, 1471 (1986).

[3]S. Etemad, R. Thomson and M. J. Andrejco, Phys. Rev. Lett. 57, 575 (1986); S. Etemad, R. Thompson, M.J. Andrejco, S. John and F. MacKintosh, Phys. Rev. Lett. 59, 1420 (1987).}

[4]M. J. Stephen and G. Cwilich, Phys. Rev. B 34 7564 (1986).

[5]G. H. Watson, P. A. Fleury and S. L. McCall, Phys. Rev. Lett. 58, 945 (1987).

[6]G.~Maret and P.~E.~Wolf, Z.~Phys.~B 65, 409 (1987).

[7]D. J. Pine, D. A. Weitz, P. M. Chaikin, E. Herbolzheimer, Phys. Rev. Lett. 60, 1134 (1988).

[8]F. C. MacKintosh and Sajeev John, Phys. Rev. B, 40, 2383 (1989)

[9]M. Rosenbluh, M. Hoshen, I. Freund and M. Kaveh, Phys.~Rev. Lett.~58, 2754 (1987).

[10]G. K. Batchelor, J. Fluid Mech., 74, 1 (1976)

[11]M. J. Stephen, Phys. Rev. B 37 1 (1988).

[12]M. Kerker, *The Scattering of Light*, (Academic Press, New York, 1969).

Chapter V

TIME DEPENDENT HYDRODYNAMIC INTERACTIONS OF BROWNIAN PARTICLES

ABSTRACT

We study the effect of hydrodynamic interactions on the short time non-diffusive motion of Brownian particles suspended in a fluid. We use Diffusing Wave-Spectroscopy to measure the mean square displacement, $\langle \Delta r^2(\tau) \rangle$, for concentrated suspensions at times short to observe the retarded nature of hydrodynamic interactions. A power-law decay of the velocity autocorrelation function, $R(\tau) \sim \tau^{-3/2}$, is observed for all concentrations. A remarkable scaling behavior of the time dependent diffusion coefficient, $D_s(\tau)=\langle \Delta r^2(\tau) \rangle/6\tau$, with particle volume fraction is observed: if $D_s(\tau)$ is scaled by its asymptotic value and if time is scale by a viscous time constant inversely proportional to the shear viscosity of the suspension, all the data fall onto a single universal curve.

5.1. INTRODUCTION

This chapter is concerned with the dynamics of hard spheres suspended in a fluid at thermal equilibrium. The hard spheres are small enough to perform random Brownian motion. Although small, the hard sphere particles are sufficiently large compared with the liquid molecules, and the fluid is considered to be incompressible. In this two-component system, composed of rigid spheres and liquid, the particles undergo three types of interactions. The first is the *Brownian* interaction arising from thermal collisions with the liquid molecules. This interaction is responsible for the rapid fluctuations of the particle velocities. The characteristic time of these velocity fluctuations, τ_h, for a Brownian particle is typically less than one microsecond. The second type of interaction results from the direct collision between particles, and is called "hard sphere" or "excluded volume" interaction between rigid particles. The third interaction is called hydrodynamic interaction which results from the fact that the particles interact through the fluid. The motion of a particle can be divided into three time scale, reflecting the characteristic time scales of the three types of interactions. The time evolution of the mean square displacement, $\langle \Delta r^2(\tau) \rangle$, of the particle reflects the consequences of these types of interactions and describes the dynamics of the random motion which results. At long times, $\langle \Delta r^2(\tau) \rangle$ increases linearly with time, reflecting the diffusive motion of the particle resulting from the interaction with the surrounding fluid and the random encounters with other particles. The long time diffusion coefficient of the particle is considerably less than the Stokes-Einstein diffusion coefficient, D_0, due to these interactions with its neighbors, which tend to trap the particle in a "cage", impeding large scale motions and thereby reducing the diffusion coefficient. At shorter times, $\langle \Delta r^2(\tau) \rangle$ also increases linearly with time, but at a faster rate, reflecting the diffusive motion of the particle in the fluid before it approaches its nearest neighbors. This short

time diffusion coefficient, D_S, is also reduced from D_0 not due to the potential of hard sphere interactions between particles, but due to the hydrodynamic interactions. Finally, at even shorter times, $\langle \Delta r^2(\tau) \rangle$ must increase even more rapidly than linear, as the ballistic motion, arising from the velocity imparted to the particle by random collisions with the fluid molecules, is viscously damped. These complex dynamics of the particles can be represented by the time dependent self-diffusion coefficient defined as

$$D_s(\tau) \equiv \frac{\langle \Delta r^2(\tau) \rangle}{6\tau} \tag{5.1}$$

The transition from the ballistic motion to diffusive motion of the particle can also be parameterized by the time evolution of the velocity correlation function, $R(\tau) \equiv \langle v(0)v(\tau) \rangle$, which is related to $\langle \Delta r^2(\tau) \rangle$ as

$$R(\tau) = \frac{1}{6} \frac{d^2 \langle \Delta r^2(\tau) \rangle}{d^2 \tau} \tag{5.2}$$

Initially $R(0)$ is the mean square velocity of the particle which can be determined by the equipartition theory, $R(0)=k_B T/m$, where k_B is the Boltzmann constant, T the temperature, and m the mass of the particle. As the velocity of the particle is viscously damped, $R(\tau)$ decreases as a function of time. At long times, when $R(\tau)$ decay to zero, the motion of the particle reaches the short time diffusive regime.

It is commonly assumed that the very early ballistic motion and short time diffusive motion of Brownian particles have well separated time scales. For a single sphere in an infinite fluid the dynamics of the Brownian motion were traditionally described by the simple Langevin equation. Using a time independent viscous drag on the particle, one finds that $R(\tau)$ decays exponentially as a function of time. However, molecular dynamics

computer simulations by Alder *et al*[1,2,3] showed that $R(\tau)$ has a much slower, $\tau^{-3/2}$, decay at long times, which is called the "long time tail". Physically the "long time tail" results from the time required to develop to the flow field in the fluid as the particle moves. The viscous drag exerted by the fluid depends not only on the present particle velocity but also on the history of the particle motion, reflecting the fact that hydrodynamic interaction between the particle and the fluid is time-dependent or retarded. For one particle in an infinite fluid, Zwanzig *et al*[4] solved the Langevin equation using the full time dependent viscous drag and correctly predicted which showed the asymptotic decay of $R(\tau)\sim\tau^{-3/2}$. Hinch[5] further developed the one particle theory to give an explicit analytical expression for $R(\tau)$ for all times.

Despite the early development of the theory of the long time tail for one particle in an infinite fluid, the experimental evidence of the effect has remained scarce. The reason for this is that the length scale over which a particle moves while its velocity correlation decays is so short that the technique of quasi-elastic light scattering (QELS) is unable to resolve the particle motion. Therefore, the data quality at this length scale from QELS is very poor. Nevertheless, early experimental evidence of the "long time tail" was reported by Paul and Pusey[6] using QELS. They measured $\langle \Delta r^2(\tau) \rangle$ for particles at very dilute concentrations. Their data were fitted using the theories both with and without considering the retarded hydrodynamic interaction. By analyzing the residual of the fits, they found the data were best described by the theory which included the "long time tail". More recently, Weitz *et al*[7] used Diffusing Wave-Spectroscopy (DWS)[8] to study the short length scale motion of more concentrated colloidal particles, and clearly demonstrated the effect of the "long time tail". Diffusing Wave-Spectroscopy (DWS) exploits diffusive nature of photons in strongly scattering media, extending the dynamic light scattering to the multiple scattering limit. Because the multiple scattering amplifies the dephasing of the light due to the motion of particles, the measured autocorrelation

function decays an appreciable amount due to particle motion over a very short distance. Therefore, this technique is best suited for studying the short times and short length scales of the motion. However, the early data reported still had considerable noise and uncertainty.

A greater challenge is to understand the short time behavior of particles in concentrated suspensions. Here the flow field generated by one particle is modified by the presence of other particles. This complex interplay between the particle motion and the fluid field also manifests itself in the time evolution of $\langle \Delta r^2(\tau) \rangle$. The theoretical calculations of this many body problem are extremely difficult. Van Sarloos and Mazur[9]calculated the frequency dependent mobility tensor and predicted that for all volume fractions $R(\tau)$ should also behave as $\tau^{-3/2}$ at long times. Very recently, Clercx and Schram[10] calculated the time dependent diffusion coefficient for two particle interactions in an unbounded fluid. As only two particle interactions were considered, the theory should be valid only for dilute suspensions. To date, there has been no experimental investigation of the retarded hydrodynamic interactions in concentrated suspensions. In this chapter we use DWS in the transmission geometry to measure $\langle \Delta r^2(\tau) \rangle$ for hard sphere suspensions as a function of particle volume fraction. At low volume fraction we compare our data with the theoretical predictions for dilute suspensions. Our data are of sufficiently high quality that we can numerically differentiate them twice to directly obtain $R(\tau)$. We find that $R(\tau)$ exhibits the $\tau^{-3/2}$ decay at long times predicted by the theory. Furthermore, our data agree with the theory for the whole range of times we can measure. At higher volume fractions, we also find a $\tau^{-3/2}$ decay of $R(\tau)$ reflecting the fact that the flow field around the particle also evolves in time, in agreement with the theoretical predictions. Moreover, we find a surprising scaling behavior of $D_s(\tau)$ with volume fraction: if $D_s(\tau)$ is scaled by its asymptotic value, $D_s(\phi)$, and if time is scaled by a viscous time constant inversely proportional to the shear

viscosity of the suspension, all the data fall onto a single universal curve. To compare with the theoretical calculation, we find that the two particle theory at the volume fractions less than or around 10% also shows a similar scaling behavior, in good agreement with our data.

This chapter is organized as follows. In section 5.2 we present a theoretical treatment of light scattering for interacting samples. The theory of the dynamics of the particles suspended in a fluid are discussed in section 5.3. The experimental details and the data analysis are included in section 5.4. In section 5.5, we present the results and discuss this the physical implications.

5.2. LIGHT SCATTERING THEORY FOR INTERACTING SAMPLES

In this section, we present the theory for Diffusing Wave Spectroscopy for interacting systems. In the previous chapters we assumed that the interactions between particles suspended in a fluid could be neglected. As a result, a particle occupy take any position within the sample volume. Moreover, the phases of the photons traveling along different paths are completely uncorrelated. Thus the temporal autocorrelation function of the intensity of multiply scattered light may be calculated by taking a statistical average over all possible contributions of single scattering events. This allows the relationship between the fluctuations of the light intensity and the particle dynamics to be established. However, this non-interacting system is approached only in the limit dilute samples, in the absence of other potential interactions. More generally, the particles do interact with one another. For example, colloidal particles can not inter-penetrate each other, resulting in the "excluded volume" or hard sphere repulsive interaction. As another example, charge stabilized colloidal spheres interact with each other through Coloumbic interactions. Any form of potential interaction, such as these, leads to a correlation in the positions of the particles. We note here that potential interactions are distinct from hydrodynamic interactions, as the latter depend on the particle velocities and hence do not influence the equilibrium structure of particles, unlike potential concern here. The previous analysis of DWS must be modified to include the effect of the inter particle interactions. The interpretation of DLS from interacting particles in the single scattering limit is well understood. Traditional dynamic light scattering measures density fluctuation at length scale of $1/q$, where q is the magnitude of the scattering wavevector. A detailed discussion of traditional DLS from interacting systems can be found by Pusey and Tough[11]. By contrast, no general scheme of treating multiple scattering from interacting systems is available. For the special case where the correlation length ξ,

defined as the distance over which the particles are correlated, is small compare with ℓ, Mackintosh and John[12] used a Green's function method to extended DWS calculations to interacting systems. In this case, each scattering event can still be considered as independent, and the effect of multiple scattering can be calculated by averaging the contributions of single scattering events. In this chapter we present an alternative derivation of the theory for DWS using another method for analyzing the contributions of optical path. We begin by discussing the most fundamental physical quantity, the scattered field. Then, we show that the intensity autocorrelation function can be derived from the field autocorrelation function, with the assumption that the illuminated sample is much larger than the correlation volume. The particle correlation results in a change in both the scattering and transport mean free paths, which in turn modifies the average transmitted intensity. We discuss the difficulties in extracting information from multiply scattered light in the general conditions of interacting particles, as we can no longer separate the multiple scattering into independent single scattering events. However, there exist two special cases where we can obtain useful information about the dynamics of the system. The first is when the particle correlation length ξ is small compared to the mean free path ℓ. In this case, a photon is successively scattered by particles uncorrelated in positions, allowing multiple scattering to be calculated by averaging the contributions of single scattering events. The second case is when the particle diameter d is large compared to the wavelength of light λ, $d>>\lambda$. In this case the inter particle separation, measured by the center to center distance, is so large that the phases of scattered photons by different particles can still be considered as independent. We will show that these two limits will account for most systems of interest. The first case accounts for systems with small particles which generally scatter less, thus increasing the optical mean free path and making it larger than the correlation length. The second case accounts for suspensions of

large particles. Therefore, DWS is a very useful tool to study the dynamics of interacting systems.

The goal of the theory of dynamic light scattering is to establish the relationship between the temporal autocorrelation function of the scattered light intensity and the dynamics of the colloidal particles in the sample. The fundamental approach taken in this chapter in deriving the autocorrelation function is to separate the multiply scattering into a product of the contributions of single scattering events, each averaged over all scattering vectors, weighted by the scattering amplitude. We begin with the expressions for the field of the multiply scattered light, and determine the relationship between the intensity autocorrelation function and the field autocorrelation function. We explain that, in two special cases, the ensemble averaged field autocorrelation function can be obtained as the average of the contribution of all possible single scattering events, or the average of the dynamic structure factor, $S(q,\tau)$, thereby establishing the relationship between the particle dynamics and the intensity fluctuations. Finally, we show that most scattering sample do in fact fall into the two special cases. Therefore, the technique we discuss here is quite general.

We consider a sample comprised of identical spherical particles of radius a. The sample geometry is that of a slab of thickness L, and with the transverse dimensions much greater than L. We assume that the sample dimension, L, is much larger than the correlation length ξ, the average distance over which the particles are correlated in space. We also assume that coherent light beam is incident to one side of the slab and the scattered light exits from the other side of the slab. Although we analyze only this slab geometry in transmission, our analysis can be extended to other geometry as well. The light transport within the sample is once again assumed to be diffusive and is described by the diffusion equation

$$\frac{\partial U}{\partial t} - D\nabla^2 U = f(x,y,z,t) \tag{5.3}$$

where U is the density of photons, $D=v\ell^*/3$ is the diffusion coefficient of light, v the speed of the light inside the sample, ℓ^* the transport mean free path, and $f(t,x,y,z)$ the source of diffusing light. Use of the diffusion equation assumes that the photons are conserved. The path of each diffusing photon is determined by random multiple scattering from a sequence of scatterers. The multiply scattered electrical field, E, emerging from the sample is made up of the contributions of fields following many different scattering paths

$$E=\sum_p E_p \tag{5.4}$$

where p denotes a scattering path and Σp denotes the sum over all possible paths. We show a typical path p in Fig. 5.1. We assume that a photon enters the sample and follows a path p consisting of n scattering sequences, from particles located at positions $\mathbf{r}_1$, $\mathbf{r}_2$, ..., and $\mathbf{r}_n$, and finally exits the sample. We define reference points, $\mathbf{r}_o$ and $\mathbf{r}_o'$, on each side of the slab. The phase of the scattered photon, ϕ_p, is the total distance over which the photon travels multiplied by the wavevector of the light at each point along the path. Thus,

$$\phi_p = \mathbf{k}_0\cdot(\mathbf{r}_1-\mathbf{r}_o)+\mathbf{k}_1\cdot(\mathbf{r}_2-\mathbf{r}_1)+\ldots+\mathbf{k}_n\cdot(\mathbf{r}_n-\mathbf{r}_{n-1})+\mathbf{k}_n\cdot(\mathbf{r}_o'-\mathbf{r}_n) \tag{5.5}$$

where we denote $\mathbf{k}_0$ and $\mathbf{k}_n$ as the input and outgoing wavevectors, and $\mathbf{k}_1$, $\mathbf{k}_2$, ...$\mathbf{k}_{n-1}$ as the intermediate wavevectors. We further define the intermediate *scattering* wavevector $\mathbf{q}_i \equiv \mathbf{k}_i - \mathbf{k}_{i-1}$, and from fig. 5.1 we see that

$$\phi_p = -\mathbf{k}_0\cdot\mathbf{r}_o + \mathbf{k}_n\cdot\mathbf{r}_o' + \mathbf{q}_1\cdot\mathbf{r}_1 + \ldots + \mathbf{q}_n\cdot\mathbf{r}_n \tag{5.6}$$

Thus, from Eq. (5.4) we obtain the total phase shift which is the sum of the contributions from the individual scattering events plus a constant phase factor, $-\mathbf{k}_0\cdot\mathbf{r}_o + \mathbf{k}_n\cdot\mathbf{r}_o'$. We define the amplitude form factor as

$$f(q) \equiv \frac{|E_{sc}(q)|}{|E_{in}|} \tag{5.7}$$

where $E_{sc}(q)$ is the field scattered at the wavevector q and E_{in} the field incident on the scattering particles. Thus, the field contribution of the path p is

$$E_p = E_o e^{i(-\mathbf{k}_o\cdot\mathbf{r}_o + \mathbf{k}_n\cdot\mathbf{r}_o')} \prod_{j=1}^{n} f(q_j) e^{i\mathbf{q}_j\cdot\mathbf{r}_j} \tag{5.8}$$

where E_o is the output electrical field.

Before discussing the theory of DWS for correlated systems, we first review the theory of DWS for uncorrelated systems, for the purpose of illustrating the procedure used in the derivation. We first show that the intensity correlation function, $G_2(\tau)$, can be obtained from the field autocorrelation function, $G_1(\tau)$. We calculate the contribution of an arbitrary optical path to $G_1(\tau)$ and then obtain the full $G_1(\tau)$ by summing over the

contributions of all paths. Finally, we use a similar procedure to derive the theory of DWS for correlated systems.

For an uncorrelated system, the scattering intensity is given by

$$I=\sum_{pp'} E_p E_{p'}^* \tag{5.9}$$

As the phase of E_p of different path, p, is random, the resultant scattering intensity, I, is also random depending upon the configurations of the particles inside the sample. The ensemble-averaged intensity, defined as an average over all particle configurations, is given by

$$\langle I\rangle=\sum_{p,p'}\langle E_p E_{p'}^*\rangle=\sum_{p}\langle E_p E_p^*\rangle \tag{5.10}$$

where $\langle\rangle$ indicates the ensemble average. The second equality follows from our assumption that the positions of the scatterers are uncorrelated and that the relative phases of fields from different paths are uncorrelated and therefore average to zero. Thus, the only non-vanishing terms in summation over $\langle E_p E_{p'}^*\rangle$ are those with $p=p'$, where the random phases of the fields are canceled by their conjugates. The argument in Eq. (5.10) is the contribution of path p to the total scattering intensity, $\langle I\rangle$, which is obtained by using Eq. (5.8).

$$\langle E_p E_p^*\rangle = I_o \prod_{j=1}^{n} F(q_j) \tag{5.11}$$

where $F(q)=f(q)f^*(q)$ is the form factor, and $I_o=E_oE_o^*$ is the output intensity. For large n, we can relax the condition that the sum of the intermediate scattering vectors must equal the difference between the incident and exiting wavevectors, $\sum_{i=1}^{n}\mathbf{q}_i=\mathbf{k}_n-\mathbf{k}_0$. Thus, we can assume that each scattering event is independent, and so the contribution of each path is the product of the contribution from each independent scattering event, averaged over angles. Thus, we have

$$\langle E_p E_p^* \rangle = I_o \langle F(q) \rangle_q^n$$

where $\langle\rangle_q$ indicates the average over all scattering angles. By definition, $\langle F(q)\rangle_q$ can be written as

$$\langle F(q)\rangle_q = \frac{\int F(q)\mathrm{d}\Omega}{\int \mathrm{d}\Omega} = \frac{\int F(q) q \mathrm{d}q}{8k_0^2} \qquad (5.12)$$

where Ω is the solid angle. The second equality follows from the relationship of $\mathrm{d}\Omega=\sin\theta \mathrm{d}\theta \mathrm{d}\phi = q\mathrm{d}q\mathrm{d}\phi/4k_0^2$, where θ and ϕ are the angular coordinates. We denote $Q(n)$ as the number of paths with n scattering events. The total contribution of paths of n scattering events, $I(n)$, is $I_oQ(n)\langle F(q)\rangle_q^n$. The total scattering intensity is the sum of contribution of all scattering events.

$$\langle I \rangle = \sum_{n=1}^{\infty} I(n) \qquad (5.13)$$

For large n, the transport of light through a sample is accurately described within the diffusion approximation. This allows $I(n)$ to be calculated using the diffusion equation.

The temporal autocorrelation function of the scattered intensity, $G_2(\tau)$, is defined as

$$G_2(\tau) \equiv \langle I(0)I(\tau)\rangle = \sum_{p,p',p'',p'''} \langle E_p(0)E^*_{p'}(0)E_{p''}(\tau)E^*_{p'''}(\tau)\rangle \qquad (5.14)$$

where τ is the delay time. Once again, because the relative phases of fields are random, the leading non-zero terms are those with $p=p'$ and $p''=p'''$ or $p=p'''$ and $p'=p''$. Then Eq. (3.5) factorizes:

$$G_2(\tau) \equiv \langle I(0)I(\tau)\rangle = \sum_{p,p',p'',p'''} \langle E_p(0)E^*_{p'}(0)\rangle \delta_{p,p'} \langle E_{p''}(\tau)E^*_{p'''}(\tau)\rangle \delta_{p'',p'''}$$

$$+ \sum_{p,p',p'',p'''} \langle E_p(0)E^*_{p'''}(\tau)\rangle \delta_{p,p'} \langle E_{p''}(\tau)E^*_{p'}(0)\rangle \delta_{p',p''}$$

$$= \langle I\rangle^2 + \left| \sum_p \langle E_p(0)E^*_p(\tau)\rangle \right|^2 \qquad (3.6)$$

For later use, we define

$$g_2(\tau) \equiv \frac{G_2(\tau)}{\langle I\rangle^2} - 1 \qquad (3.7)$$

and

$$g_1(\tau) \equiv \frac{\sum_p \langle E_p(0)E^*_p(\tau)\rangle}{\langle I\rangle} \qquad (5.15)$$

From Eq. (3.6), we see that $g_2(\tau)$ and $g_1(\tau)$ are related:

$$g_2(\tau)=|g_1(\tau)|^2 \qquad (5.16)$$

This equation, known as the Siegert relation, allows us to obtain intensity correlation functions from calculations of the field correlation functions. Thus, in subsequent

sections we always calculate the field correlation functions and use Eq. (5.32) to obtain intensity correlation functions for comparison with our experiments.

To calculate these autocorrelation functions we first determine the contribution of a single diffusive light path due to the particle motion inside the sample. This corresponds to calculating the argument of the summation in Eq. (5.15). Then the contributions of all paths, weighted by the distribution of the paths, are summed to obtain the desired correlation function. Using Eq. (5.8), the contribution of path p , denoted as $G_p(\tau)$, is given by

$$G_p(\tau)=\langle E_p(\tau)E_p^*(0)\rangle=I_o\left\langle \prod_{j=1}^{n} F(q_j)e^{i\mathbf{q}_j\bullet\Delta\mathbf{r}_j(\tau)} \right\rangle \qquad (5.17)$$

where $\Delta\mathbf{r}_i(\tau) = \mathbf{r}_i(\tau) - \mathbf{r}_i(0)$ is the distance the i^{th} particle moves in a time τ. The argument of the exponential,

$$\Delta\Phi^{(n)}(\tau) = \sum_{i=1}^{n}\mathbf{q}_i\,\Delta\mathbf{r}_i(\tau) \qquad (5.18)$$

represents the aggregate phase shift of the scattered light due to the motion of all n scatterers in the time interval τ. For n large, we again take a statistical approach and consider each individual scattering events as independent. As the fields belonging to different paths add incoherently, the average contribution to the normalized autocorrelation function of all paths of order n is

$$G_p(\tau)=I_oQ(n)\left\langle F(q)e^{i\mathbf{q}\bullet\Delta\mathbf{r}(\tau)}\right\rangle_q^n \qquad (5.19)$$

Here $\langle\rangle$ denotes averages over both the particle displacement, $\Delta\mathbf{r}(\tau)$, and the distribution of wavevectors $\mathbf{q}$. Furthermore, the large number of scattering events in each path greatly simplifies the evaluation of the averages in Eq. (5.19). At very small τ where $\mathbf{q}\cdot\Delta\mathbf{r}(\tau)\ll 1$, we can expand the right side of Eq. (5.19)

$$
\begin{aligned}
& I_0 Q(n)\left\langle F(q) e^{i\mathbf{q}\cdot\Delta\mathbf{r}(\tau)}\right\rangle_q^n \\
& \cong I_0 Q(n)\left\langle F(q)\left[1 - i\mathbf{q}\cdot\Delta\mathbf{r}(\tau) - \frac{q^2\cdot\Delta r^2(\tau)}{6}\right]\right\rangle_q^n \\
& \cong I_0\, Q(n)\, \langle F(q)\rangle_q^n e^{-n\bar{q}^2\langle\Delta r^2(\tau)\rangle/6} \\
& = I(n)\, e^{-n\bar{q}^2\langle\Delta r^2(\tau)\rangle/6}
\end{aligned}
\tag{5.20}
$$

where

$$
\bar{q}^2 \equiv \frac{\langle F(q)q^2\rangle_q}{\langle F(q)\rangle_q} = 2k_0^2\frac{\ell}{\ell^*} \tag{5.21}
$$

For simple diffusion, $\langle\Delta r^2(\tau)\rangle = 6D\tau$ where D is the diffusion coefficient of the particles. The field autocorrelation function, $g_1(\tau)$, is obtained by summing over contributions of all paths.

$$
g_1(\tau) = \frac{\sum_{n=1}^{\infty} I(n)\, e^{-n2k_0^2\frac{\ell}{\ell^*}\langle\Delta r^2(\tau)\rangle/6}}{\langle I\rangle} = \sum_{n=1}^{\infty} P(n)\, e^{-nk_0^2\frac{\ell}{\ell^*}\langle\Delta r^2(\tau)\rangle/3} \tag{5.22}
$$

where $P(n)=I(n)/\langle I\rangle$ is the n^{th} order fraction of the total scattering intensity $\langle I\rangle$. For simplicity, we pass to the continuum limit by approximating $n=s/\ell$, where s is the path length.

$$g_1(\tau) = \int_0^\infty dsP(s)\, e^{-\frac{s}{\ell^*}k_0^2 \langle \Delta r^2(\tau)\rangle/3} \qquad (5.23)$$

where $P(s)$ is calculated by solving the diffusion equation using the boundary conditions discussed in Chapter 3. Thus we establish the relationship between the particle dynamics and the autocorrelation functions.

We use a similar procedure to derive the theory of DWS for interacting systems. Because of the particle correlations, the phases of different paths are no longer uncorrelated. Paths within a radius of a correlation length, ξ, are correlated. Therefore we define a *tube* in which one path is not separated by the distance ξ from another path. We first calculate the contribution of the tube to the scattering intensity and the autocorrelation function. We then sum over all possible tubes to obtain the desired autocorrelation functions. The ensemble averaged intensity is

$$\langle I\rangle = \sum_{p,p'} \langle E_p E_{p'}^*\rangle = \sum_t \left[\sum_{|p-p'|<\xi} \langle E_p E_{p'}^*\rangle \right] \qquad (5.24)$$

where t is a tube and ξ the sample correlation length. The second equality follows from our assumption that the positions of particles are correlated only over a length scale of ξ and that the phases of fields from paths separated by more than ξ are uncorrelated and therefore average to zero. Equation (5.24) reflects the fact that different paths must be close to each other to contribute to the total average intensity. The only non-vanishing terms from Eq. (5.24) are those with p and p' separated by no more than ξ. For uncorrelated systems, a tube is equivalent to a path and, thus, Eq. (5.10) is recovered

from Eq. (5.24). The argument in the right side of Eq. (5.24) is the contribution of a tube, I_t, given by

$$I_t = \sum_{|p-p'|<\xi} \langle E_p E_{p'}^* \rangle = I_o \sum_{|p-p'|<\xi} \langle \prod_{j=1}^{n} f(q_j) f^*(q'_j) e^{-i\mathbf{q}_j \cdot \mathbf{r}_j + i\mathbf{q}'_j \cdot \mathbf{r}'_j} \rangle \quad (5.25)$$

where $I_o = E_o E_o^*$ is the incident intensity, and n is the number of scattering events. As expected, Eq. (5.25) shows that the average intensity is modified by the correlation of the scatterers. In general, Eq. (5.25) is a many-point correlation function which can not be written as an average of the static structure factor, $S(q)$, as the different scattering centers may be correlated. However, there exist two cases where $\langle I \rangle$ can be written as an average of $S(q)$. The first is when the interparticle distance, d, is large compared to the wavelength of light, λ, and the second is when the scattering mean free path, ℓ, is large compared to the correlation length, ξ.

In the first case, large interparticle distances ensure that the phase difference for two different paths in the tube is always large compared with the wavelength of light. Therefore, the contribution of this pair of paths varies very rapidly with the path length difference and thus, these contributions are averaged to zero. Therefore, although the particle positions are correlated, they can be treated just like uncorrelated systems. Thus, all the discussion of uncorrelated systems apply to these systems. This category covers dilute systems as well as particles whose diameter is large compared to λ.

In the second case, the assumption, $\ell >> \xi$, ensures that successive scattering centers can be regarded as uncorrelated. Furthermore, $\ell >> \xi$ ensures that the tube width is sufficiently narrow so that $\mathbf{q} \cong \mathbf{q}'$. Thus, Eq. (5.25) factorizes.

$$I_t = I_o \prod_{j=1}^{n} \langle F(q_j) \sum_{\mathbf{r}_j, \mathbf{r}'_j} e^{-i\mathbf{q}_j \cdot [\mathbf{r}_j - \mathbf{r}'_j]} \rangle = I_o \prod_{j=1}^{n} N \langle F(q_j) S(q_j) \rangle \qquad (5.26)$$

where N is the number of particles in a scattering volume and $S(q)$ is the static structure factor, defined as

$$S(q) = \frac{1}{N} \langle \sum_{\mathbf{r},\mathbf{r}'} e^{-i\mathbf{q} \cdot [\mathbf{r} - \mathbf{r}']} \rangle \qquad (5.27)$$

where the summation is over all particles in the correlation volume. Equation (5.26) shows that the contribution of a tube is modified by the structure factor. For n large, we again take a statistical approach by averaging over all scattering angle, and obtain

$$I_t = I_o N^n \langle F(q) S(q) \rangle_q^n \qquad (5.28)$$

Since there are N^n number of paths in a tube with n scattering events and N particles in a correlation volume, the average contribution of one path of n events is $I_o \langle F(q) S(q) \rangle_q^n$. The total contribution of paths of n scattering events, $I(n)$, is $Q(n) I_o \langle F(q) S(q) \rangle_q^n$. Thus we obtain the scattering intensity by summing over all possible tubes.

$$\langle I \rangle = \sum_{t} N^n \langle F(q)S(q) \rangle_q^n = \sum_{n=1}^{\infty} I_o Q(n) \langle F(q)S(q) \rangle_q^n = \sum_{n=1}^{\infty} I(n) \quad (5.29)$$

For uncorrelated system where $S(q) = 1$, we recover the expressions for uncorrelated systems.

Our purpose is to calculate the intensity autocorrelation functions of the multiply scattered light as the particles undergo Brownian motion. In previous case, we showed that the intensity autocorrelation function can be obtained from the field autocorrelation function for uncorrelated systems. Here we show that for correlated systems this relation also holds provided that the geometric dimensions of the sample are much larger than the correlation length. The autocorrelation function of a scattered intensity is defined as

$$G_2(\tau) \equiv \langle I(0)I(\tau) \rangle = \sum_{p,p',p'',p'''} \langle E_p(0) E^*_{p'}(0) E_{p''}(\tau) E^*_{p'''}(\tau) \rangle \quad (5.30)$$

where τ is the delay time. Because the phases of fields from paths separated by distances larger than ξ are uncorrelated, the leading non zero terms are paths with $|p\text{-}p'| < \xi$ and $|p''\text{-}p'''| < \xi$ or $|p\text{-}p'''| < \xi$ and $|p'\text{-}p''| < \xi$, where $|p\text{-}p'| < \xi$ indicates that paths p and p' are not separated by a distance longer than ξ. Following our assumption that the correlation length is much smaller than the sample dimensions, the contribution of 4 distinct paths staying in one correlation volume is small, and therefore can be neglected. Thus, Eq. (5.30) factorizes:

$$G_2(\tau)=\sum_{p,p'}\langle E_p(0)E_p^*(0)\rangle\sum_{p'',p'''}\langle E_{p''}(\tau)E_{p'''}^*(\tau)\rangle+\sum_{p,p'''}\langle E_p(0)E_{p'''}^*(\tau)\rangle\sum_{p',p''}\langle E_{p'}^*(0)E_{p''}(\tau)\rangle$$

$$=\langle I\rangle^2+\left|\sum_{p,p'}\langle E_p^*(0)E_{p'}(\tau)\rangle\right|^2 \qquad (5.31)$$

Once again, we use the definitions of $g_1(\tau)$ and $g_2(\tau)$. From Eq. (5.31), we see that $g_2(\tau)$ and $g_1(\tau)$ are again related:

$$g_2(\tau)=|g_1(\tau)|^2 \qquad (5.32)$$

Equation (5.32) shows that for correlated systems we can also obtain the intensity autocorrelation function from the field autocorrelation function. In deriving Eq. (5.32) we assume that the detection area is a point. In reality, since we always detect scattered light from a small but finite area, the effect of the spatial averaging must be considered. It can be shown that Eq. (5.32) is modified to

$$g_2(\tau)=\beta|g_1(\tau)|^2 \qquad (5.33)$$

where the parameter β is a function of detection area.

To calculate the autocorrelation function for correlated systems, we first determine the contribution of one tube and then sum over all tubes. The contribution of a tube, $g_t(\tau)$, is given by

$$G_t(\tau) = \sum_{|p-p'|<\xi} \langle E_p(0) E^*_{p'}(\tau) \rangle$$

$$= I_o \sum_{|p-p'|<\xi} \langle \prod_{j=1}^{n} F(q_j) e^{i\mathbf{q}_j \cdot [\mathbf{r}_j(\tau) - \mathbf{r}'_j(0)]} \rangle \qquad (5.34)$$

Once again, we used the assumption, $\ell >> \xi$, so that $\mathbf{q}'=\mathbf{q}$. Furthermore, as the successive scattering centers are uncorrelated, Eq. (5.34) factorizes.

$$G_t(\tau) = I_o \sum_{|p-p'|<\xi} \prod_{j=1}^{n} \langle F(q_j) e^{i\mathbf{q}_j \cdot [\mathbf{r}_j(\tau) - \mathbf{r}'_j(0)]} \rangle = I_o \prod_{j=1}^{n} N \langle F(q_j) S(q_j, \tau) \rangle \qquad (5.35)$$

where $S(q,\tau)$ is called dynamic structure factor, defined as

$$S(q,\tau) = \frac{1}{N} \langle \sum_{\mathbf{r},\mathbf{r}'} e^{-i\mathbf{q} \cdot [\mathbf{r}(\tau) - \mathbf{r}'(0)]} \rangle \qquad (5.36)$$

For n large, we again can take a statistical approach. The contribution of each scattering event is averaged over all possible scattering angles. We obtain the average contribution of a tube of n scattering events.

$$G_t(\tau) = I_o N^n \langle F(q) S(q,\tau) \rangle_q^n \qquad (5.37)$$

Since a tube of n scattering events has N^n number of paths, the average contribution of each path, $g_n(\tau)$, is $I_o\langle F(q)S(q,\tau)\rangle_q^n$. Similarly, the total contribution of paths of n scattering events is $Q(n)I_o\langle F(q)S(q,\tau)\rangle_q^n$. Finally, we obtain the autocorrelation function by summing over all possible tubes.

$$G_1(\tau)=\sum_t I_o N^n\langle F(q)S(q,\tau)\rangle_q^n = I_o\sum_{n=1}^{\infty} Q(n)\langle F(q)S(q,\tau)\rangle_q^n \qquad (5.38)$$

To study the particle dynamics by measuring the correlation function, we must establish the relationship between $g_1(\tau)$ and the particle motion. To do this we first do a short time expansion of $S(q,\tau)$. For ergodic systems where the time average is equivalent to the ensemble average, it can be shown[13] that the following theorem is true

$$\frac{d^2\langle A(0)B(\tau)\rangle}{d^2\tau}=-\langle \dot{A}(0)\dot{B}(\tau)\rangle \qquad (5.39)$$

From Eq. (5.40), we have

$$\frac{d^2S(q,\tau)}{d^2\tau}=\frac{1}{N}\sum_{i,j=1}^{N}\langle v_j(0)\ v_i(\tau)e^{-iq\,(r_i(\tau)-r_j(0))}\rangle \qquad (5.40)$$

where v denotes the velocity. At times short enough to observe the decay of the velocity correlation function, the particle has not moved significantly from its position at τ=0. Eq. (5.40) becomes

$$\frac{d^2S(q,\tau)}{d^2\tau}=\frac{1}{N}\sum_{i,j=1}^{N}\langle \mathbf{v}_j(0)\ \mathbf{v}_i(\tau)e^{-iq\,(\mathbf{r}_i(0)-\mathbf{r}_j(0))}\rangle$$

$$=-\langle v(0)\ v(\tau)\rangle-\frac{1}{N}\sum_{i\neq j}^{N}\langle \mathbf{v}_j(0)\ \mathbf{v}_i(\tau)e^{-iq\,(\mathbf{r}_i(0)-\mathbf{r}_j(0))}\rangle \qquad (5.41)$$

To obtain $S(q,\tau)$ at short time, we need to integrate Eq. (5.41) twice. We use the following relationships

$$\Delta r(\tau)=\int_0^{\tau} v(t)dt \qquad (5.42)$$

and

$$\langle \Delta r^2(\tau)\rangle=6\int_0^{\tau}dt_1\int_0^{t_1}\langle v(0)\ v(t_2)\rangle dt_2$$

$$\langle \Delta \mathbf{r}_j(\tau)\ \Delta \mathbf{r}_i(\tau)e^{-iq\bullet(r_i(0)-r_j(0))}\rangle=\frac{1}{6}\int_0^{\tau}dt_1\int_0^{t_1}\langle v_j(0)\ v_i(t_2)e^{-iq\bullet(r_i(0)-r_j(0))}\rangle dt_2 \qquad (5.43)$$

Finally, we obtain

$$S(q,\tau)=S(q)\left\{1-\frac{q^2}{6S(q)}H(q,\tau)\right\} \tag{5.44}$$

where $H(q,\tau)$ is defined as

$$H(q,\tau)\equiv\langle\Delta r^2(\tau)\rangle+\frac{1}{N}\sum_{i\neq j}\langle\Delta r_j(\tau)\ \Delta r_i(\tau)e^{-iq\ [r_i(0)-r_j(0)]}\rangle \tag{5.45}$$

For q large compared with the typical interparticle spacing, the $i\neq j$ terms in Eq. (5.45) are negligible compared with the $i=j$ terms. Thus for large q, $H(q,\tau)$ reduces to the mean square displacement, $\langle\Delta r^2(\tau)\rangle$. Physically, this reflects the fact that $H(q,\tau)$ measures the correlation of the displacement between particles at the length scale of $1/q$. If the length scale of $1/q$ is small compared with the particle diameter, $H(q,\tau)$ only measures the self diffusion of the particles, regardless of the particle concentration. Similarly, the structure factor, $S(q)$, at large q is unity as it probes the structure of one particle. Thus for large q, we obtain

$$H(q,\tau)=\langle\Delta r^2(\tau)\rangle$$

$$S(q)=1 \tag{5.46}$$

The autocorrelation function for the multiple scattering may be obtained by substituting Eq. (5.44) into Eq. (5.38).

$$g_1(\tau)=\frac{\sum^{n} I_0Q(n)\langle F(q)S(q)[1-\frac{H(q,\tau)q^2}{6S(q)}]\rangle_q^n}{\langle I\rangle}$$

$$= \frac{\sum_n I_0 Q(n) \left[\langle F(q)S(q) \rangle_q^n - \frac{\langle F(q)H(q,\tau)q^2 \rangle_q^n}{6} \right]}{\langle I \rangle}$$

$$= \frac{\sum_n I_0 Q(n) \langle F(q)S(q) \rangle_q^n \left[1 - \frac{\langle F(q)H(q,\tau)q^2 \rangle_q^n}{6\langle F(q)S(q) \rangle_q^n} \right]}{\langle I \rangle}$$

$$= \frac{\sum_n I(n) e^{-\frac{\langle F(q)H(q,\tau)q^2 \rangle_q^n}{6\langle F(q)S(q) \rangle_q^n}}}{\langle I \rangle}$$

$$= \sum_n P(n) e^{-\frac{\langle F(q)H(q,\tau)q^2 \rangle_q^n}{6\langle F(q)S(q) \rangle_q^n}} \qquad (5.47)$$

Once again, $P(n)$, defined as $I(n)/\langle I \rangle$, is calculated by using the diffusion equation. For convenience we define the average of the scattering wavevector as

$$\overline{Y}(q) \equiv \frac{\langle F(q)Y(q)q^2 \rangle_q}{\langle F(q)q^2 \rangle_q} = \frac{\int dq F(q) q^3 Y(q)}{\int dq F(q) q^3} \qquad (5.48)$$

The extra q is from the fact that we integrate over all scattering angles. The key to the solution of Eq. (5.47) is the determination of $P(n)$. This task is greatly simplified if we pass to continuum limit. Thus we approximate the sum over n by an integral over the path length $s=nl$, and we use the relationship[8]

$$l^* = 2k_o^2 l \frac{\langle F(q)S(q)\rangle_q}{\langle F(q)S(q)q^2\rangle_q} \tag{5.49}$$

We obtain

$$g_1(t) = \int_0^\infty ds P(s) e^{-\frac{s}{l^*}\frac{k_o^2 \overline{H}(q,\tau)}{3\overline{S}(q)}} \tag{5.50}$$

In this case, $P(s)$, is the fraction of the scattered photons which travel a path length s through the medium.

The intensity distribution of the total intensity, $P(s)$, depends the experimental geometry, the place where the incident light enters the sample, and the point from which the exiting light is collected. In our case we use the slab geometry. In the coordinate system shown in Fig. 5.2 the incident surface is at $z=0$, and the other side is at $z=L$ where L is the thickness of the slab. The incident light is focused to a point, $r_{in}=(0,0,0)$, on the surface of the slab and the scattered light is collected from the point, $r_{out}=(0,0,L)$, on the other side of the slab. The calculation of $I(s)$ can be determined by a thought experiment. Initially, we deposit a pulse, $f(x,y,z,t)=\delta(x,y,z,t)$, at r_{in} into the medium. Thus $I(s)$ is the flux exiting from r_{out} as a function of time $t=s/c$, where c is the speed of light. This can

be determined by solving the diffusion equation Eq. (5.3) together with the proper boundary conditions for the experimental geometry. Detailed discussions of the boundary conditions for this geometry have been given in Chapter 3. We choose the boundary conditions such that there is no incoming diffusive flux at the surfaces of the sample. Thus,

$$U-\frac{2l^*}{3}\frac{\partial U}{\partial z}=0 \qquad (z=0)$$

$$U+\frac{2l^*}{3}\frac{\partial U}{\partial z}=0 \qquad (z=L) \qquad (5.51)$$

The exiting flux is given by

$$I(s)=U-\frac{2l^*}{3}\frac{\partial U}{\partial z} \qquad (z=L) \qquad (5.52)$$

Rather than solving for $I(s)$, we notice that Eq. (5.50) is a Laplace transform of $I(s)$. Thus we need only solve the Laplace transform of the diffusion equation, simplifying our task. The solution is given by Carslaw and Jaeger[14] for this geometry and the boundary conditions, and the procedure of obtaining the solution of Eq. (5.50) has been discussed by in detail Pine *et al*[8]. Following their procedure, we obtain

$$g_1(t)=\int_{\frac{L}{l^*}\sqrt{\frac{k_o^2\overline{H}(q,\tau)}{S(q)}}}^{\infty}\left[A(s)\sinh(s)+e^{-s(1-l^*/L)}\right]ds \qquad (5.53)$$

For monodisperse hard sphere suspensions, the quantities $F(q)$, $S(q)$, and l^* can be calculated theoretically. Therefore, by measuring the autocorrelation function, we are able to extract the evolution of the quantity $\overline{H}(q,\tau)$ as a function of time.

In general, $\overline{H}(q,\tau)$ is not strictly equal to the mean square displacement. Physically, the autocorrelation function in multiple scattering does not measure self-diffusion, since multiply scattered light has components of all scattering angles. From Eq. (5.48) the weighting factor of $\overline{H}(q,\tau)$ is $F(q)q^3$. The form factor $F(q)$ favors small q whereas the factor q^3 favors large q. Fig. 5.3 shows $F(q)q^3$ as a function of qa where the form factor $F(q)$ is calculated with Mie theory and a is the particle radius. The scattering wavevector q ranges from 0 in forward scattering to $q_{max}=4k_0$ in backscattering. In the case of $a>>\lambda$, most of the weight is in the range where $1/q$ is large compared with the particle diameter. Physically, for suspensions of large spheres the interparticle spacing is sufficiently large, at least a particle diameter, that $\overline{H}(q,\tau)$ approximately equals the mean square displacement. For the same reason $\overline{S}(q)$ is approximately unity. Thus for large spheres Eq. (5.53) becomes

$$g_1(\tau)=\int_{\frac{L}{l^*}\sqrt{k_o^2\langle\Delta r^2(\tau)\rangle}}^{\infty}\left[A(s)\sinh(s)+e^{-s(1-l^*/L)}\right]ds \qquad (5.54)$$

For a given size and volume fraction of a hard sphere suspension, the value of l^* can be calculated. Therefore, for large spheres we can directly extract the mean square displacement from the autocorrelation functions. This conclusion for large spheres is consistent with our analysis for large spheres in the first case.

Although the theory outlined in this section applies only the systems at the two limits, it is quite general as most of systems of interests fall within these two limits. The first case covers both dilute systems and or systems with large particles. The second case covers small particles as they generally scatter light less strongly, and therefore, the scattering mean free path is long. Furthermore, the correlation length, ξ, is short as ξ is usually proportional to the particle diameter. Thus, DWS is a useful technique for the study of correlated systems.

5.3. PARTICLE DYNAMICS THEORY

In this section, we discuss the theory for the dynamics of hard sphere suspensions at very early times. The particles are assumed to be small enough to perform Brownian motion but are sufficiently large compared with the solvent molecules so the solvent may be described as an incompressible fluid. The Brownian motion of a colloidal particle arises from thermal agitation. At a fixed point of time $t=t_0$, a particle velocity is denoted as $\mathbf{v}(t_0)$. At very early times, meaning $t - t_0$ very small, the particle retains its original velocity, $\mathbf{v}(t_0)$. After suffering many random collisions with solvent molecules, the particle velocity rapidly decays and its motion becomes diffusive. At times long compared with the molecular collision time scale, the forces acting on the particle can be divided into a viscous drag by the solvent and a random force. We study the particle motion at time scales before it becomes diffusive. For simplicity, we first consider the Brownian motion of a *single* particle suspended in an unbounded fluid. We begin with a simple model which does not include the time dependence of the viscous drag. We then proceed to a more sophisticated model where the time dependence is fully taken into account. Finally, we consider a system of N hard spheres suspended in an incompressible fluid, and discuss the basic equations. We emphasize that no exact solution exists for a system with $N>2$.

We consider a spherical particle suspended in a unbounded fluid. The displacement, $\Delta\mathbf{r}(\tau)$, is given by

$$\Delta r(\tau) = \int_0^{\tau} dt\, v(t)$$

where v(t) is the instantaneous velocity. The mean square displacement, $\langle \Delta r^2(\tau) \rangle$, can be expressed in terms of the velocity autocorrelation function, $R(\tau)$, defined as,

$$R(\tau) \equiv \langle v(0) \cdot v(\tau) \rangle \tag{5.55}$$

as

$$\langle \Delta r^2(\tau) \rangle = 2 \int_0^{\tau} dt\, (t-\tau)\, R(\tau) \tag{5.56}$$

In the time scale of interest, numerous collisions between the particle and the fluid molecules have already taken place, and the motion of the particle can be described by the Langevin equation

$$m\frac{dv}{dt} = -f(t) + F(t) \tag{5.57}$$

where m is the mass of the particle. The force acted on the particle due to the collisions of the solvent molecules is divided into a viscous drag force, $-f(t)$, and a random force, F(t). The random force is assumed to be uncorrelated in time

$$\langle F(t)F(t') \rangle = A\delta(t-t') \tag{5.58}$$

where the amplitude, A, is chosen to ensure that the equipartition theory is satisfied,

$$\langle v^2 \rangle = \frac{k_B T}{m} \tag{5.59}$$

where k_B is the Boltzmann's constant and T is the absolute temperature. Eqs. (5.57) and (5.58) are so called fluctuation-dissipation (FD) theory. The simplest approach is to use the Stokes expression for the viscous drag [15]

$$f(t) = -\xi v(t) \tag{5.60}$$

The friction coefficient, ξ, is given by, $\xi = 6\pi\eta a$, where a is the radius of the particle, and η the viscosity of the fluid. Then from Eq. (5.57) the velocity correlation function is given by

$$R(\tau) \equiv \langle v(0)(\tau) \rangle = \frac{k_B T}{m} e^{-\tau/\tau_b} \tag{5.61}$$

With the assumption of a constant value for ξ, Eq. (5.57) results in an exponential decay of the velocity correlation function. The rate of decay is determined by the viscous damping time, $\tau_b = m/\xi$. For a 1μm polystyrene sphere suspended in water at a room temperature, $\tau_b = 0.23\mu s$. Thus a particle rapidly loses any memory of its original velocity and becomes diffusive at times longer than τ_b .

To correctly treat the behavior at the very shortest times, the frequency or time dependence of the viscous drag, ξ, must be included. This requires the full description of the velocity field of the fluid. The Brownian motion of the particles induce a flow in the fluid, characterized by the pressure and the velocity fields $p(\mathbf{r},t)$, $u(\mathbf{r},t)$. In macroscopic

hydrodynamics the conservation laws for mass and momentum in an incompressible fluid are

$$\nabla \cdot u = 0$$

$$\rho \frac{\partial u}{\partial t} + \rho(u \cdot \nabla)u - \eta \nabla^2 u + \nabla p = 0 \qquad (5.62)$$

Here ρ is the fluid density. This equation, known as Navier-Stokes equation, enables us to calculate the pressure and the velocity fields. In the case of the flow induced by the Brownian motion of the particles u is so small that the non-linear term, $\rho(u \cdot \nabla)u$, can be neglected. Therefore, Eq. (5.66) becomes

$$\nabla \cdot u = 0$$

$$\rho \frac{\partial u}{\partial t} - \eta \nabla^2 u + \nabla p = 0 \qquad (5.63)$$

The usual stick boundary conditions are such that the fluid velocity at the surface of the particles, $u(r,t)|_S$, equals the velocity of the particles, $v(t)$.

$$u(r,t)|_S = v(t) \qquad (5.64)$$

Once the $u(r,t)$ and $p(\mathbf{r},t)$ are determined, the viscous drag force acted on the particle can be calculated by

$$f(t) = \int_S \sigma \cdot ds \qquad (5.65)$$

where s denotes the surface of the particle and σ is the stress tensor, whose element are defined as

$$\sigma_{jk}=-p\delta_{jk}+\eta\left(\frac{\partial u_j}{\partial x_k}+\frac{\partial u_k}{\partial x_j}\right) \tag{5.66}$$

The solution is given by Landau and Lifshits[16]

$$f(t)=2\pi\rho a^3\left\{\frac{1}{3}\frac{dv}{dt}+\frac{3\eta v}{a^2}+\frac{3}{a}\sqrt{\frac{\eta}{\pi}}\int_{-\infty}^{t}\frac{dv\ d\tau}{d\tau\sqrt{t-\tau}}\right\} \tag{5.67}$$

Equation (5.67) shows that the drag force acting on the particle depends not only on the current particle velocity, but also its past history. Physically, this results from the fact that the fluid velocity field generated by the particle motion at earlier times will act back on the particle at later times. The Langevin equation for a single sphere in a infinite fluid can be obtained by substituting Eq. (5.67) into Eq. (5.57). The analytical solution of the velocity correlation function was obtained by Hinch[5]

$$R(\tau)=\frac{k_B T}{m}\frac{2\Sigma}{3\sqrt{5-8\Sigma}}\left[\alpha_+ e^{\alpha_+^2\tau}\,erfc(\alpha_+\tau)-\alpha_- e^{\alpha_-^2\tau}\,erfc(\alpha_-\tau)\right] \tag{5.68}$$

The ratio of particle to fluid density is given by $\Sigma=\rho'/\rho$, with $ercf(x)$ is the complex compliment of the error function, and

$$\alpha_\pm=\frac{3}{2}\frac{3\pm\sqrt{5-8\Sigma}}{1+2\Sigma} \tag{5.69}$$

At long times, the decay of $R(\tau)$ is algebraic instead of exponential,

$$\lim_{\tau\to\infty} R(\tau)=\frac{D_o}{2\tau_h\sqrt{\pi}}\left[\frac{\tau}{\tau_h}\right]^{-3/2} \tag{5.70}$$

where $D_o=k_BT/\xi$ is the Stokes value for the free diffusion coefficient, and the characteristic time $\tau_h=\rho a^2/\eta$ is the time the vorticity takes to diffuse a particle radius. This slow algebraic decay of $R(\tau)$ is called the "long time tail". Physically, the "long time tail" can be understood using the following simple picture. As the particle moves, it drags along the neighboring fluid. This results a flow field which favors the original direction of the particle motion. Therefore, the particle motion is more likely in the same direction as before.

The theory becomes much more complicated when there are more than one sphere in the fluid. Then, the flow field generated by one particle will be modified by the presence of other particles. This modified flow field acts back on the motion of the particle. These complex interactions between the particles through the fluid are called hydrodynamic interactions. To use the Langevin equation to calculate the motion of a particle, we must first determine the viscous drag acting on the particle. This requires the solution of Eq. (5.63) with boundary conditions reflecting the many-body interactions. The exact solutions for particle numbers $N>2$ are not available. The theory for two particles has been calculated by Clercx and Schram[10].

The essential goal of the hydrodynamic theory for two identical spheres in an unbounded fluid is similar to the one particle case: to calculate the viscous drag forces, $f_1(t)$ and $f_2(t)$, acting on the particles 1 and 2. The velocity and pressure fields are

obtained by solving the Navier-Stokes equation with stick boundary conditions on the two spheres. This is done by expanding the solution in terms of a complete set of the eigenfunctions for the Navier-Stokes equation. The expansion coefficients are determined such that the boundary conditions are satisfied. The viscous drag on the particles 1 and 2, $f_1(t)$ and $f_2(t)$, are then calculated by integrating over the stress tensor σ using Eq. (5.66). For the two particles, $f_1(t)$ is not only a function of the velocity particle 1, v_1, and the history of v_1, but also the velocity particle 2, v_2, and the history of v_2. This interaction between the particles is called the hydrodynamic interaction, and reflects the fact that the flow field around particle 1 is not only influenced by the particle 1 itself, but also by the motion of particle 2. Once the viscous drag forces are obtained, the velocity correlation functions can be calculated by solving the Langevin Equation. Finally, the velocity correlation function is averaged over all particle configurations. Because only two particles interactions are considered, the validity of the theory is limited to suspensions with low volume fractions. Clercx and Schram[10] numerically calculated the time derivative of the mean square displacement, $D(\tau)$, which they defined as $\frac{d\langle \Delta r^2(\tau)\rangle}{6d\tau}$ for volume fractions of 10%, 20%, and 30%. This quantity, $D(\tau)$, behaves very much like the quantity which we defined as the time dependent diffusion coefficient $D_S(\tau)=\frac{\langle \Delta r^2(\tau)\rangle}{6\tau}$. Both start from zero at τ=0, and both saturate to the same asymptotic value at long time limit. The calculation by Clercx and Schram[10] showed that for volume fractions ϕ up to 20%, $D(\tau)$ increases monotonically to its asymptotic value as a function of time. For ϕ=30%, $D(\tau)$ increases to a peak then decreases to a plateau.

An alternative approach was employed by Van Sarloos and Mazur[9], who calculated the frequency dependent mobility tensor $\mathbf{b}(\omega)$, in the low frequency or long time limit using a many particles hydrodynamic theory. The frequency dependent mobility tensor is the inverse of the frequency dependent resistance tensor. The frequency dependent

viscous drag force on the particles is the product of the resistance tensor and the particle velocity. Therefore, the velocity correlation function, $R(\tau)$, can be calculated from the mobility tensor. They found that at low frequency the mobility tensor has a $\omega^{1/2}$ dependence. From this they concluded that $R(\tau)$ should have a $\tau^{-3/2}$ behavior at long times. The limitation of their calculation is the range of the validity which only covers long times.

5.4. EXPERIMENTS

In our experiments we use uniform aqueous polystyrene spheres purchased from Duke Scientific. Polystyrene spheres suspended in water have very narrow size distributions and are commercially available in a various sizes. The spheres are stabilized by their surface charge so that the Coulomb interaction prevents particles from aggregating. The Coulomb interaction is screened by the presence of counter ions in the solution and the pair interaction potential decays exponentially as a function of the interparticle distance. The screening length, which is the inverse of the decay rate of the screened Coulomb interaction, is experimentally controllable by varying the concentration of counter ions. Higher concentrations of counter ion result in shorter screening lengths. For screening lengths short compared with the average interparticle surface to surface separation, the system behaves approximately as a hard sphere suspension. The average interparticle separation is proportional to the particle size, and thus is large for large spheres. Therefore, we can choose large spheres which have a screen length short compared with the interparticle separations yet still large enough to prevent particles to aggregation. To measure self diffusion with DWS at short times, we must also choose the particle sizes to be large compared with the wavelength of light.

We use two sets of sample. The first set has a diameter of 1.53μm, with a very small standard deviation of 0.018μm; the second set has a diameter of 3.09μm, with a standard deviation of 0.077μm. The density of the polystyrene is comparable to that of water at room temperature, ρ'=1.05 g/cm^3. The counter ion concentrations are sufficiently high to ensure a short screen length, resulting in a equivalent hard sphere interaction between particles. As purchased, the samples have a volume fraction of 10%. To obtain samples with lower volume fractions, we dilute with water. To obtain samples with higher

volume fractions, we let the particles fully sediment for a day and remove the required amount of water. To accurately determine the volume fraction, ϕ, of a sample, we measure the weight fraction, w, by weighing a small portion of the sample before and after drying it in a vacuum oven at room temperature. We calculate ϕ using the relationship

$$\phi=\frac{w}{w+\rho'(1-w)} \qquad (5.71)$$

The sample cells are glass cuvettes. The thickness, L, of the sample cells are between 1mm and 5mm. To ensure multiple scattering, we ensure that the ratio, L/l^* is greater 20.

The experimental setup is illustrated in Fig. 5.4. We use the transmission geometry. The light source is the 488-nm or 514.5-nm line from a Ar^+ ion laser. The laser beam is focused to a point on the surface of one side of the sample. The multiply scattered light from the surface of the other side of the sample is imaged one to one onto a 50-μm diameter pinhole using a lens. To ensure that only one speckle spot is detected we place a 1mm aperture before the lens to limit the solid angle of the collection optics. After the final pinhole, the scattered light is split equally with a beam splitter and directed to two photon-multiplier tubes (PMT). The signals from the two PMT are cross correlated, eliminating spurious correlation due to the effects of after pulsing in a single PMT. We use an ultra fast correlator, built specially for this experiment, with a sample time as short as 12.5ns. To obtain good statistics at these very short times, data are typically collected for about 12 hours. A rotational stage inverts the sample every 10 minutes to remix the sample and avoid sedimentation. The sample is immersed in a water bath maintained at a fixed temperature of 22.3±.05^{o}C.

We use a temperature stabilized etalon in the laser cavity to force the laser to operate at a single longitudinal frequency. There are two reasons for using a single frequency laser. First we need a long coherence length due to the multiple scattering where photons may travel over very long paths inside the sample. If the coherence length is not long enough, the photons that traveled long paths will not be coherent with photons that traveled shorter paths. This reduces the amplitude of the intensity fluctuations and distorts the shape of the correlation function. Second, we must eliminate the beating between adjacent longitudinal modes to ensure a stable intensity at the shortest time scales. For our Ar^+ ion laser, the longitudinal modes typically have a spacing of about 125Mhz, and the resultant amplitude fiuctuation due to their beating can be detected by our correlator, which operates at 80Mhz. We monitor the laser beam with a fast photo diode and use a fast oscilloscope to measure the mode beating of the laser output. The etalon is tuned until the mode beating disappears, ensuring that laser is operating at a single frequency.

One of the problems in measuring fluctuation correlation at very short times is the dead time of the detection system. Most amplifier discriminator used with PMTs require at least 30ns to recover after detecting a photon. This time scale is commonly called the "dead time". If a photon is registered at t=0, a second photon will be not registered during the dead time period. Therefore, the measured autocorrelation function $g_2(\tau)$ is zero for τ<30ns. Our cross correlation scheme eliminates this effect. Suppose at t=0 a photon arrives and is registered by PMT1. At any small time τ later, a second photon arrives. This second photon will have 50% chance to be detected by PMT2. Since PMT2 did not register a photon at t=0, it is able to register the second photon enable us to measure the desired intensity correlation function at times shorter than the dead time by cross correlating the signals from the two PMTs. What happens if the second photon

goes to PMT1 and gets lost? This effect has been shown[17] to be negligible as long as the average intensity is below 0.2 times the inverse of the dead time, which in our case is about 6Mhz. Our typical intensity is below 1 Mhz, far below the threshold.

We are able to measure correlation functions at both short and long times in a single measurement. The first 16 channels of our correlator are evenly spaced have sample times of 12.5ns. Then the correlator doubles the sample time every eight successive channels. This way, the correlator covers delay times from 12.5ns to a little more than a hour with 342 channels.

To obtain the desired autocorrelation function, $g_2(\tau)$, we must minimize all contributions to the noise. The measured autocorrelation functions have two kind of noise, statistical noise and systematic noise. The statistical noise can be reduced by making repetitive measurements over a long period of time. The systematic noise come mainly from noise on the input laser intensity. The scattered intensity, $I_S(t)$, therefore has superimposed on it an additional fluctuation due to the laser noise,

$$I_S(t)=I(t)n(t) \tag{5.72}$$

where $I(t)$ is the system response and $n(t)$ is the laser noise. The measured autocorrelation function $g_S(\tau)$ is

$$g_S(\tau)=\frac{\langle Is(0)Is(\tau)\rangle}{\langle I_S\rangle^2} - 1 = \beta(N_2(\tau) + 1)\,|g_1(\tau)|^2 + N_2(\tau) \tag{5.73}$$

where the noise correlation function, $N_2(\tau)$, is defined as

$$N_2(\tau)\equiv\frac{\langle n(0)n(\tau)\rangle}{\langle n\rangle^2}-1 \qquad (5.74)$$

Usually the noise $N_2(\tau)$ is much smaller than one. Therefore, Eq. (5.73) means that the measured autocorrelation function is the sum of the desired autocorrelation function $\beta g_2(\tau)$ and the noise correlation function $N_2(\tau)$. To correct for this systematic error, we need to know $N_2(\tau)$. This can be accomplished if $N_2(\tau)$ and $g_2(\tau)$ have very different decay times. If $N_2(\tau)$ decays much slower than $g_2(\tau)$, we can extract $N_2(\tau)$ from $g_S(\tau)$ at long times where $g_2(\tau)$ already decays to zero. On the other hand, if $N_2(\tau)$ decays much faster than $g_2(\tau)$, $N_2(\tau)$ decay to zero before $g_2(\tau)$ decays. An extreme example is white noise where $N_2(\tau)=0$ for $\tau\neq 0$. Unless the laser noise is known, or has a very different decay time from that of $g_2(\tau)$, the effect of the noise can be serious. In addition, a smaller intercept, β, will also reduce the signal to noise ratio.

The noise $N_2(\tau)$ of our laser intensity is typically $\leq 10^{-3}$. The time scale of the noise fluctuations is several milliseconds which is about one decade longer than the decay time of $g_2(\tau)$. A typical measured autocorrelation function, $g_s(\tau)$, is shown in log-log plot as a function of time in Fig. 5.5. There are two separable time scales here, enabling us to subtract the laser noise. We use an exponential form to approximate the behavior of $N_2(\tau)$.

$$N_2(\tau)=Be^{-\tau/T} \qquad (5.75)$$

where B and T are fitting parameters. From Eq. (5.73) one can see that at times long compare with the decay time of $g_1(\tau)$, $g_s(\tau)$ is the same as $N_2(\tau)$. We fit $N_2(\tau)$ to Eq. (5.75) to obtain the parameter B and T. We then use a third order polynomial fit to a few points near $\tau=0$ to obtain the intercept β. Finally we again use Eq. (5.73) to extract $g_1(\tau)$.

To obtain the mean square displacement, $\langle \Delta r^2(\tau) \rangle$, we numerically invert $g_1(\tau)$ using the formula predicted for DWS in this transmission geometry Eq. (5.54). The only parameter in the formula is the transport mean free path, ℓ^*, which is calculated using Mie theory. This is done by numerically looking for the roots, $\langle \Delta r^2(\tau) \rangle$, for $g_1(\tau_n)$ so that the Eq. (5.36) holds. The time dependent velocity correlation function can then be obtained by numerically differentiating the data two times. However, numerical differentiation of the data amplifies the high frequency noise as the noise is multiplied by the frequency. This artifact effect can be eliminated by smoothing the data before differentiating. We fit a three order polynomial to every three points of $\langle \Delta r^2(\tau) \rangle$ to smooth the data, and differentiate the fit to obtain the derivative.

5.5. RESULTS

We first show our results for samples at very low volume fractions where we expect particles to behave like a single particle in an infinite fluid. Here the particles are separated so far apart that the interparticle interactions can be neglected. We then show the effect of the hydrodynamic interactions on the short time motion as we increase the volume fractions.

To demonstrate the power of DWS to probe motion on very short length scales, we plot the square root of the mean square displacement as a function of time for a sample with d=1.53μm and ϕ=2.1% in Fig. 5.6. The range of $\sqrt{\langle \Delta r^2(\tau) \rangle}$ probed is from ~1Å at times below 10^{-7} seconds to over 100 Å at times above 10^{-4} seconds . This is in sharp contrast to the traditional dynamic light scattering which typically probes length scales comparable to a wavelength, which, in our case, is 4,880 Å. This figure clearly illustrates the power of DWS to probe motion on very short length scales. The noises at very early times demonstrates that the resolution of the length scale in this experiment is on the order of 1Å. There is also some noise at very long times, as the correlation function has decayed nearly to the level of the noise of the laser.

In order to compare our experiment with the theory developed for one particle suspended in an infinite fluid. we plot the time dependent diffusion coefficient $D_s(\tau)=\langle \Delta r^2(\tau) \rangle/6\tau$ normalized by the Einstein-Stokes value D_0 in Fig 5.7. As expected, the data starts from zero at τ=0 and slowly approaches unity at long times, reflecting the very slow decay of the velocity correlation function of the particle.. The solid line through the data is the calculation of Eq. (5.68), which takes into account the retarded hydrodynamic interaction. It is in excellent agreement with the data. By contrast, the dashed line is the theoretical prediction with out considering the retarded

hydrodynamic interaction between the fluid and the particle. It obviously rises too fast by comparison with the data.

The data are of sufficient quality that we can numerically differentiate them to obtain the velocity correlation function, $R(\tau)$. We show a plot of $R(\tau)$ vs time in Fig. 5.8 for the same sample described above. The straight dashed line above the data indicates a $\tau^{-3/2}$ behavior. The data clearly show the $\tau^{-3/2}$ decay of the long time tail, reflecting the pronounced effect of the retarded interaction between the fluid and particles. The solid line through data is the theoretical calculation, Eq. (5.68), and is in excellent agreement with the experimental data. We emphasize that there are *no* fitting parameters in the calculation.

As we increase the particle volume fraction, the hydrodynamic interactions between particles become more important. This is shown in Fig 5.9 where we plot $D_s(\tau)/D_o$ for several samples with the volume fractions, ϕ, ranging from 2.1% to 25.6%, we also include, by the dashed line, the theoretical calculation for $\phi=0$. The data for all volume fractions start from zero at $\tau=0$ and saturate at long times to their asymptotic values, $D_s(\phi)/D_o$. The data for samples with higher ϕ are always lower than those with lower ϕ. At earlier times, the data for all ϕ, though noisy, seem to follow the calculation for $\phi=0$. This reflects the fact that the wake generated from one particle needs time to travel to its nearest neighboring particles. Before the wake reaches the neighbors, the particle does not feel their presence. This sets the time scale for hydrodynamic interactions. At later times, the data for higher ϕ deviate from the curve for $\phi=0$ with the higher volume fraction data deviating earlier than those with lower ϕ. Presumably this reflects the fact that the interparticle spacing is shorter for samples with a higher volume fraction, and therefore, the wake propagates to the other particle earlier. The fact that the asymptotic value of $D_s(\tau)$ is smaller for higher volume fraction indicates the hydrodynamic interactions impede the motion of particles.

One of our most important findings is that the self-diffusion of Brownian particles in concentrated suspensions also has a "long time tail", regardless volume fractions. We again numerically differentiate $\langle \Delta r^2(\tau) \rangle$ to obtain the velocity correlation functions for the samples with higher ϕ. In Fig. 5.10 we show a logarithmic plot of the velocity correlation functions, $R(\tau)$, for several ϕ, values of 2.1%, 10.4%, and 25.6%. We observed that $R(\tau)$ decreases as ϕ increases. The solid line shown is the calculation for ϕ=0. The velocity correlation functions for particles at higher ϕ also clearly exhibit a $\tau^{3/2}$ decay. This demonstrates that the flow field around the particle still develops very slowly despite the presence of other particles. This is also in agreement with the theoretical predictions by Van Sarloos and Mazur[9].

In studying the evolution of the time dependent diffusion coefficient, we find a surprising scaling behavior for different volume fractions. We find that for the experimentally obtainable time range, the time dependent self-diffusion coefficients for all ϕ for both the 3.09μm and 1.53μm particles can be scaled onto the theoretical calculation for ϕ=0 as shown in Fig. 5.11, where we plot the scaled $D_s(\tau)$ as a function of scaled time. The vertical scaling factor for $D_s(\tau)$ is its asymptotic value, $D(\phi)$, while the horizontal scaling factor for the delay time τ is a volume fraction dependent time constant, $\tau_\nu(\phi)$, where $\tau_\nu(0)=\tau_h$. All data collapse onto the single universal curve determined by the theory for ϕ=0. This surprising scaling behavior suggests that not only is the long-time behavior of the particle dynamics at finite concentration similar to the one particle case, but so also are the dynamics at short time. Physically, Fig. 5.11 implies that the effect of hydrodynamic interactions makes the particle feel as if it were a single particle in a modified fluid.

To check the consistency of our data, we compare our measurements of the asymptotic value of $D_s(\phi)$ for different ϕ to the independent measurements obtained through tracer experiments[18].

We plot $D_s(\phi)/D_o$ *vs* ϕ in Fig 5.12. The solid line is the empirical relationship between the short time self-diffusion coefficient, $D_s(\phi)$, and ϕ.

$$\frac{D_s(\phi)}{D_o}=1-1.83\phi \qquad (5.76)$$

Eq. (5.76) is also consistent with the theoretical prediction by Batchlor[19] who considered the two particle hydrodynamic interactions. The theoretical prediction is valid only at low ϕ although experimentally this behavior is found to extend to much higher value of ϕ. Our data is consistent with Eq. (5.76).

In order to understand the physical meaning of the scaling constants for the time axis, we plot $\tau_\nu(\phi)$ normalized by τ_h vs ϕ in Fig. 5.13. We notice that the time scale of the evolution of the Brownian motion for one particle in an infinite fluid is the time the vorticity takes to diffuse a particle radius, $\tau_h=\rho a^2/\eta$. At higher volume fraction, the only parameter that can change is the viscosity $\eta(\phi)$ which is ϕ dependent. To determine if the time scale at higher volume fractions is determined by $\eta(\phi)$ we plot the high frequency, low strain values $\eta_\infty/\eta(\phi)$ as the solid line which are calculated by Beneeker and Mazur[20]. The solid line is in excellent agreement with the data. This behavior suggests the idea that the evolution of the Brownian motion in concentrated suspensions is determined by the bulk viscosity of the suspension. Physically, $\eta(\phi)$ is calculated on the length scales long compared to the particle dimensions. At long times, the scaling behavior makes sense because the vorticity generated by a particle has propagated through many particles in the fluid. As a result, the particles feel an average effect of the suspension. What is surprising is that the scaling behavior at times $<\tau_h$ where the vorticity has not yet diffuse a particle radius.

The only available theory is the two particle treatment given by Clercx and Schram[10]. To compare the predict behavior with our observations, we replot the numerical calculations of the

normalized time-dependent self-diffusion coefficient defined by Clercx and Schram[10] as, $\frac{1}{6D_0}\frac{d\langle\Delta r^2(\tau)\rangle}{6d\tau}$, for volume fractions of 0%, 10%, 20%, and 30% in Fig 5.14. All curves start from zero and saturate to the short time self-diffusion coefficients, consistent with our measurements. Also consistent with our observations, all curves seem to follow the same behavior as that of zero volume fraction limit at very short times. At longer times, and for volume fractions less than 20%, the predicted normalized self-diffusion coefficient increases monotonically to their asymptotic values. The short time self-diffusion coefficient is lower for higher volume fractions. This is again consistent with our experimental results. However, for ϕ=30%, the theory predicts the time-dependent self-diffusion coefficient first rises above its asymptotic value, and then decreases back to its asymptotic value. This is in disagreement with our results as all our measurements show that $D_S(\tau)$ increases monotonically. This may reflect the limited range of validity for the two particle approximation. Furthermore, the theoretical calculations for different volume fraction do not scale for higher volume fractions, as can be seen from Fig. 5.15, where we plot the theoretically calculated self-diffusion coefficients, normalized by their asymptotic values, for ϕ=0, 10%, 20%, and 30%, as a function of the normalized time, $\tau/\tau_\nu(\phi)$. For relatively low volume fraction, ϕ=10%, the theoretical calculation seems to scale reasonably well, in agreement with our experiments. However, as ϕ increases to 20%, the scaling becomes worse. The curve for 30% can not be scaled at all, unlike the behavior observed in experiments. This suggests the fact that the validity of the two particle interaction may be limited to very low volume fractions, ϕ<10%.

Clearly further theoretical work is needed to properly interpret these many body hydrodynamic interactions. We emphasize that the scaling behavior and its relationships to the viscosity is not well understood. We can not consider a particle in a concentrated suspension as the particle in an effective medium with an effective viscosity. Otherwise the terminal diffusion coefficients $Ds(\phi)$ should have had the same ϕ dependence as the viscosity, as the Stokes relation should apply.

From the scaling behavior analysis, the two particle theory is not adequate for volume fractions higher than 10%.

5.6 CONCLUSIONS

We have studied the short time transition of the Brownian particles from ballistic motion to diffusive motion at both low and high volume fractions. We showed that by using DWS in transmission geometry for monodisperse large sphere suspensions, the short time evolution of the mean square displacement of a particle can be extracted from the autocorrelation function. Using a very fast correlator, the length scale that we can probe is as short as several Angstroms. The quality of our data is sufficiently good that the velocity correlation function can be obtained by numerically differentiating the measured mean square displacement two times. The results of this paper demonstrate the power of DWS to probe the short length scale.

At low volume fraction, we have directly observed the slow algebraic behavior of the velocity correlation function, the "long time tail". This long time tail results from the retarded hydrodynamic interactions between the particle and the surrounding fluid. Furthermore, our data is in complete agreement with the theory taking into account of the retarded hydrodynamic interaction, which can in no way be explained by the theory without the interaction.

At high volume fractions, our data shows that there still exists the same long time behavior, algebraic decay of the velocity correlation function, regardless of the size or volume fraction. This is in agreement with theoretical predictions. Moreover, we find a surprising scaling behavior for the time dependent self-diffusion coefficient: if $D_S(\tau)$ is scaled by the asymptotic value of the short time self-diffusion coefficient, and the time is scaled by a viscous time inversely proportional to the shear viscosity of the suspension, all the data fall onto a single master curve. Two particle theory works well at low

volume fractions (ϕ<10%), but fails at high volume fractions. Further theoretical works is required to fully understand this behavior.

Acknowledgments.

We acknowledge many useful and stimulating discussions with S. Milner, A.J. Liu, and J.Z. Xue. We also thank E. Herbolzheimer for many helpful discussions.

[1] B.J. Alder and T.E. Wainwright, Phys. Rev. Lett. **23**,988-990 (1967)
[2] B.J. Alder and T.E. Wainwright, J. Phys. Soc. Japan Suppl. **26**,267 (1968)
[3] B.J. Alder and T.E. Wainwright, Phys. Rev. A. **1**, 18-22 (1970)
[4] R. Zwanzig and M. Bixon, Phys. Rev. A. **2**, 2005 (1970)
[5] E.J. Hinch and J. Fluid Mech. 72, 499 (1975)
[6] G.L. Paul and P.N. Pusey, J. Phys. A. **14**, 3301 (1981)
[7] D.A. Weitz, D.J. Pine, P.N Pusey, and R.J.A. Tough, Phys. Rev. Lett. **63**,1747 (1989)
[8] D.J. Pine, D.A. Weitz, J.X. Zhu, and E. Herbolzheimer, J. Phys. (France) **51**, 2101 (1991)
[9] W. Van Saarloos and P. Mazur, Physica A. 120, 77 (1983)
[10] H.J.H Clercx and P.P.J.M. Schram, Physica A. **174**, 325-354 (1991)
[11] P.N. Pusey and R.J.A. Tough, Dynamic Light Scattering, P85, Edited by R. Pecora, Plenum Press, (1985)
[12] F.C. Mackintosh and S. John, Ph.D. thesis.
[13] J.P. Hansen, and I.R. McDonald, *Theory of Simple Liquid*, P195, Academic Press, (1985)
[14] H.S. Carslaw and J. C. Yaeger, Conduction of Heat in Solids, 2nd ed. (Clarendon, Oxford, 1990)
[15] G.E. Ulenbeck, and L.S. Ornstein, *Phys. Rev.* **36**, 823 (1930)
[16] L.D. Landau and E.M. Lifshitz, *Fluid Mechanics*, P91, Pergamon Press, Oxford, England
[17] K. Shätzel
[18] W. van Megan, S. M. Underwood, R.H. Ottewill, N.St.J. Williams, and P.N. Pusey, Faraday discuss. Chem. Soc. **83**, 47 ((1987)
[19] G. K. Batchlor, J. Fluid Mech. **74**, 1 (1976)
[20] C.W.J. Beenaker and P. Mazur, Phys. Lett. A **98**,22(1983);Physica **126A**, 349 (1984)

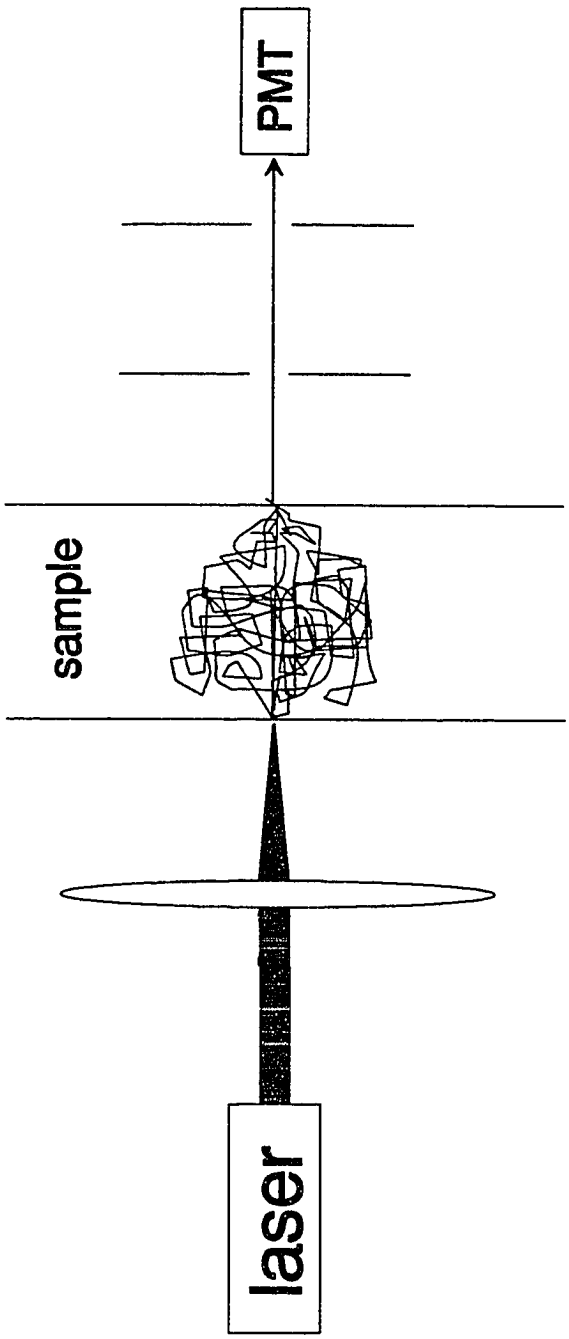

Figure 2.1

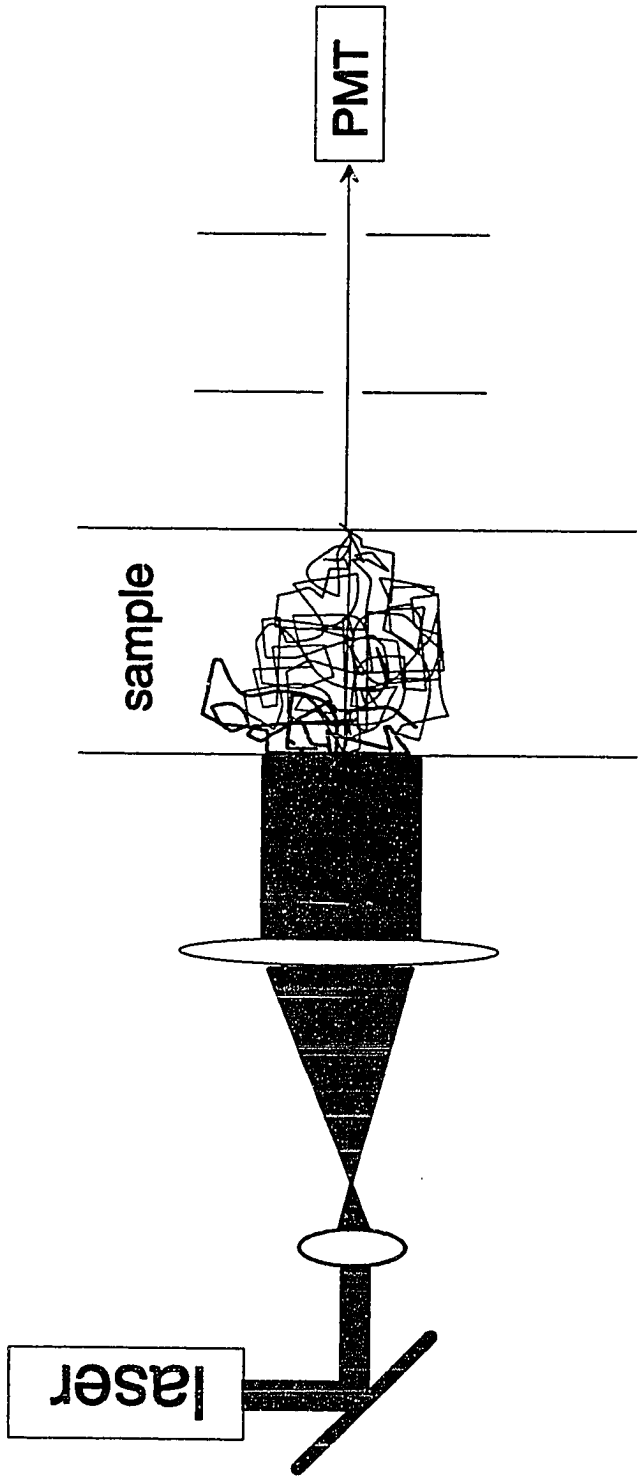

Figure 2.2

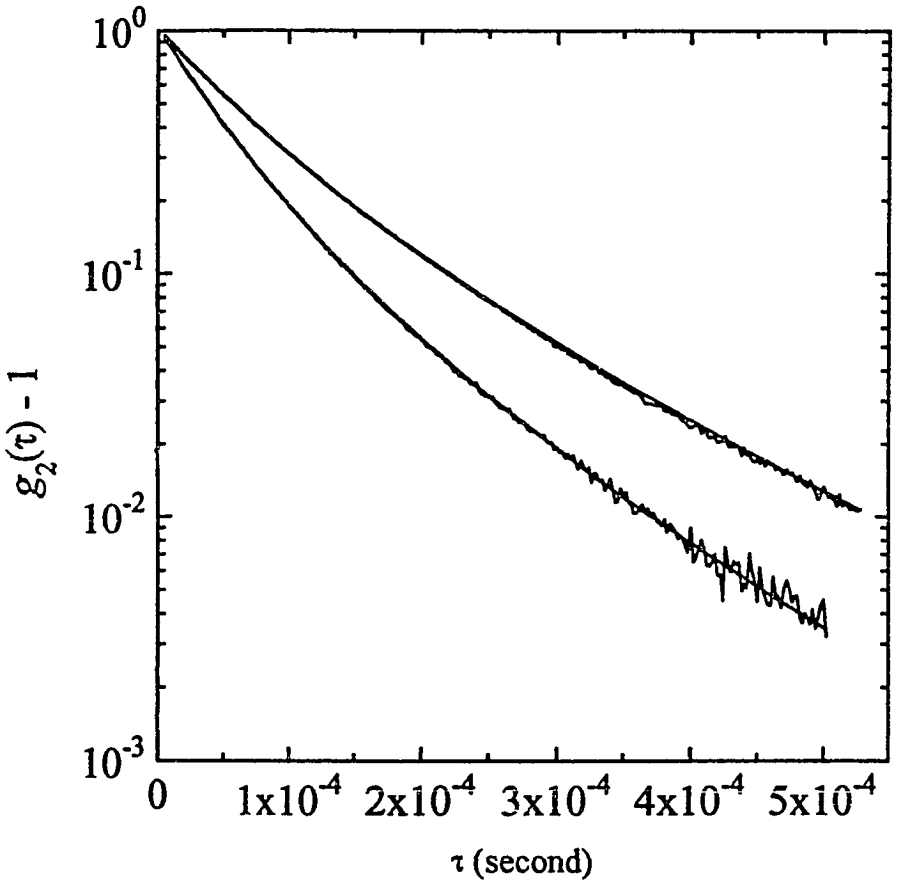

Figure 2.3

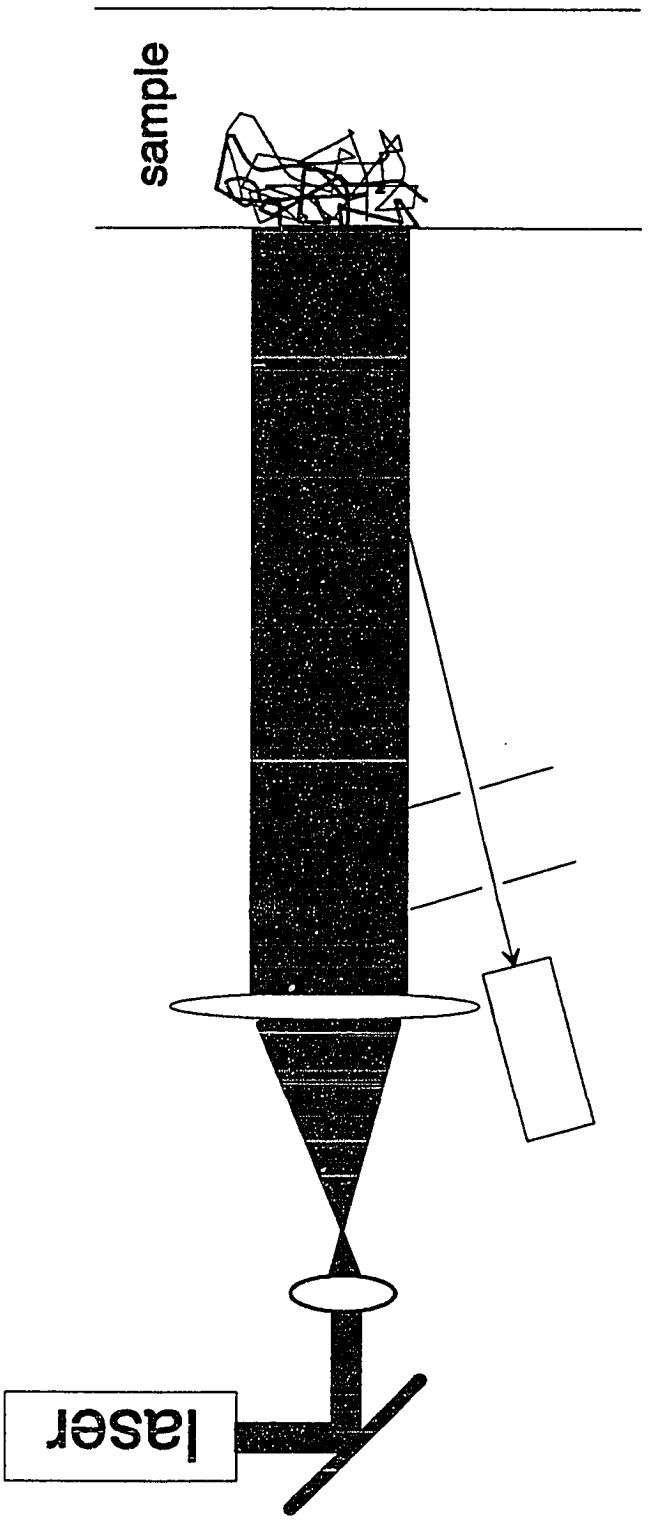

Figure 2.4

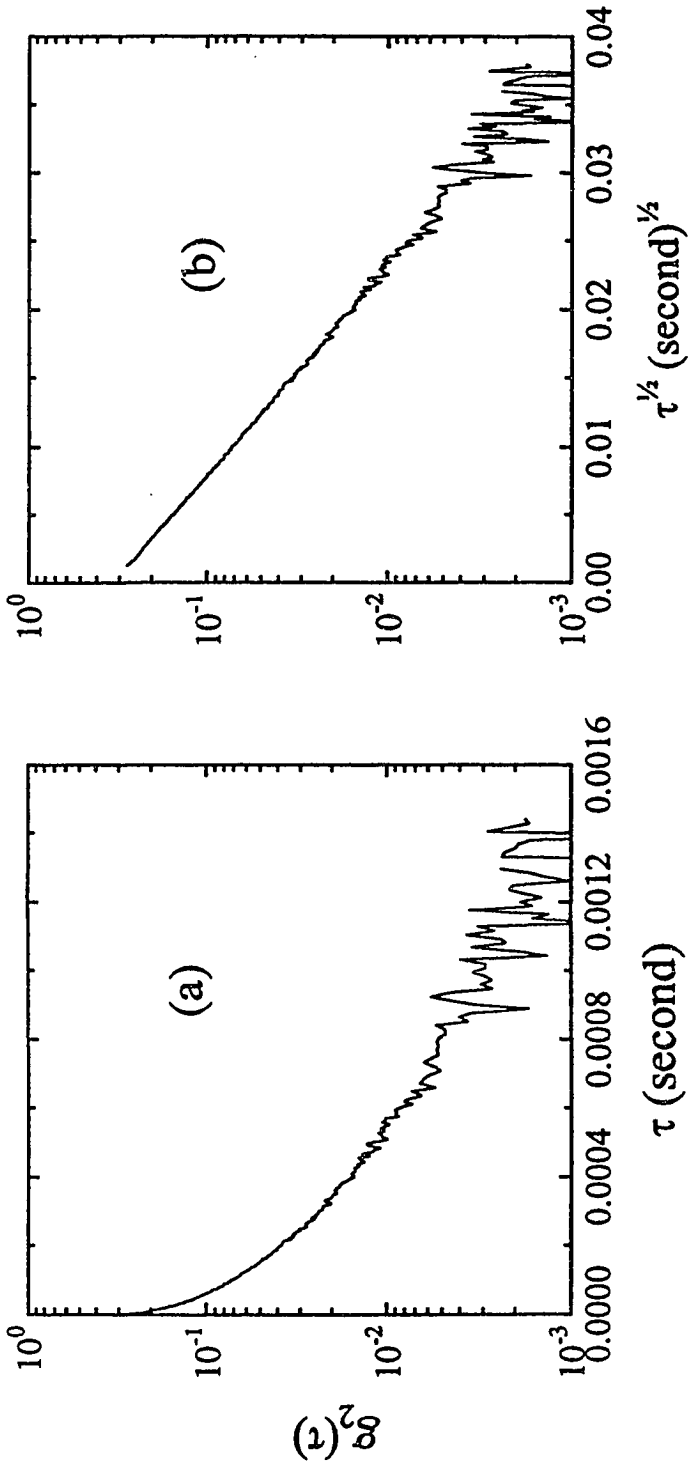

Figure 2.5

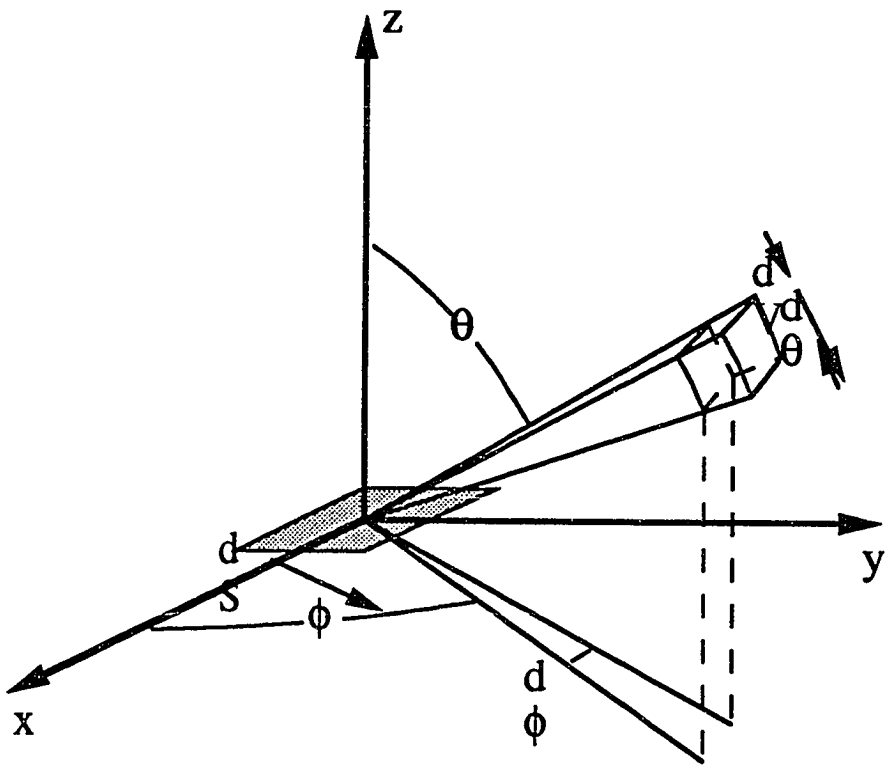

Figure 3.1

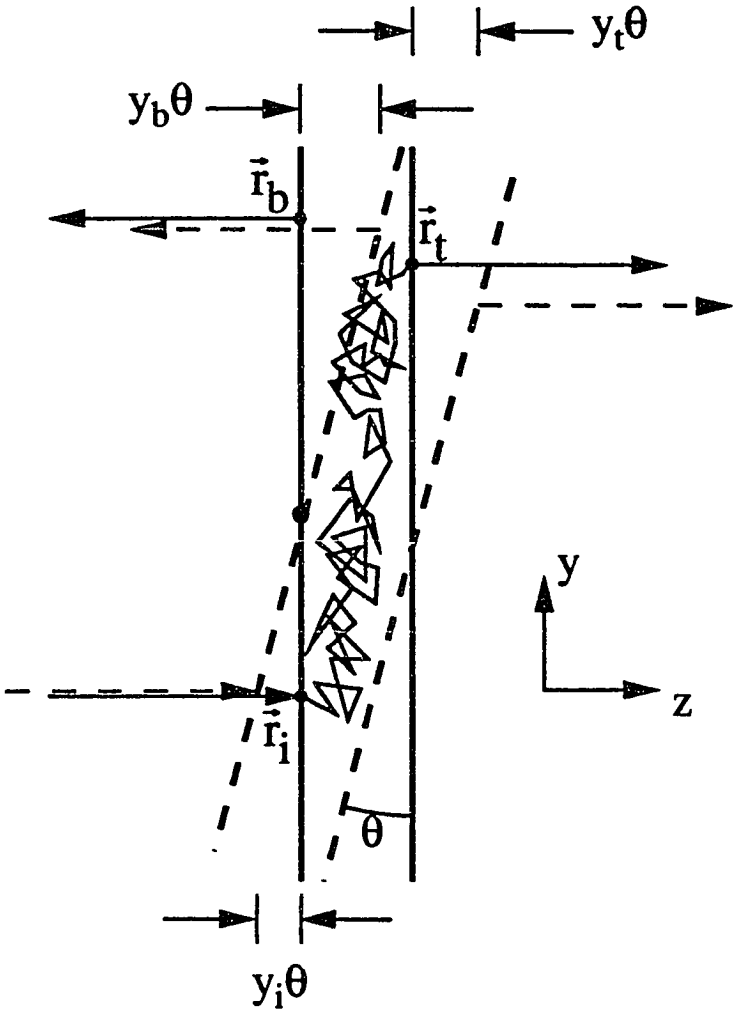

Figure 3.2

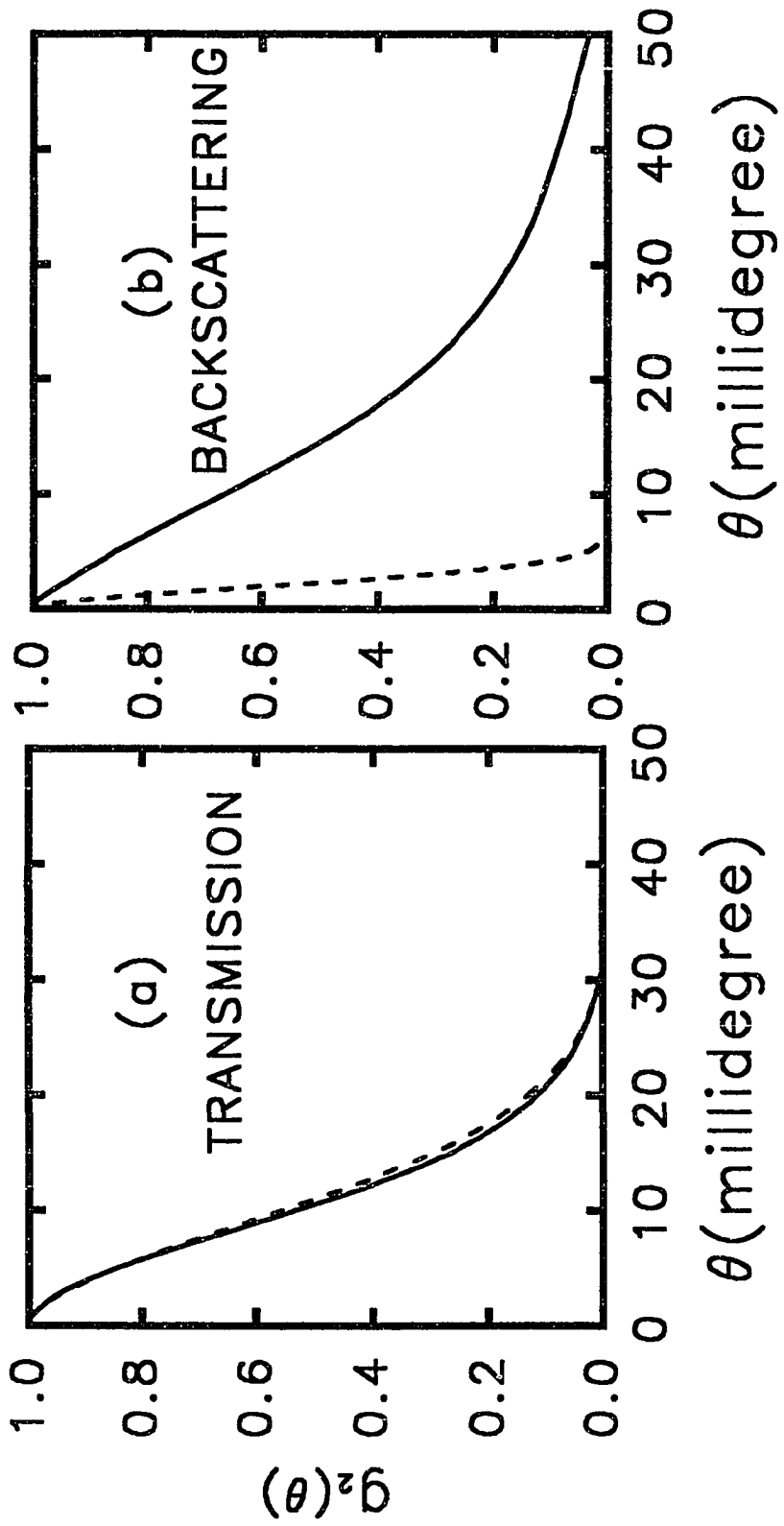

Figure 3.3

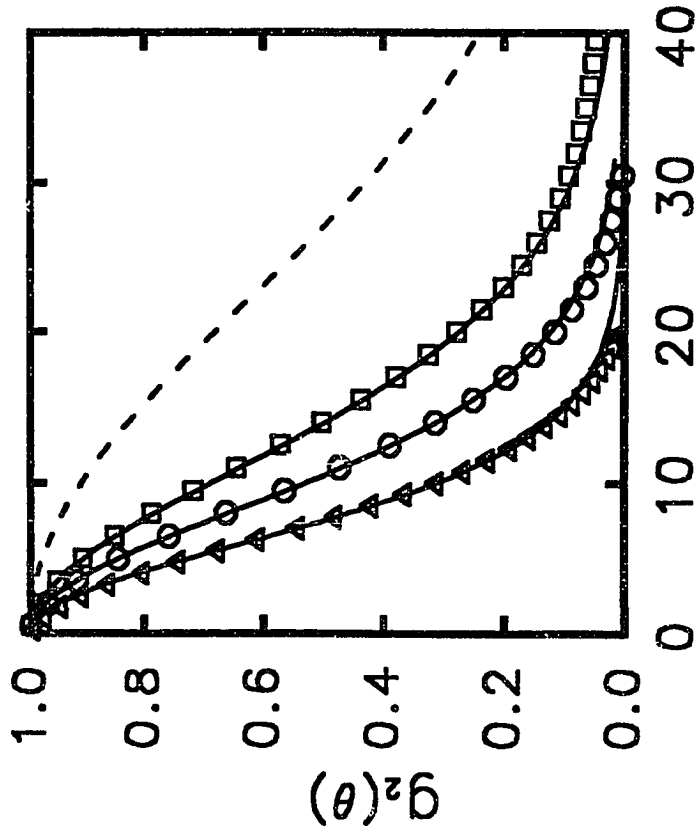

Figure 3.4

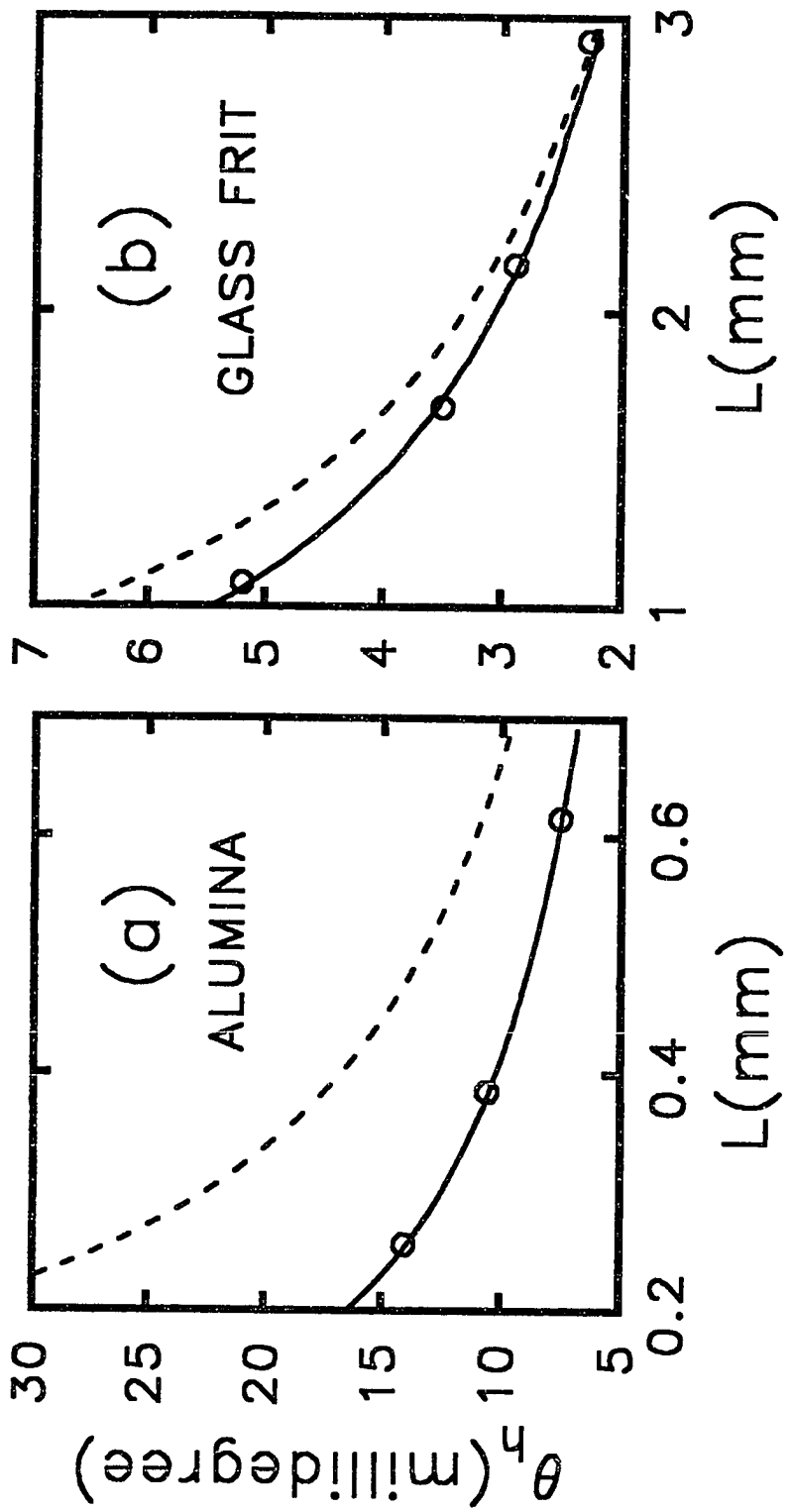

Figure 3.5

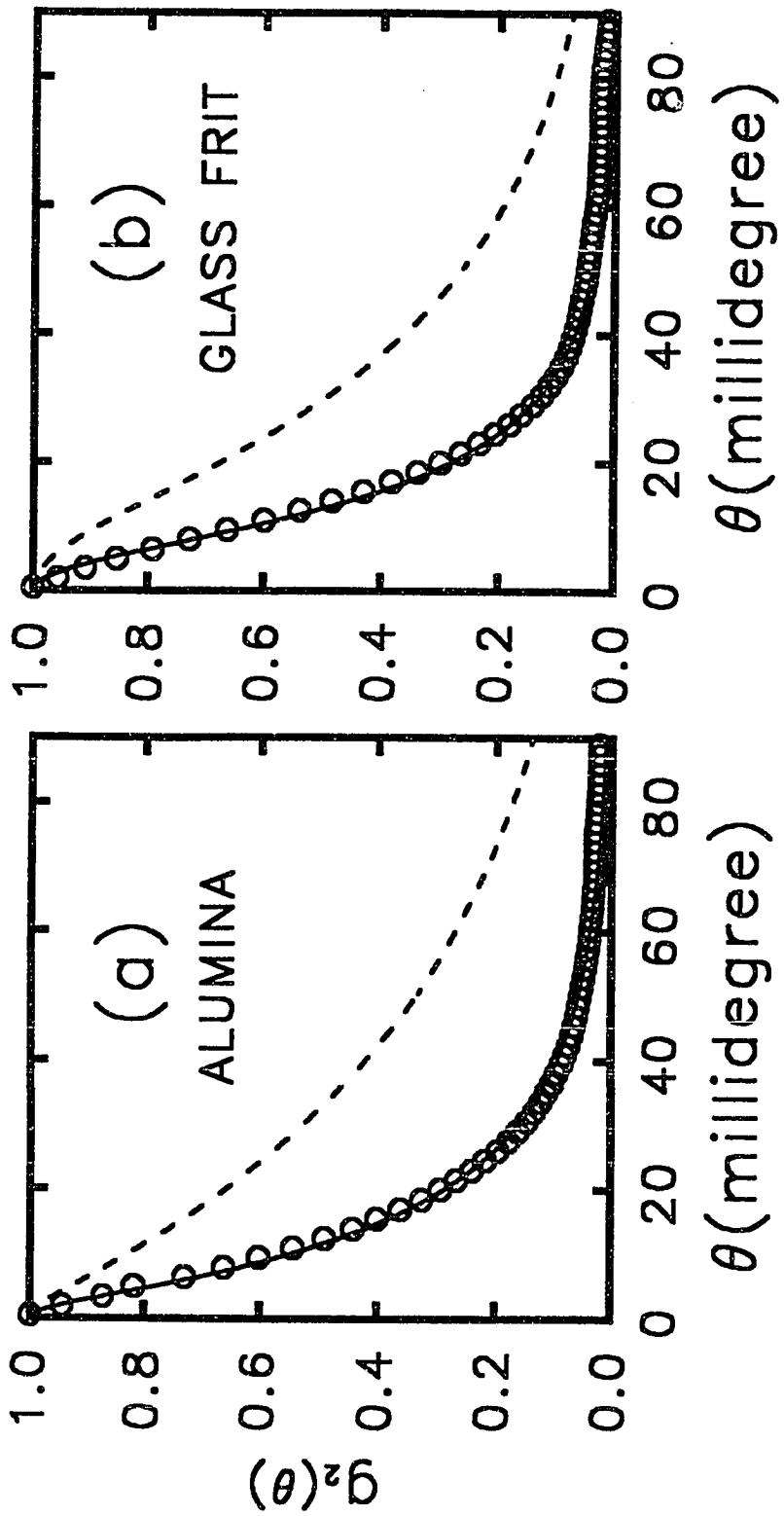

Figure 3.6

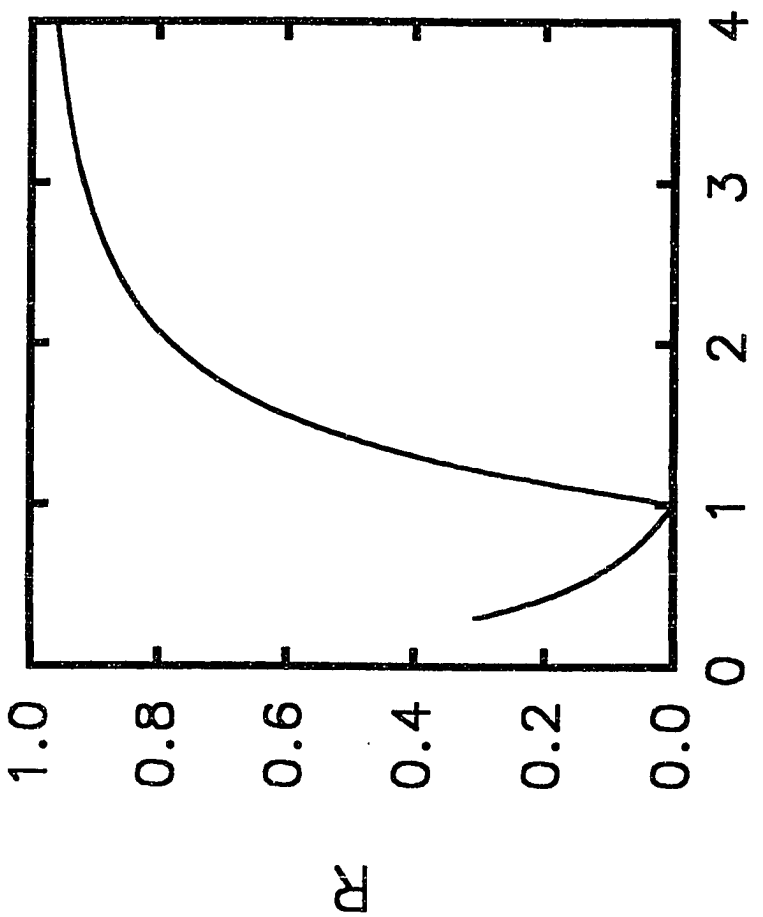

Figure 3.7

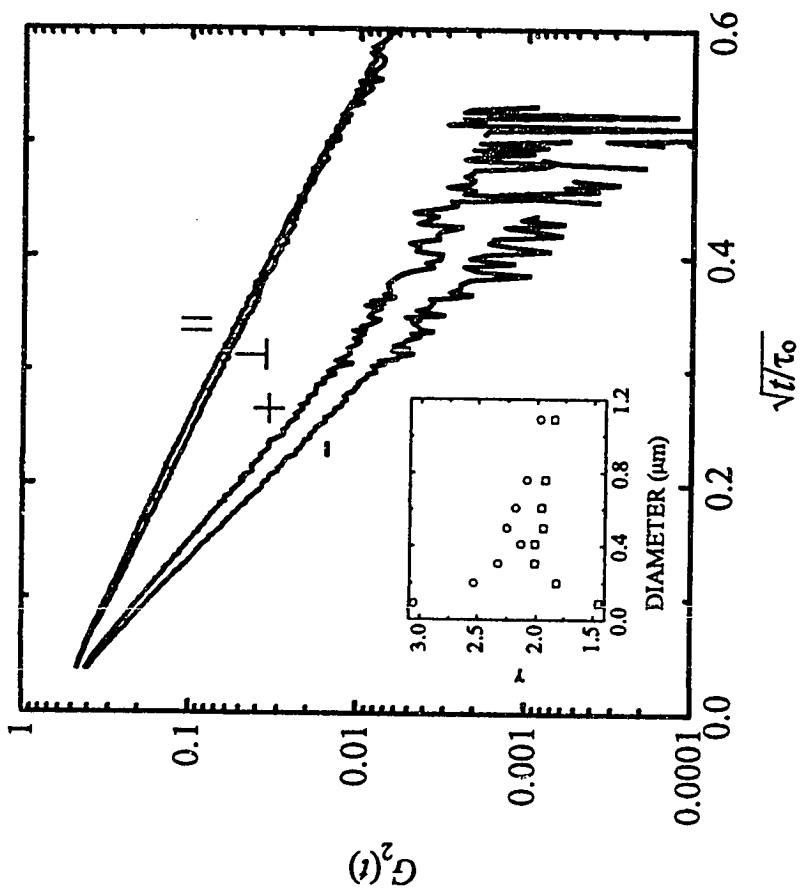

Figure 4.1

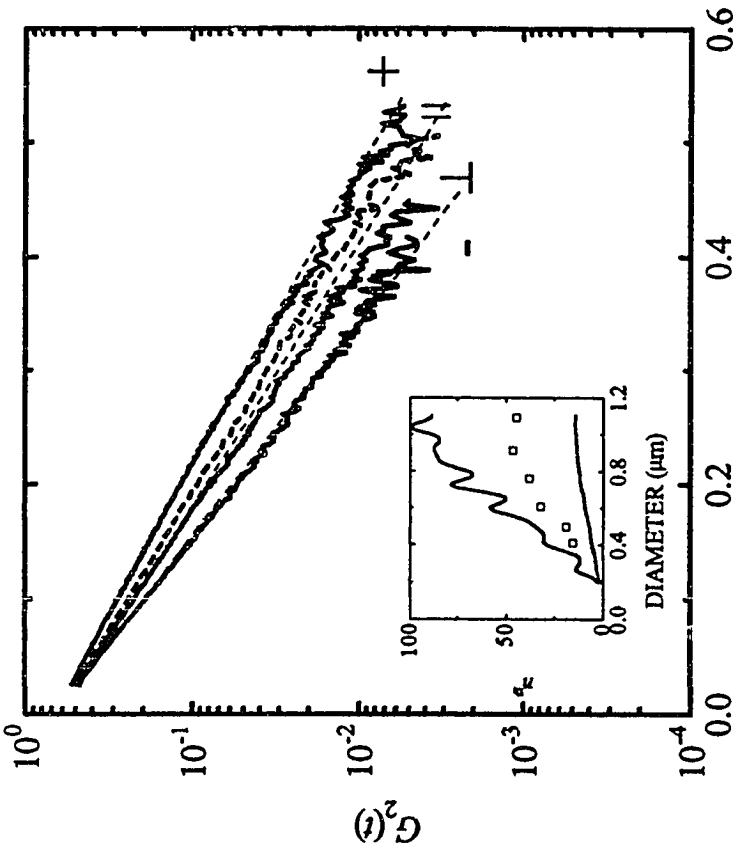

Figure 4.2

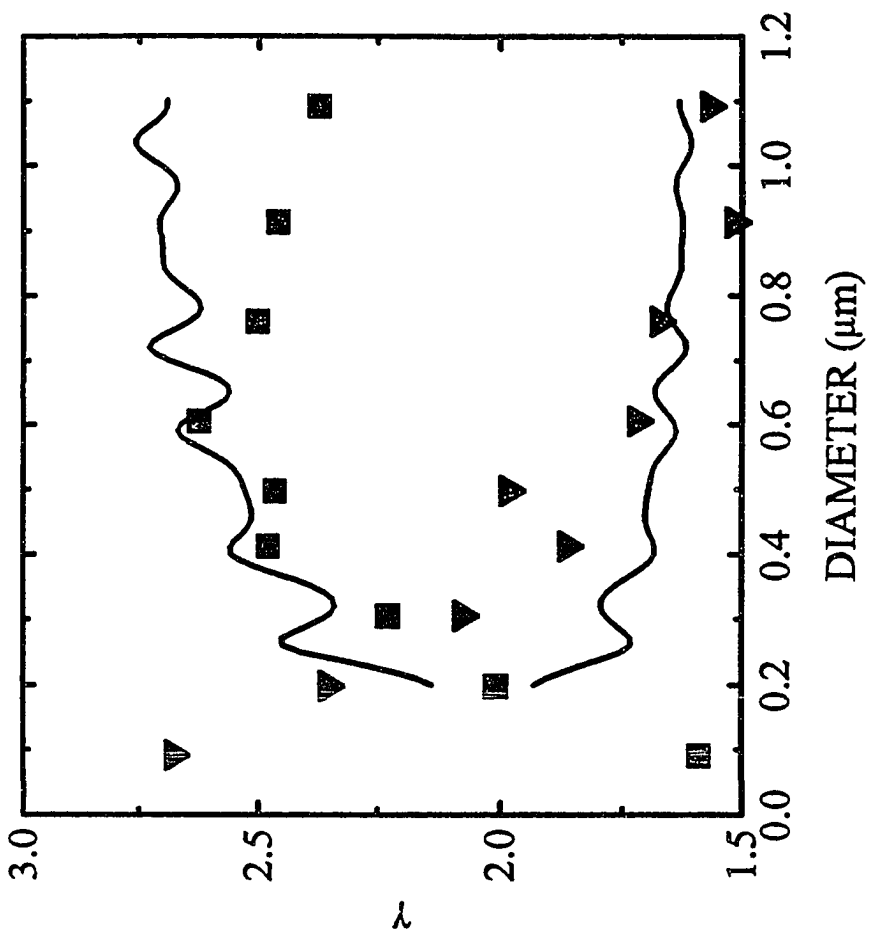

Figure 4.3

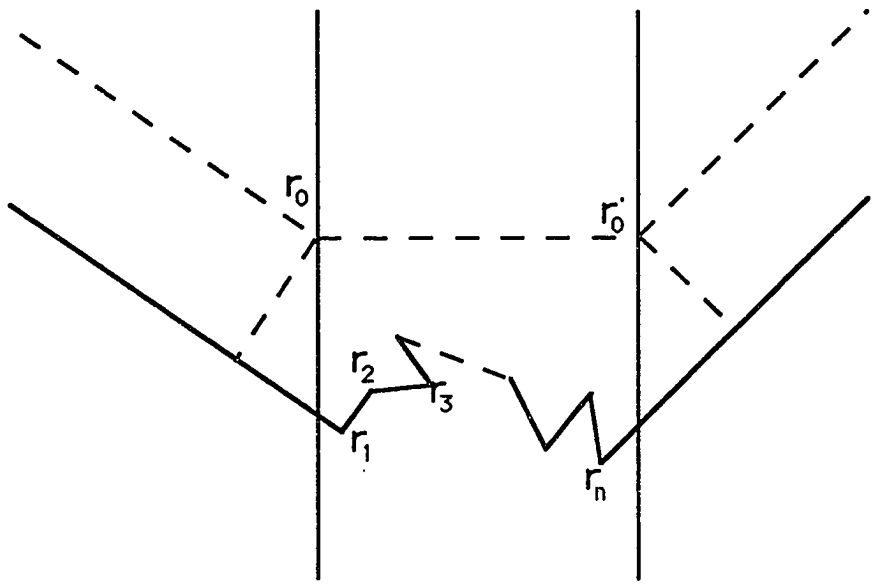

Figure 5.1

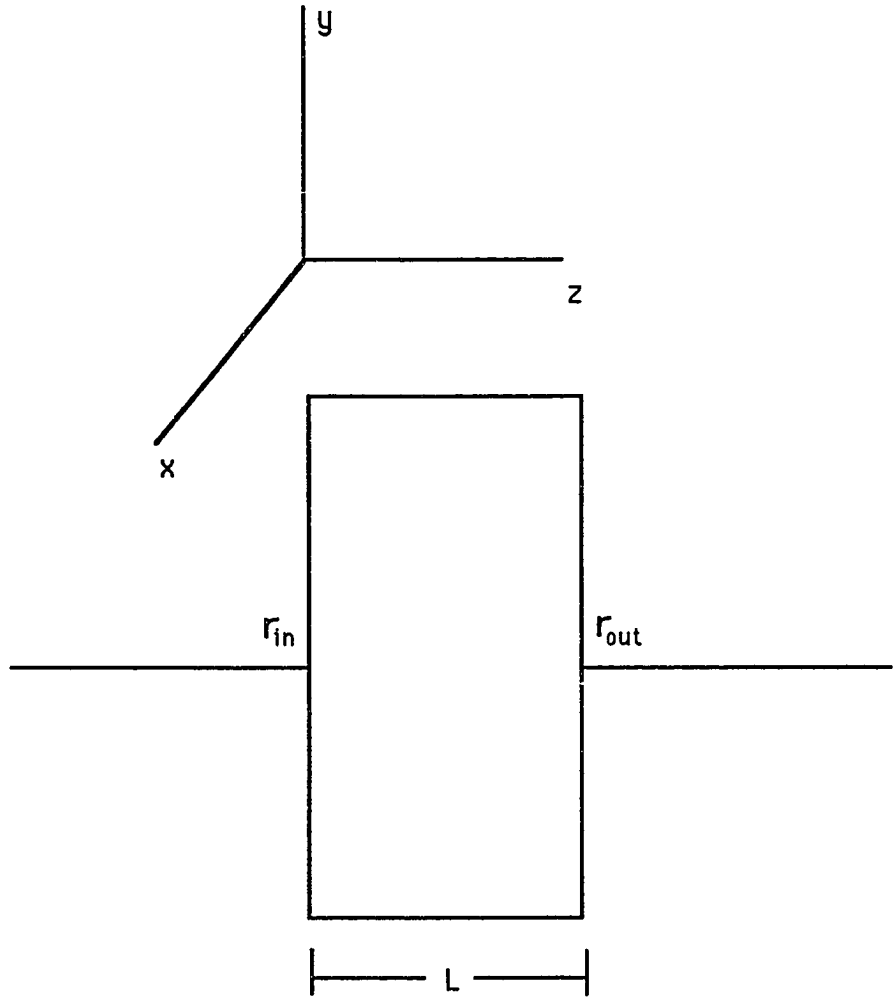

Figure 5.2

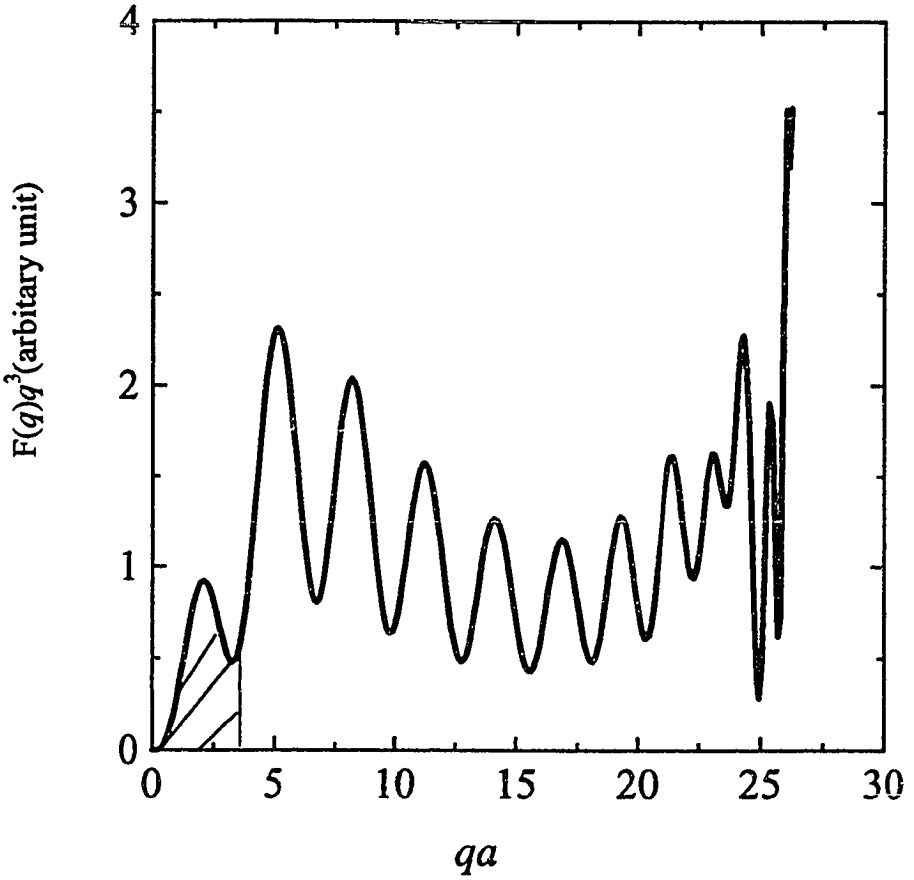

Figure 5.3

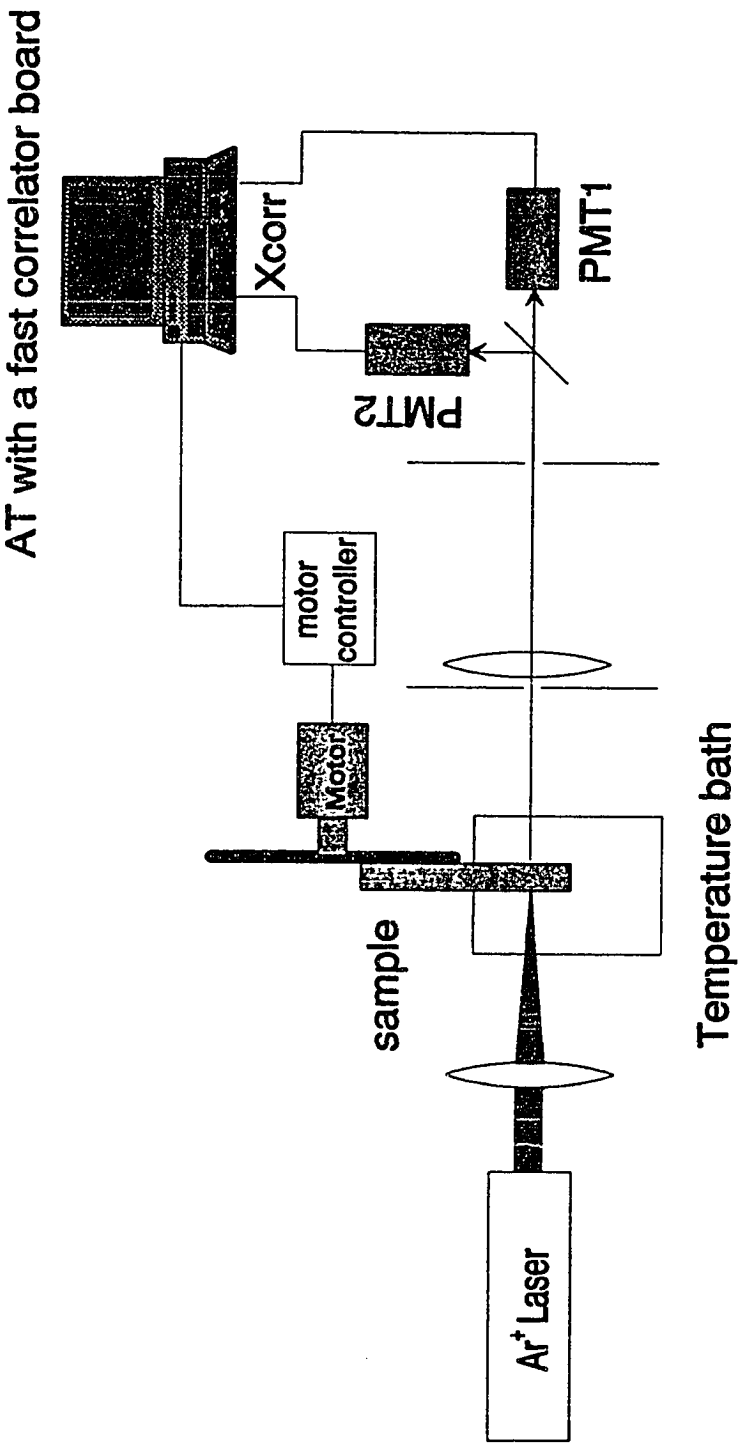

Figure 5.4

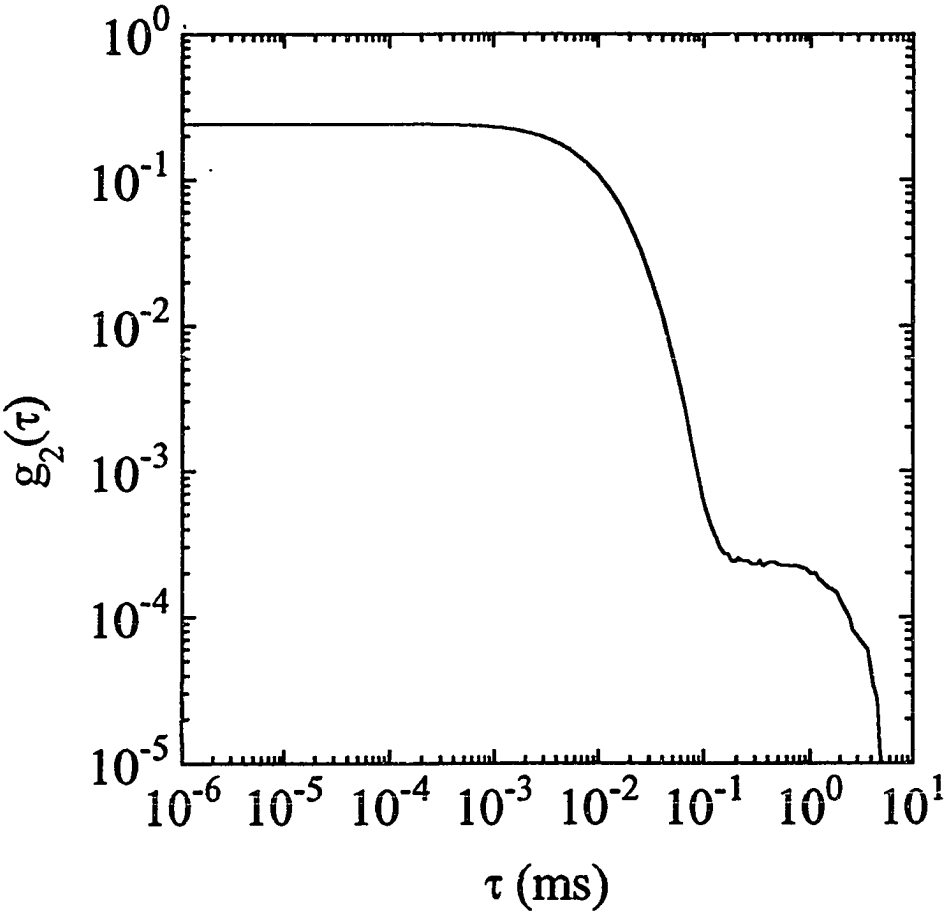

Figure 5.5

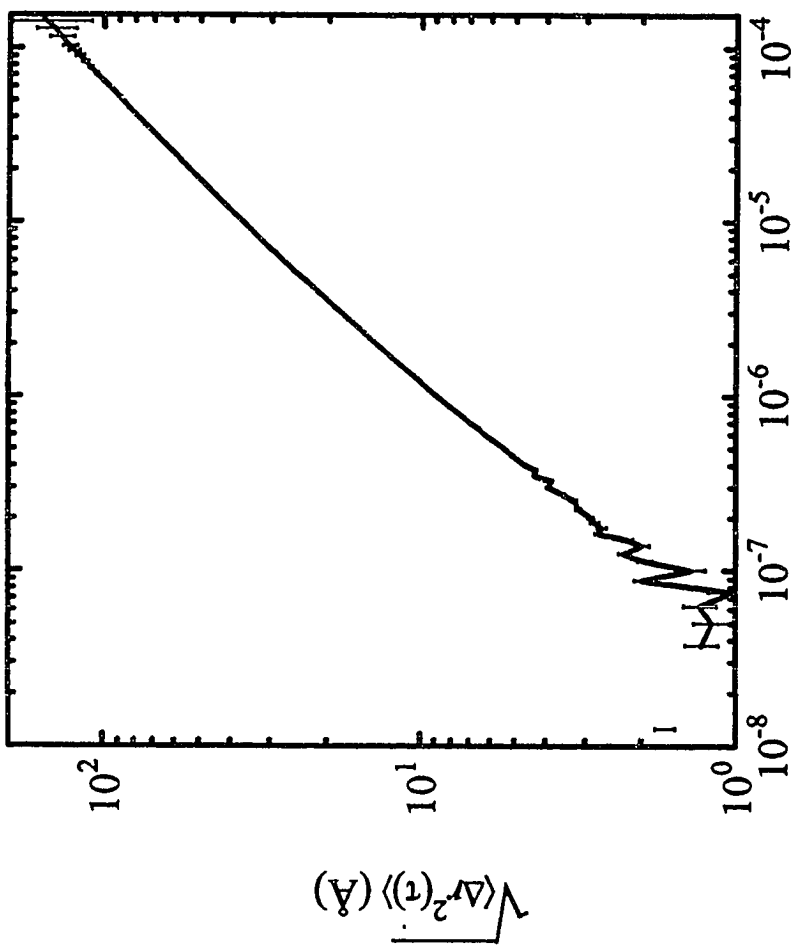

Figure 5.6

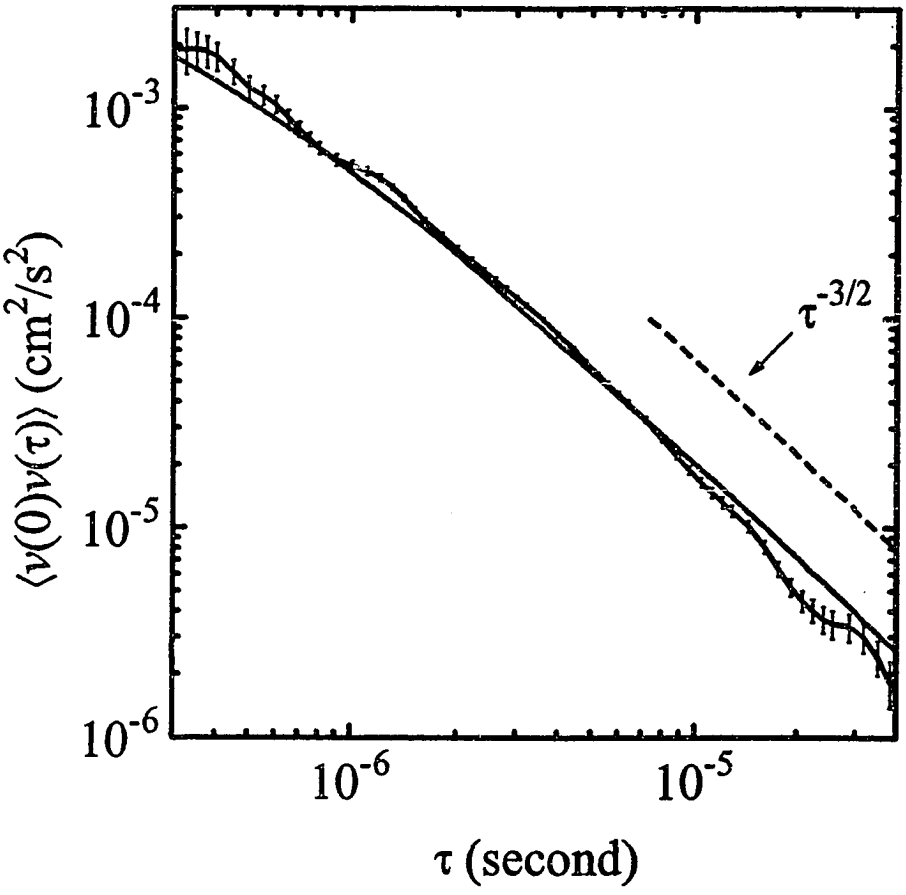

figure 5.7

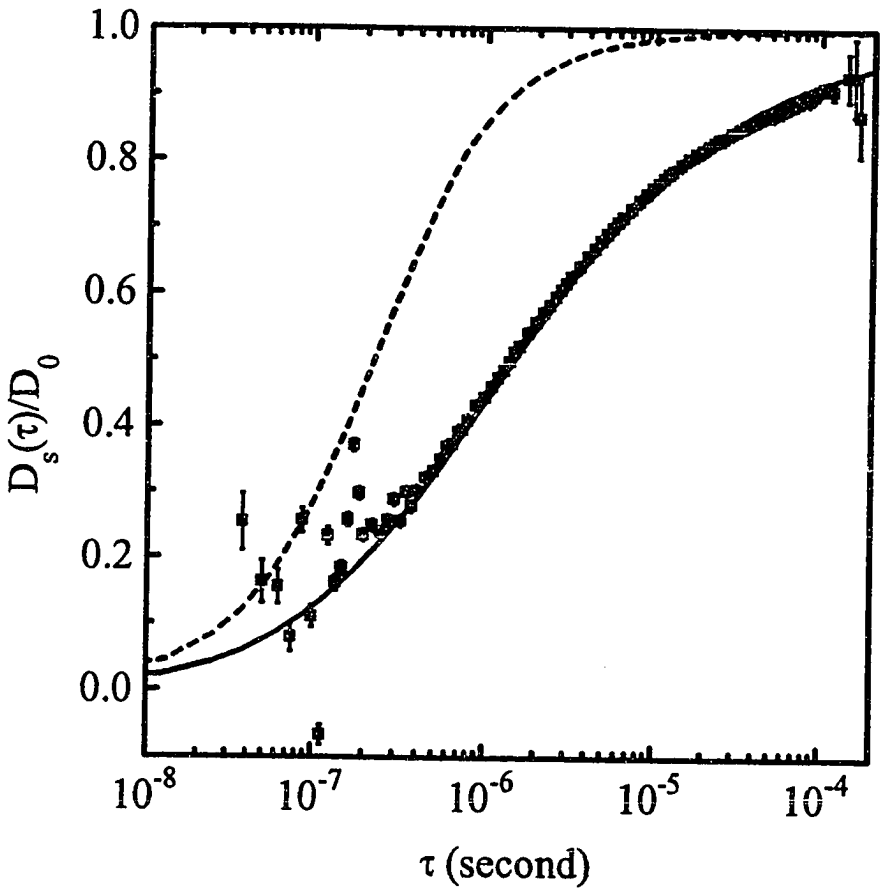

Figure 5.8

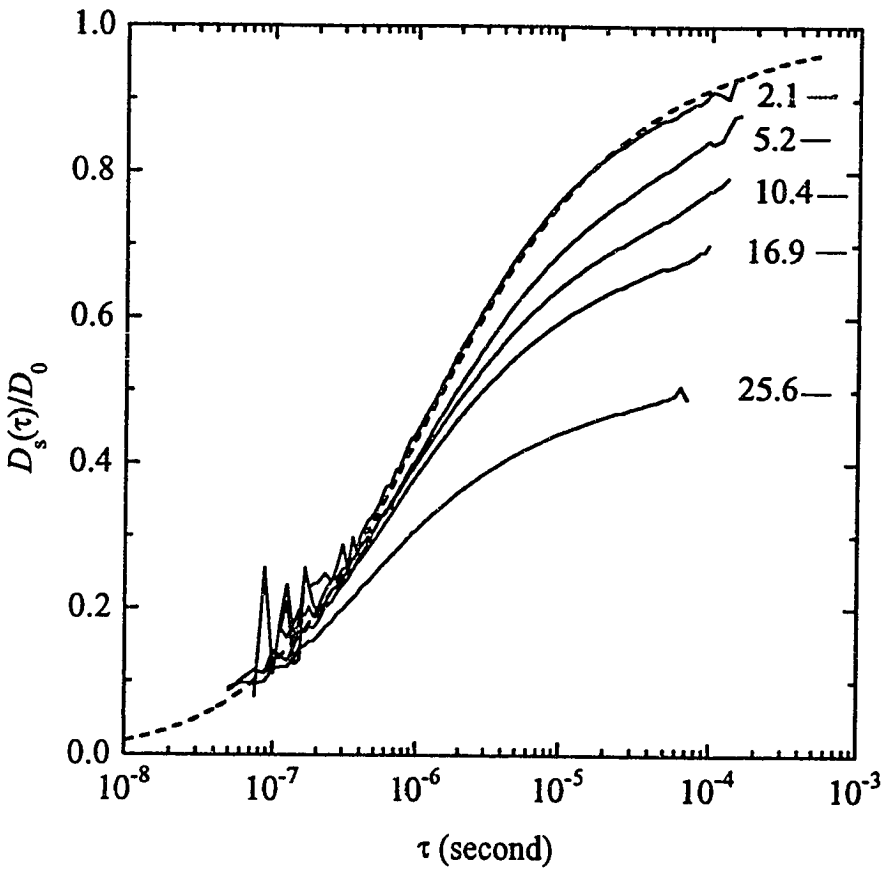

Figure 5.9

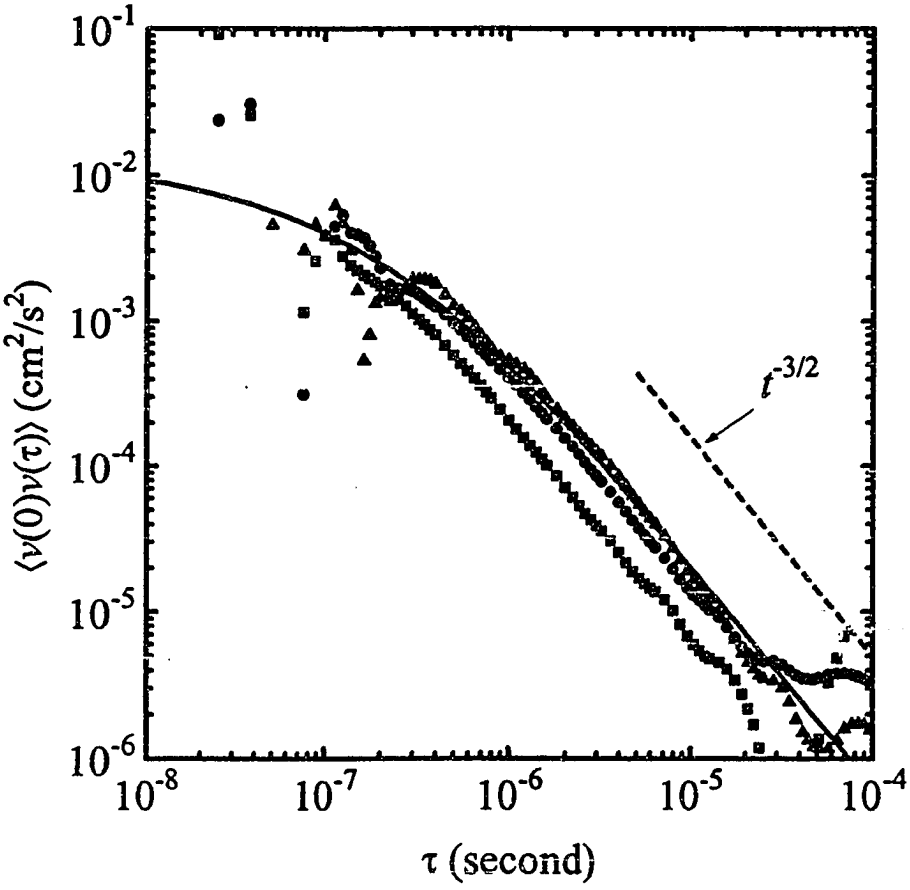

figure 5.10

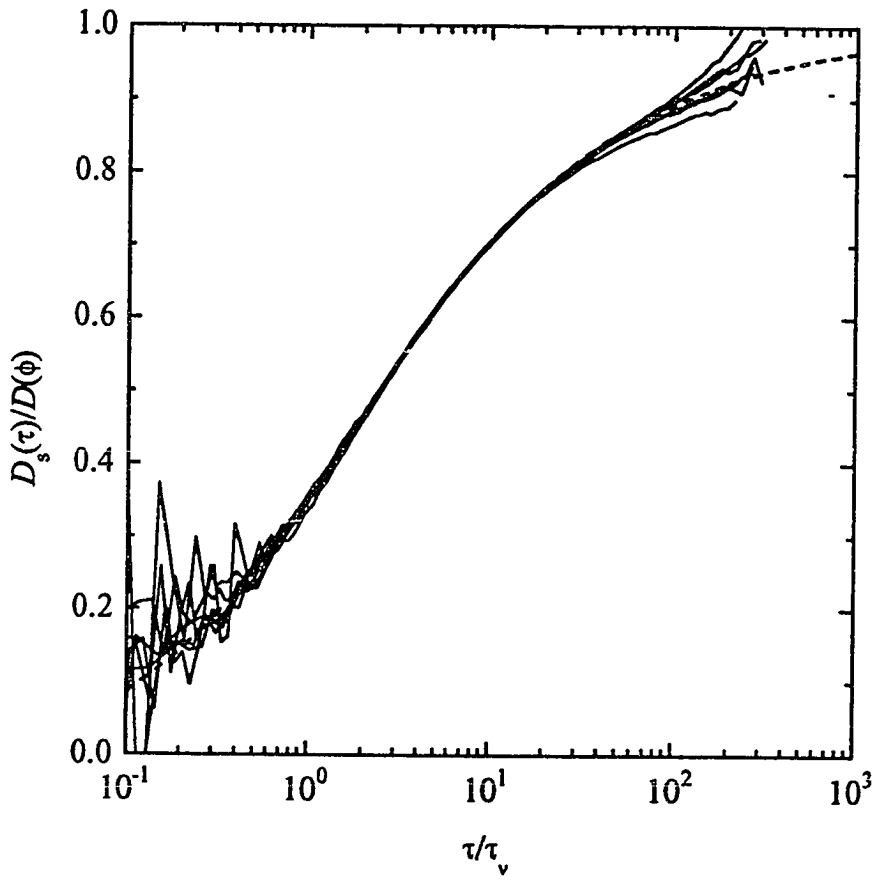

Figure 5.11

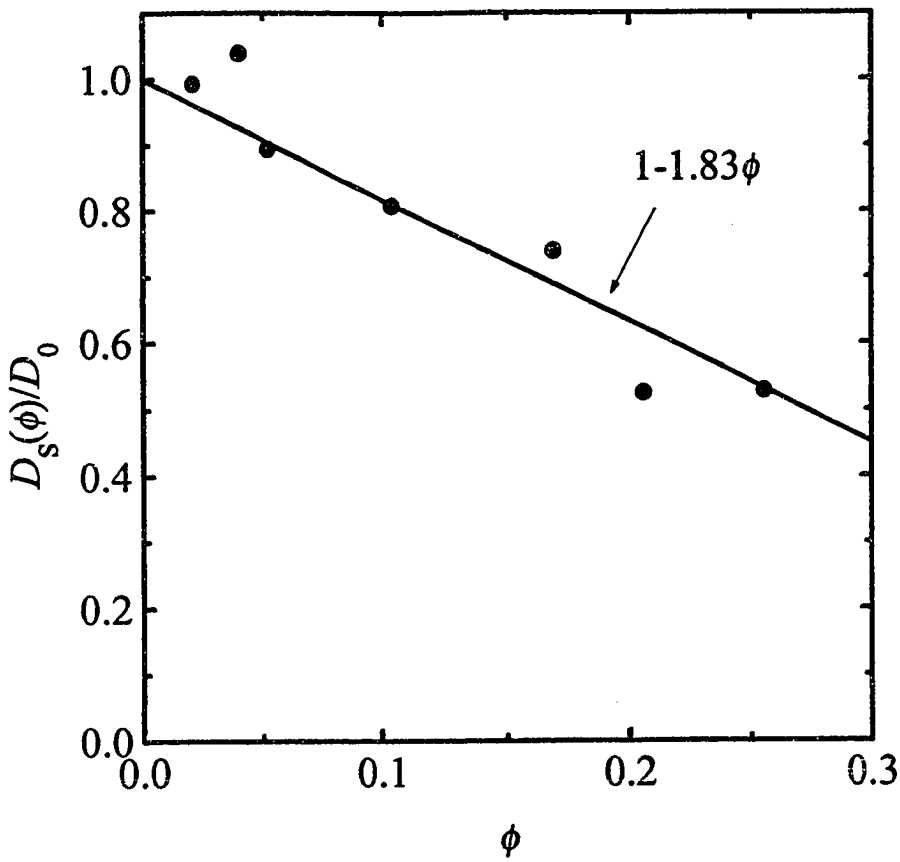

Figure 5.12

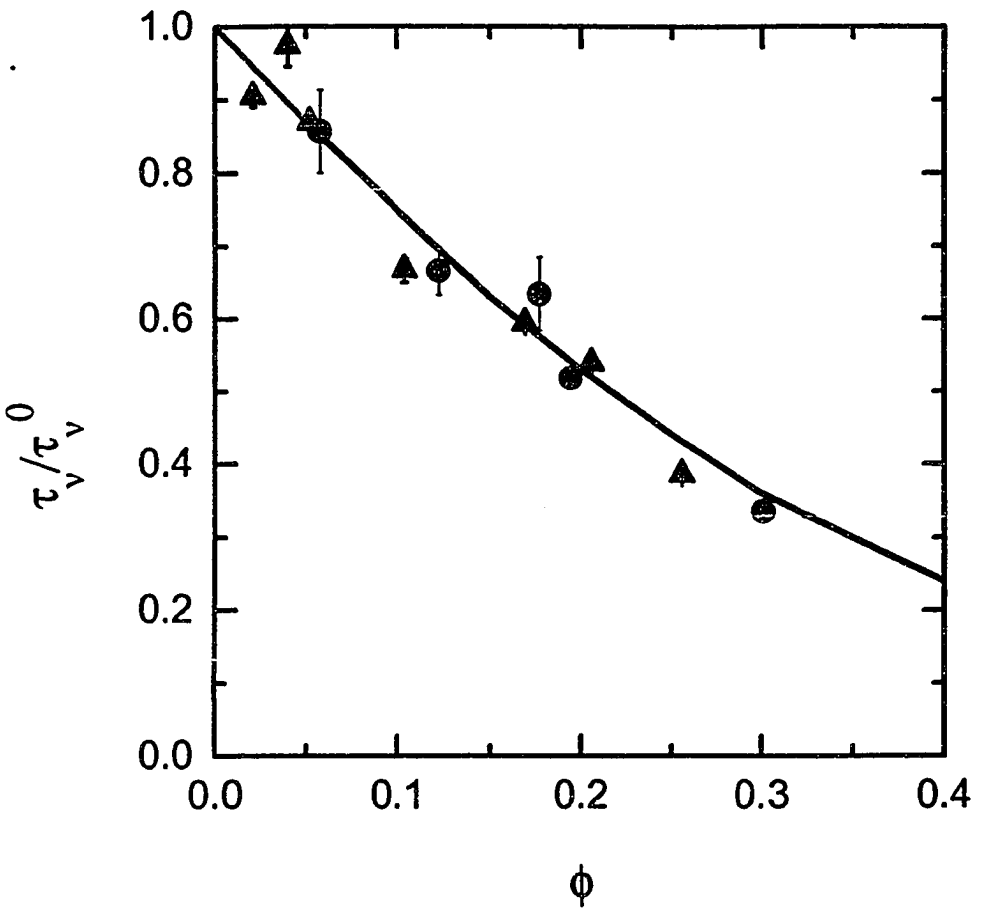

Figure 5.13

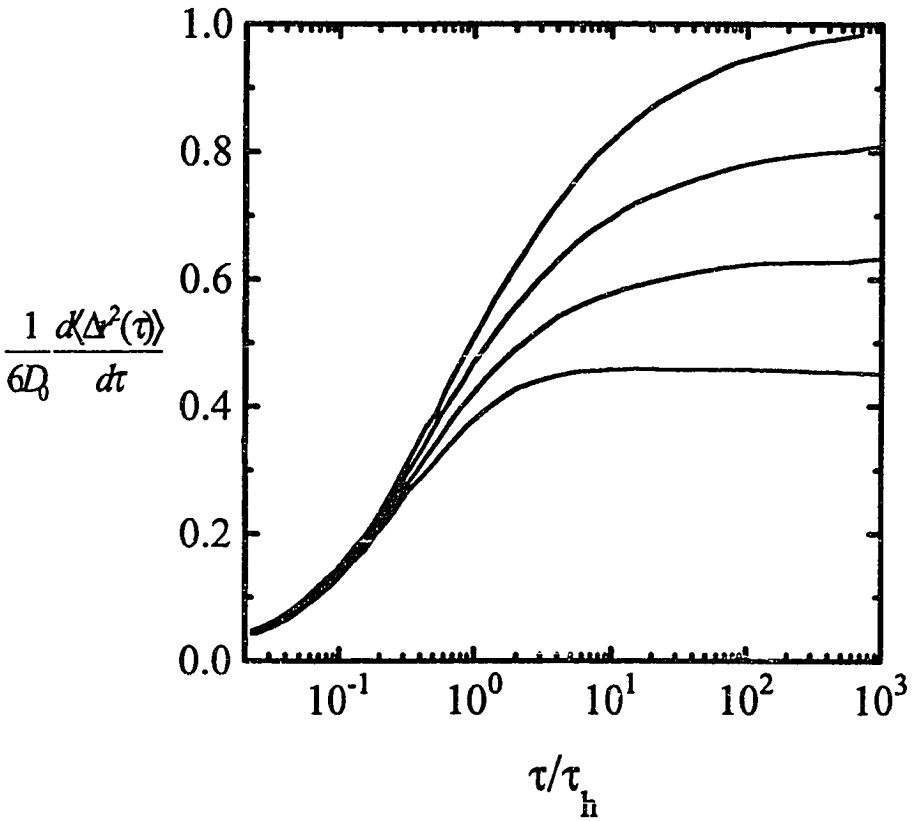

Figure 5.14

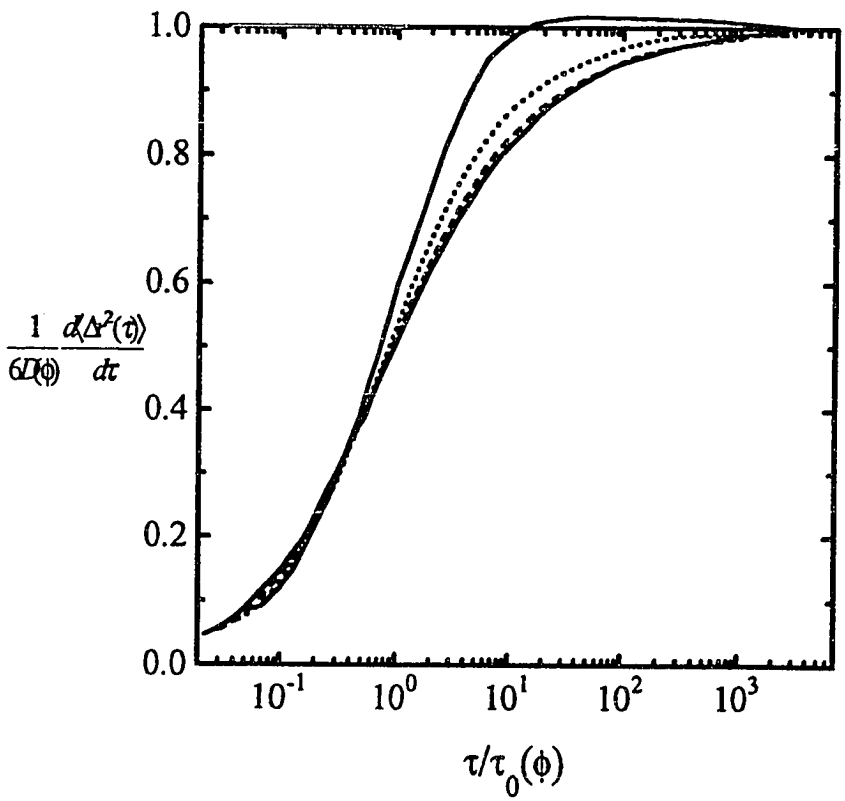

Figure 5.15

Bibiography

E. Akkermans, P. E. Wolf and R. Maynard, Phys. Rev. Lett. **56**, 1471 (1986).

B.J. Alder and T.E. Wainwright, Phys. Rev. Lett. **23**,988-990 (1967)

B.J. Alder and T.E. Wainwright, J. Phys. Soc. Japan Suppl. **26**,267 (1968)

B.J. Alder and T.E. Wainwright, Phys. Rev. A. **1**, 18-22 (1970)

G. K. Batchlor, J. Fluid Mech. **74**, 1 (1976)

C.W.J. Beenaker and P. Mazur, Phys. Lett. A **98**,22(1983);Physica **126A**, 349 (1984)

M. Born and E. Wolf, *Principles of Optics*, 4th edition (Pergamon, New York, 1990).

H.S. Carslaw and J. C. Yaeger, Conduction of Heat in Solids, 2nd ed. (Clarendon, Oxford, 1990)

H.J.H Clercx and P.P.J.M. Schram, Physica A. **174**, 325-354 (1991)

J.M. Drake and A.Z. Genack, Phys. Rev. Lett. **63**,259(1989).

S. Etemad, R. Thomson and M. J. Andrejco, Phys. Rev. Lett. **57**, 575 (1986);

Etemad, R. Thompson, M.J. Andrejco, S. John and F. MacKintosh, Phys. Rev. Lett. **59**, 1420 (1987).

S. Feng, C. Kane, and A. D. Stone, Phys. Rev. Lett. **61**, 834 (1988).

L. A. Ferarri, J. Appl. Phys. **68**, 4399 (1990).

I. Freund, M. Rosenbluh, and R. Berkovits, Phys. Rev. B **41**, 496 (1990).

I. Freund, M. Rosenbluh, and R. Berkovits, Phys. Rev. B **39**, 12403 (1989).

S. Glasstone and M. C. Edlund *The Elements of Nuclear Reactor Theory* (D. Van Nostrand Company, Princeton, New Jersey, 1955).

A.A. Golubentsev, Zh. Eksp. Teor. Fiz. **86**, 47 (1984) [Sov. Phys. JETP **59**, 26 (1984)].

J.P. Hansen, and I.R. McDonald, *Theory of Simple Liquid*, P195, Academic Press, (1985)

E.J. Hinch and J. Fluid Mech. 72, 499 (1975)

A.F. Ioffe and A.R. Regel, *Prog. Semicond.* **4**, 237, (1960)

A. Ishimaru, *Wave Propagation and Scattering in Random Media* (Academic, New York, 1978).

M. Kerker, *The Scattering of Light*, (Academic Press, New York, 1969).

A. Lagendijk, R. Vreeker, and P. DeVries, Phys. Lett. A **136**, 81 (1989).

L.D. Landau and E.M. Lifshitz, *Fluid Mechanics*, P91, Pergamon Press, Oxford, England

F. MacKintosh and S. John, Phys. Rev. B **40**, 2383 (1989).

F.C. Mackintosh and S. John, Ph.D. thesis.

F.C. Mackintosh, J.X. Zhu, D.J. Pine, and D.A. Weitz, Phys. Rev. B. **40**, 9342 (1989).

G. Maret and P.E. Wolf, Z. Phys. B **65**, 409 (1987).

G.L. Paul and P.N. Pusey, J. Phys. A. **14**, 3301 (1981)

D.J. Pine, D.A. Weitz, P.M. Chaikin, and E. Herbolzheimer, Phys. Rev. Lett. **60**, 1134 (1988).

D.J. Pine, D.A. Weitz, G. Maret, P.E. Wolf, E. Herbolzheimer, and P.M. Chaikin, *Scattering and Localization of Classical Waves in Random Media*, edited by P. Sheng (World Scientific, Singapore, 1990).

D.J. Pine, D.A. Weitz, J. X. Zhu, and E. Herbolzheimer, J. Phys. (France) **51**, (1990) 2101-2127.

P.N. Pusey and R.J.A. Tough, Dynamic Light Scattering, P85, Edited by R. Pecora, Plenum Press, (1985)

M. Rosenbluh, M. Hoshen, I. Freund, and M. Kaveh, Phys. Rev. Lett. **58**, 2754 (1987).

Scattering and Localization of Classical Waves in Random Media, edited by P. Sheng (World Scientific, Singapore, 1990).

M.J. Stephen, Phys. Rev. B **37**, 1 (1988).

M. J. Stephen and G. Cwilich, Phys. Rev. B **34** 7564 (1986).

G.E. Ulenbeck, and L.S. Ornstein, *Phys. Rev.* **36**, 823 (1930)

M. P. van Albada and A. Lagendijk, Phys. Rev. Lett. **55**, 2692 (1985).

M.P. van Albada, B.A. van Tiggelen, A. Lagendijk, and A. Tip,Phys. Rev. Lett. **66**, 3132 (1991).

W. van Megan, S. M. Underwood, R.H. Ottewill, N.St.J. Williams, and P.N. Pusey, Faraday discuss. Chem. Soc. **83**, 47 ((1987)

W. Van Saarloos and P. Mazur, Physica A. 120, 77 (1983)

G. H. Watson, P. A. Fleury and S. L. McCall, Phys. Rev. Lett. **58**, 945 (1987).

D.A. Weitz, D.J. Pine, P.N Pusey, and R.J.A. Tough, Phys. Rev. Lett. **63**,1747 (1989)

P.E. Wolf, G. Maret, E. Akkermans and R. Maynard, J. Phys. (France) **49**, 63 (1988).

P.E. Wolf and G. Maret, Phys. Rev. Lett. **55**, 2696 (1985).

R. Zwanzig and M. Bixon, Phys. Rev. A. **2**, 2005 (1970)